Dusty Plasmas

Wing-Huen Ip
wingip@astro.ncu.edu.tw
Institutes of Astronomy and Space Science,
National Central University

The 1st CPS International School of Planetary Sciences,
“Dust in Space”
January 5-9, 2009
Seapal Suma, Kobe, Japan

Outline

- Prologue
- Saturnian rings
- Lunar dust
- Cometary and asteroidal dust
- Laboratory dusty plasmas
- Summary
- Epilogue

Basic references

- Horanyi, M., Charged dust dynamics in the Solar System, Ann. Rev. Astr. Astrophys., 34, 383, 1996.
- Shukla, P.K., A survey of dusty plasma physics, Phys. Plasmas, 8, 1791, 2001.
- Ishihara, O., Complex plasma: dust in plasma, J. Phys. D: Appl. Phys., 40, R121, 2007.
- Morfill, G.E., Ivlev, A.V., Rubin-Zuzic, M., Knapek, C.A., Pompl, R., Antonova, T., and Thomas, H.M., Complex plasmas-new discoveries in strong coupling physics, Appl. Phys., B89, 527, 2007.
- Grasp, A.L., Jones, G.H., Juhasz, Al Horanyi, M. and Havnes,O., The charging of planetary rings, Space Sci. Rev., 137, 435, 2008.

Lecture 1

January 6, 2009

1. Prologue

The first generation of dusty plasma physicists

W. Ian Axford

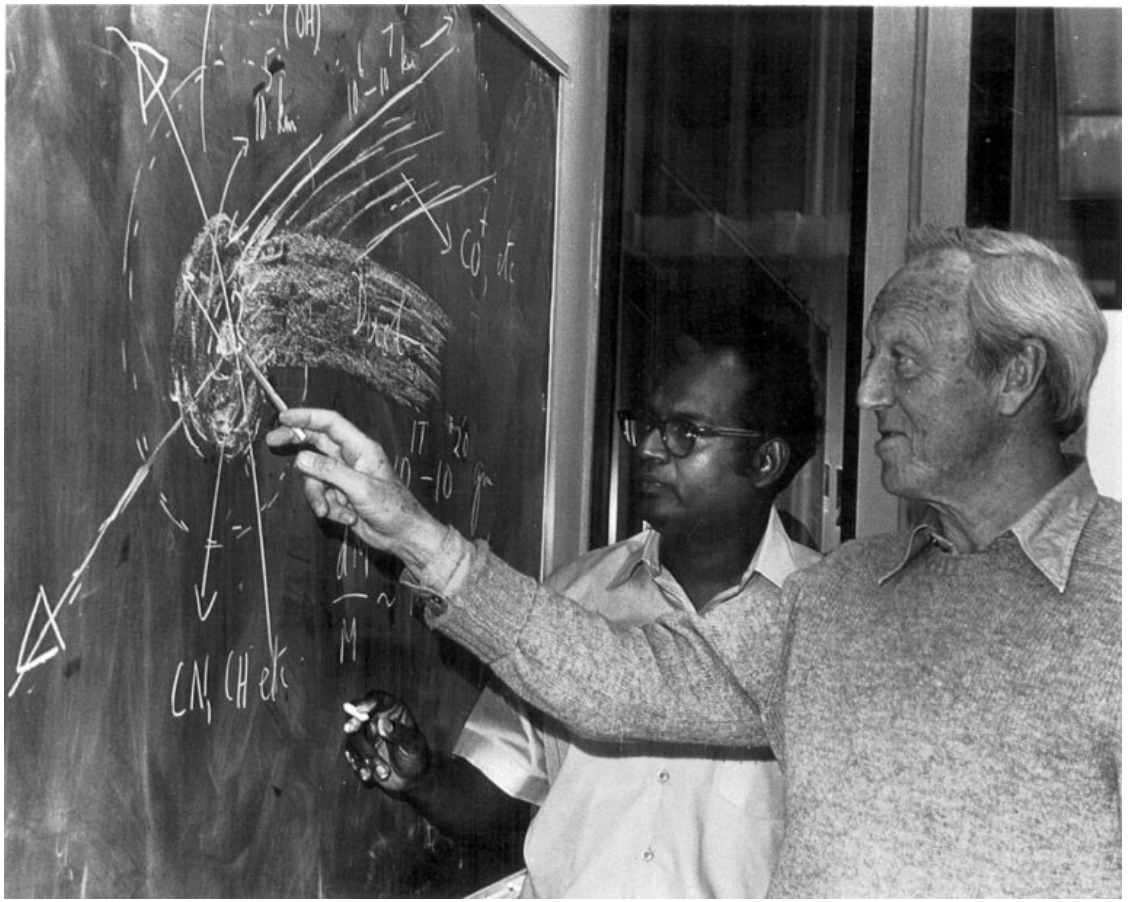

Asoka Mendis and Hannes Alfven

Saturn as A Dusty Plasma Laboratory

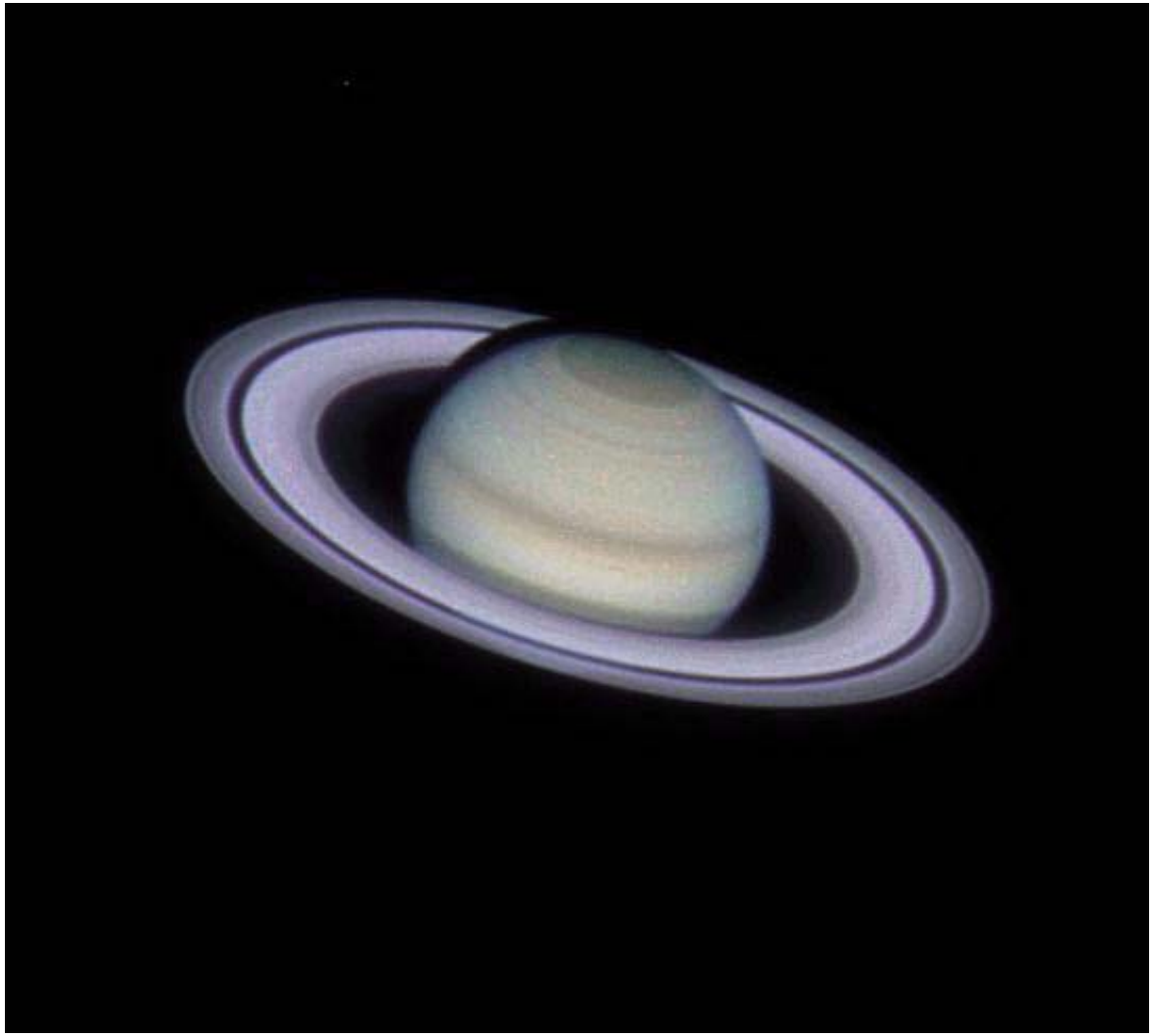

Alfven's critical ionization effect and plasma condensation model of the Saturnian rings

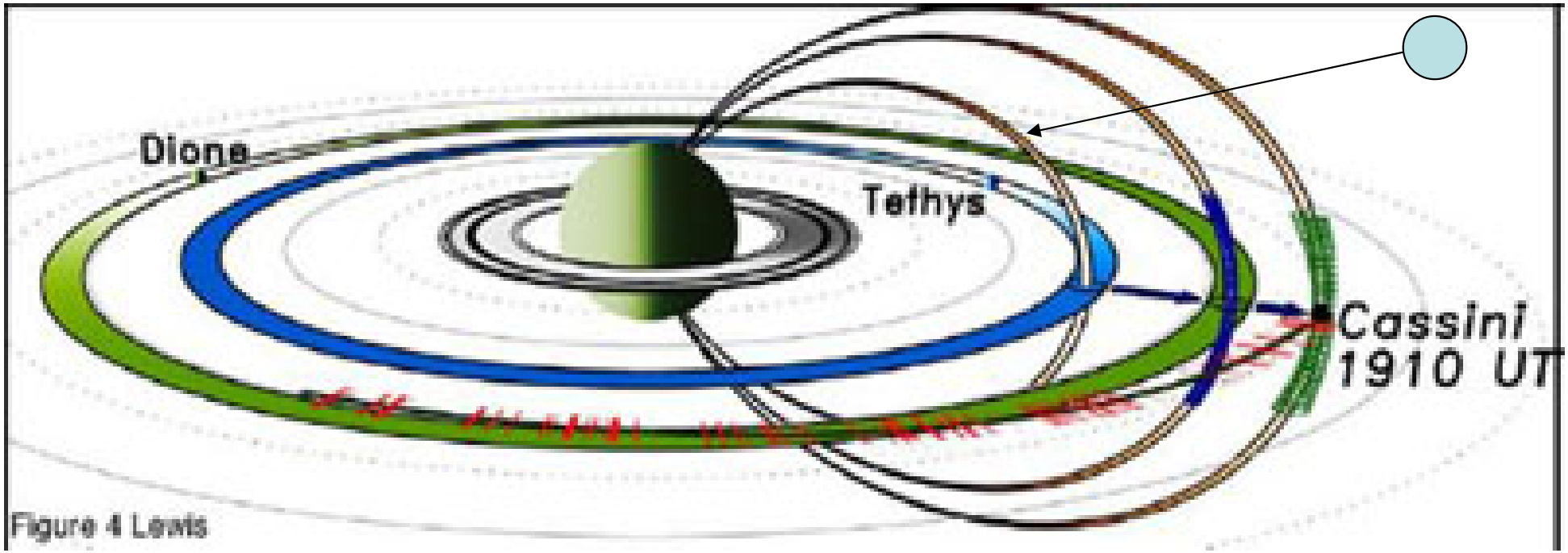

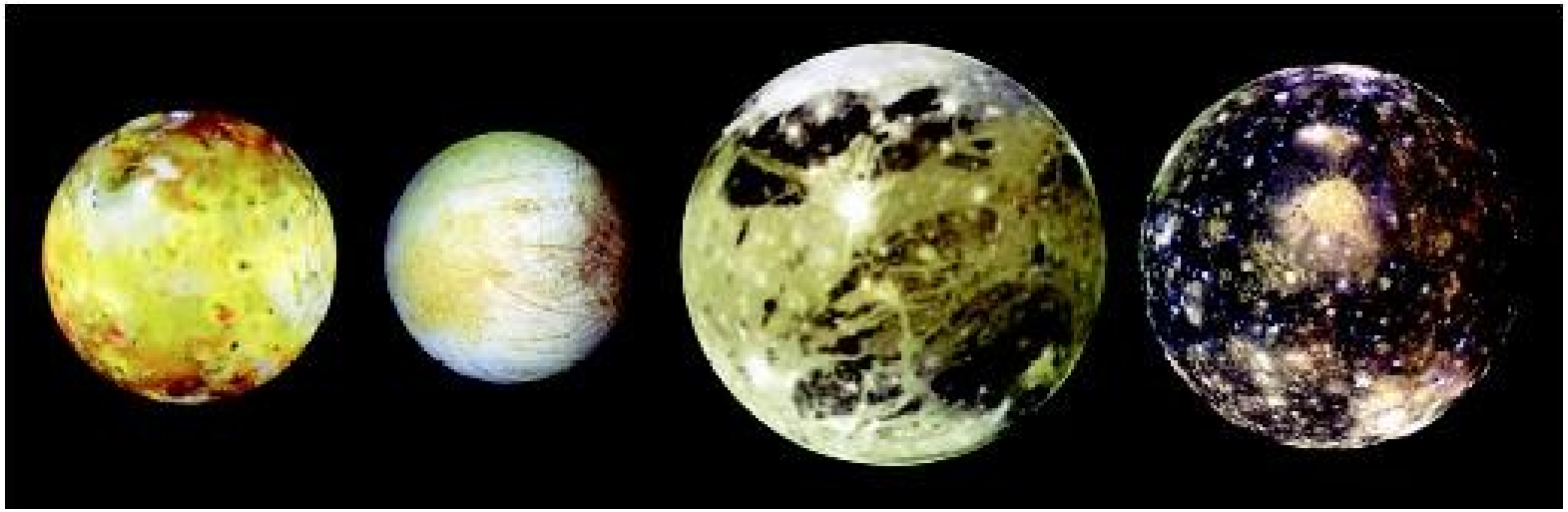

Europa

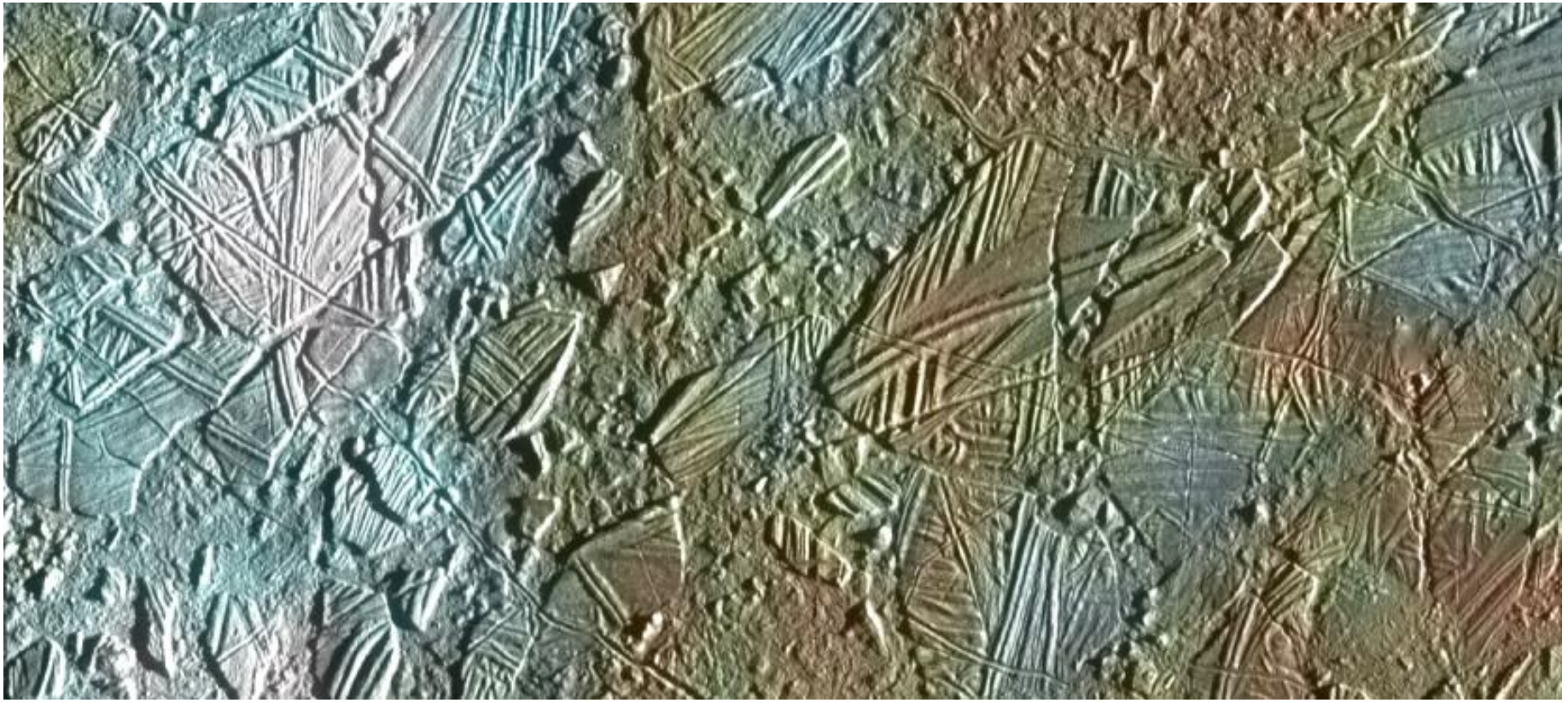

Titan for Christmas

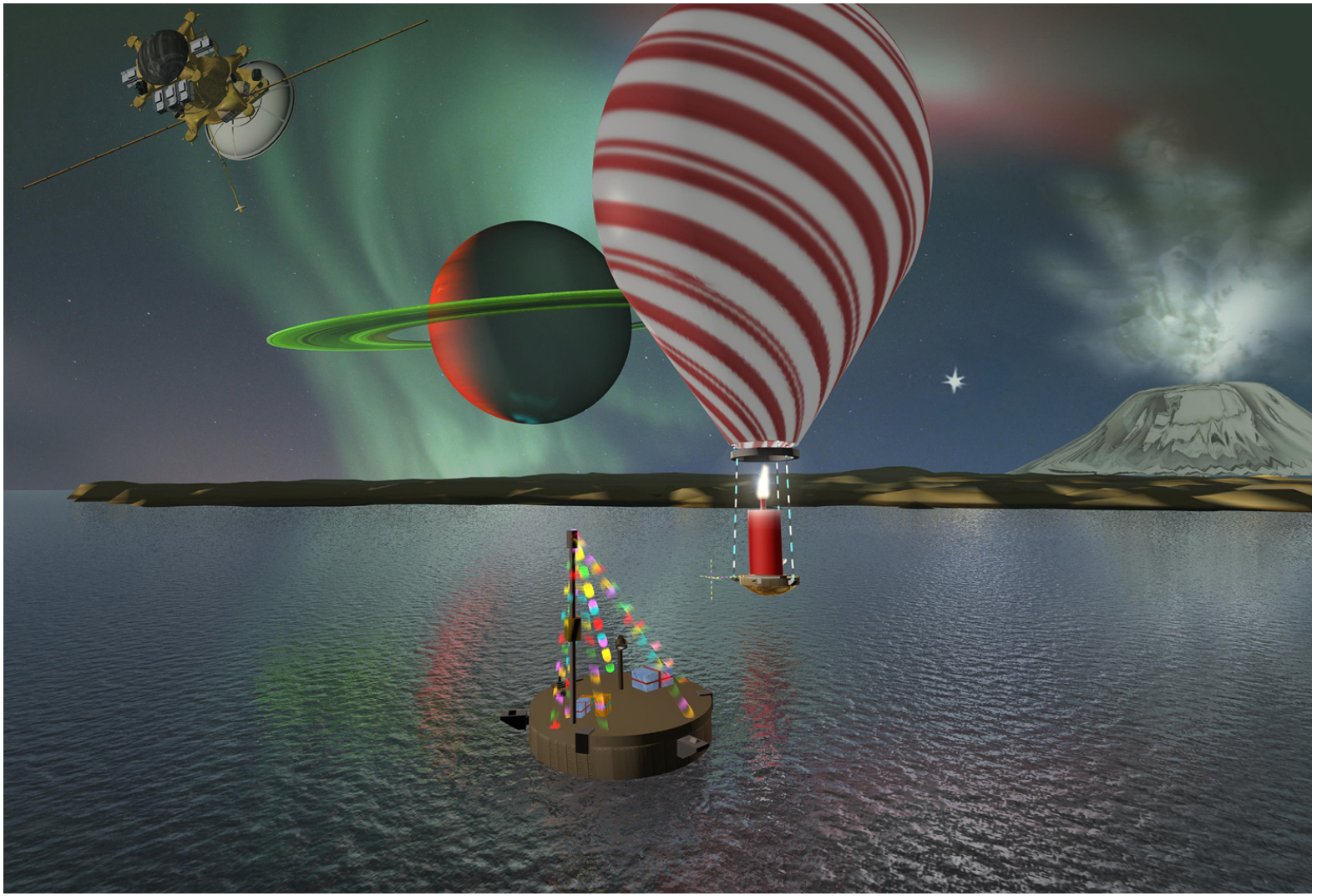

From Athena Coustenis,
X'mas 2008

Surface albedo asymmetry of Saturnian icy satellites

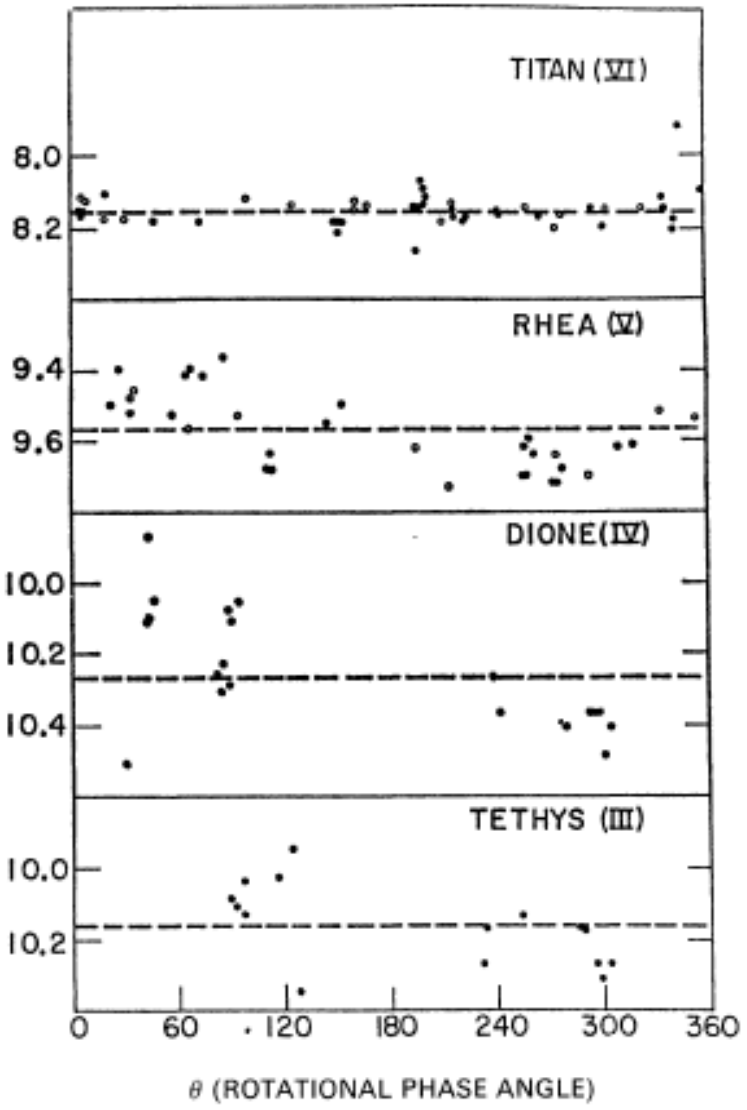

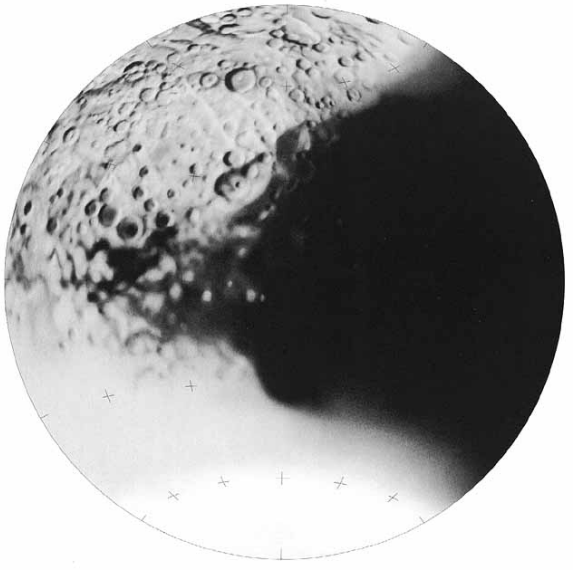

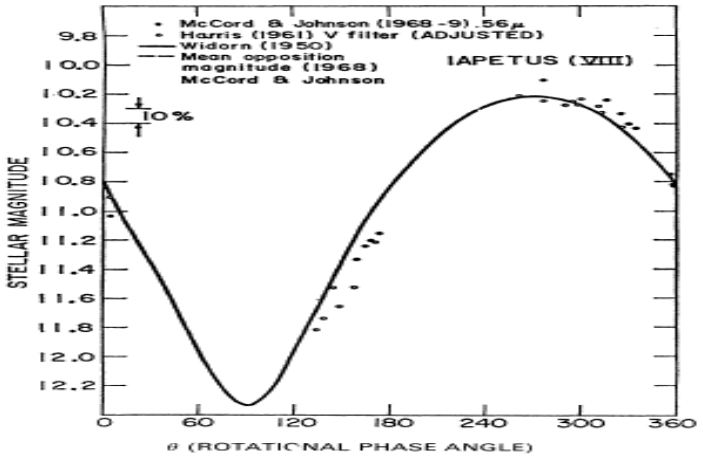

Top-down model

Soter (1974) originally proposed dust
Ejected from Phoebe could land on the
Leading hemisphere of Iapetus (see also Burns et al. (1996).

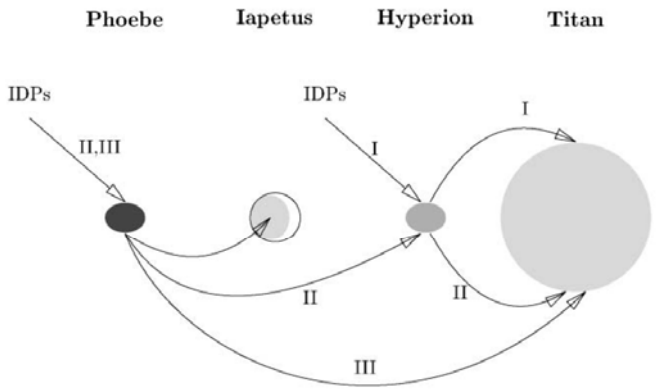

Fig. 1. Possible ways of the dust transport in the outer Saturnian system. I—dust ejected by IDPs from Hyperion and arriving at Titan; II—dust ejected by IDPs from Phoebe, impacting Hyperion and ejecting secondary particles which also arrive at Titan; III—dust ejected by IDPs from Phoebe and reaching Titan directly.

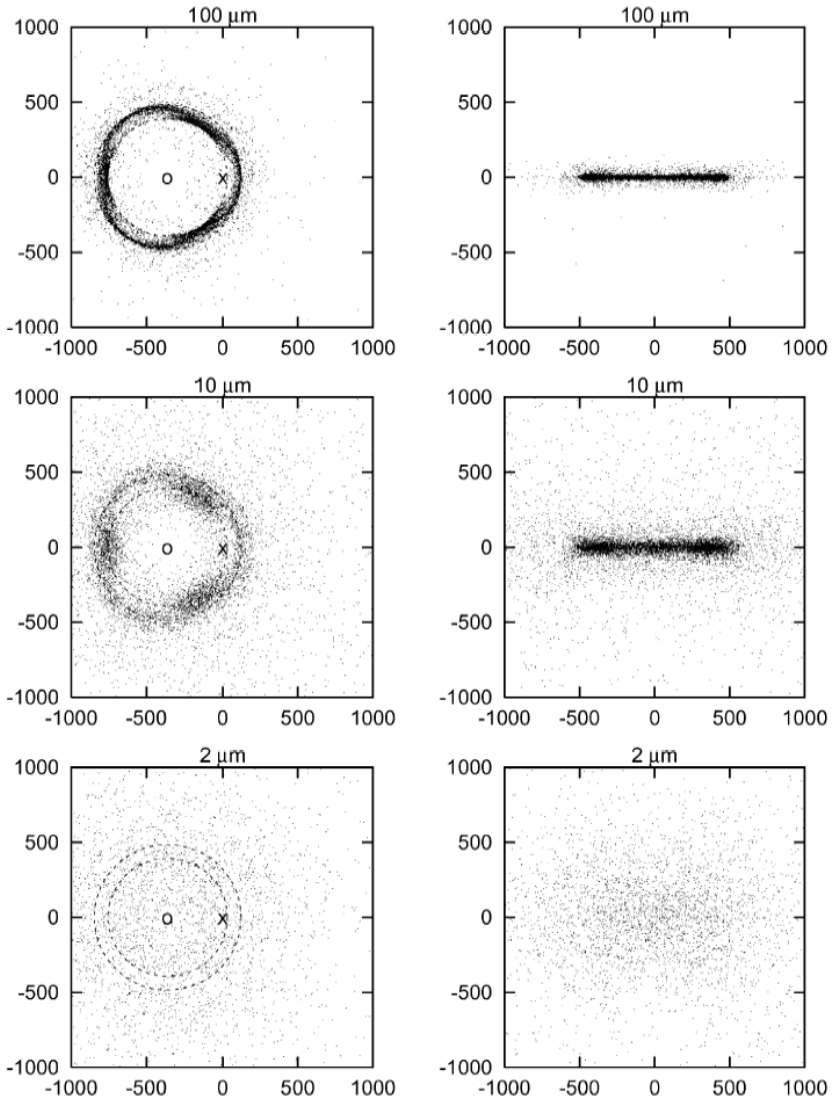

distribution of dust in the Titan-centred rotating equatorial system (x-axis along Saturn–Titan line, z-axis toward Saturn's north pole). same as in Fig. 8. Coordinates are in Titan's radii (including the atmosphere). Small circle and cross in the left panels are the position Titan, respectively, and dashed circles have the same meaning as in Fig. 8.

Krivov and Banaszkiewicz (2001)

Annual Review of Earth and Planetary Science

SATELLITES AND MAGNETOSPHERES OF THE OUTER PLANETS

* 10029

D. A. Mendis and W. I. Axford
Department of Applied Physics and Information Science, University of California, San Diego, La Jolla, Caifornia 92037

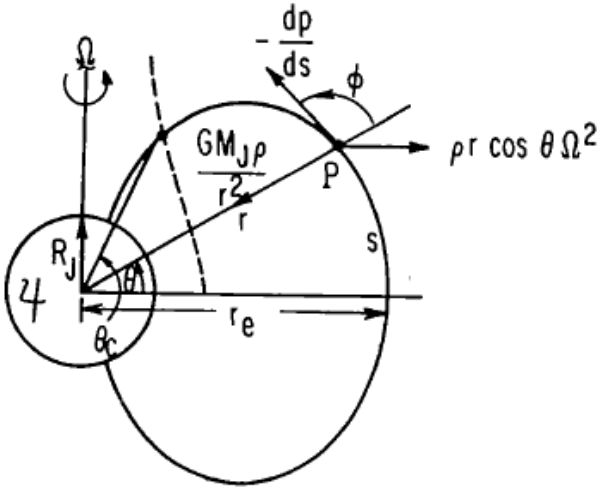

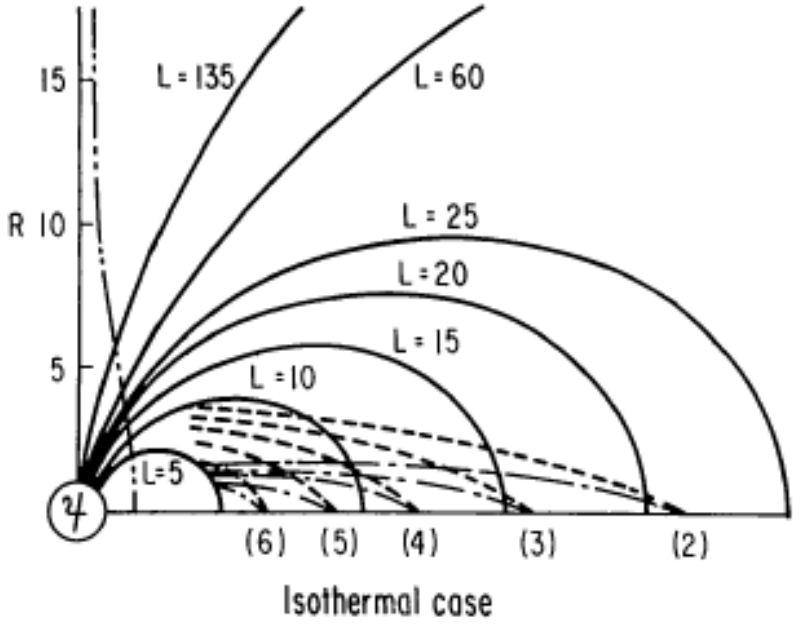

Mendis & Axford (1974)

Bottom-up model

Surface erosion mechanism of Iapetus

Meteoroids
~Ice sublimation

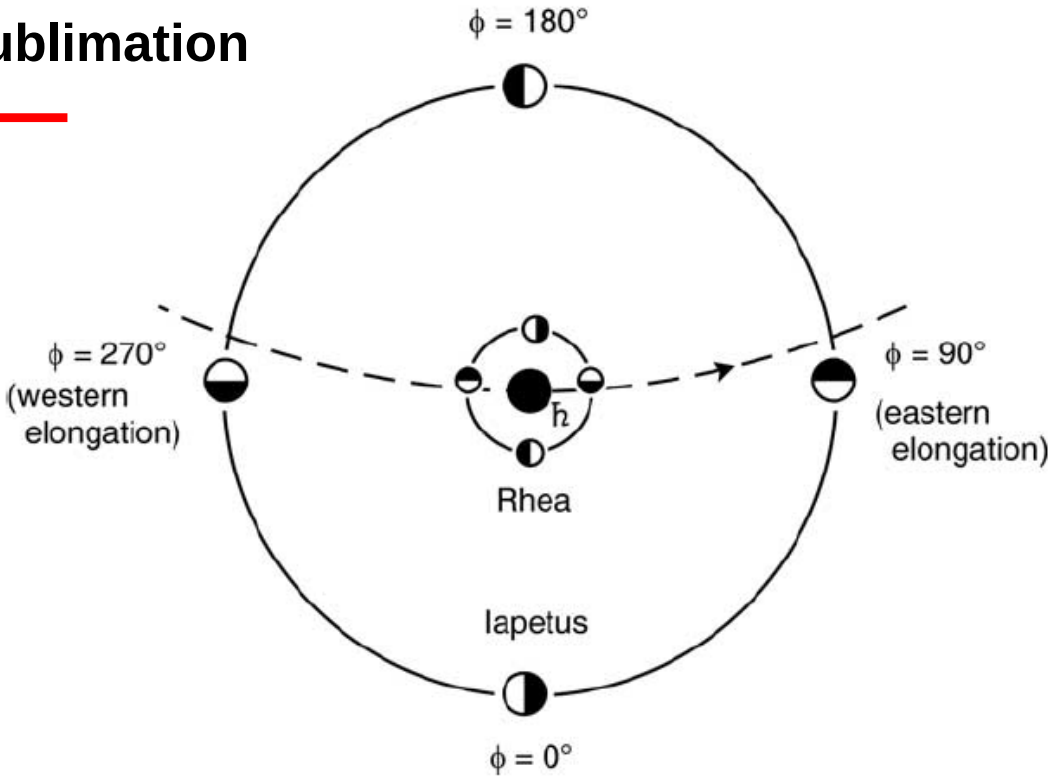

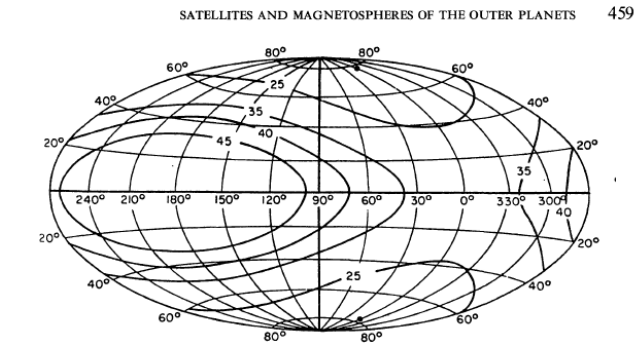

Figure 14 Lines of constant erosion rate on the complete sphere of Iapetus. Numbers are the factors by which the arrival rate of meteoroidal mass in a system at rest relative to the Sun must be multiplied to give the rate of material erosion. The center of the leading hemisphere of Iapetus in orbit about Saturn is at 180°, the trailing at 0° (Cook & Franklin, 15).

Mendis & Axford (1974)

2. Saturnian rings

Cassini view of the Saturnian ring system

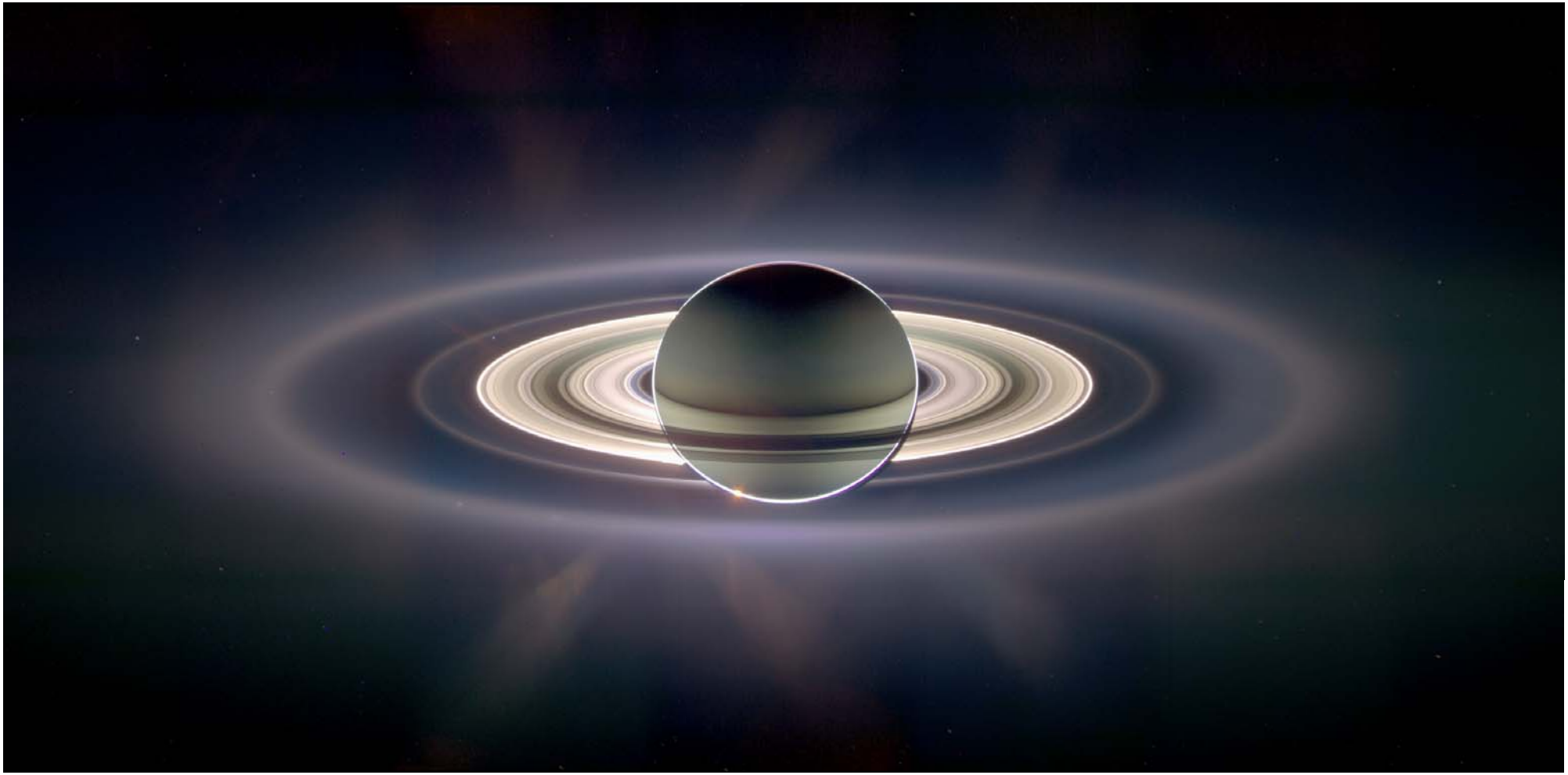

Edge-on view of the E-ring by Keck (Optical depth ~ 10^{-5})

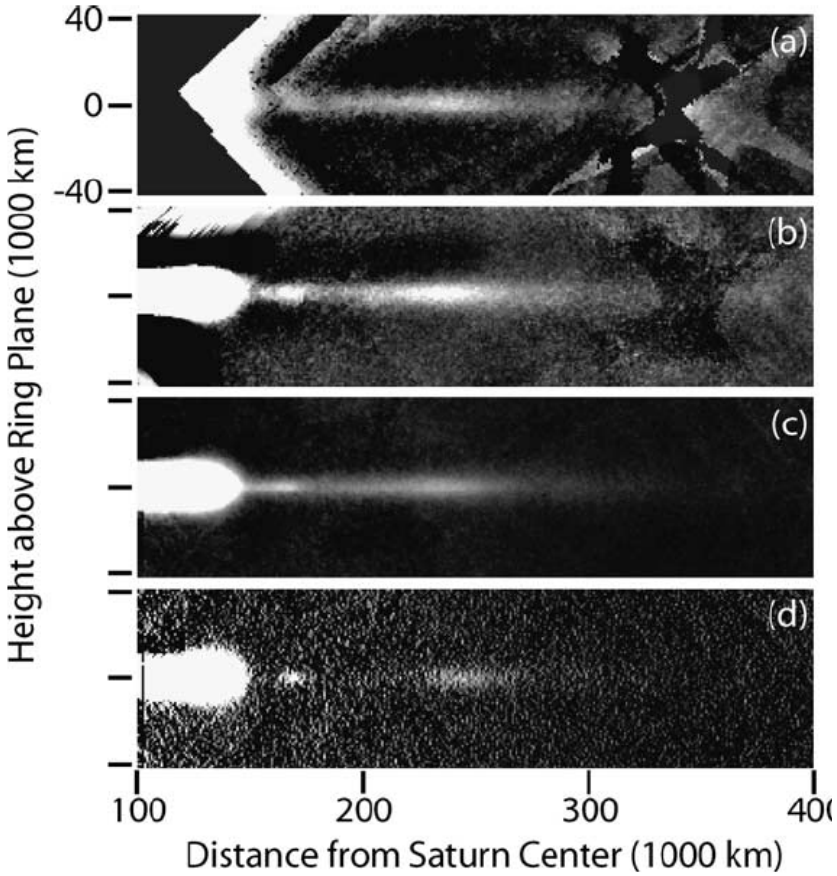

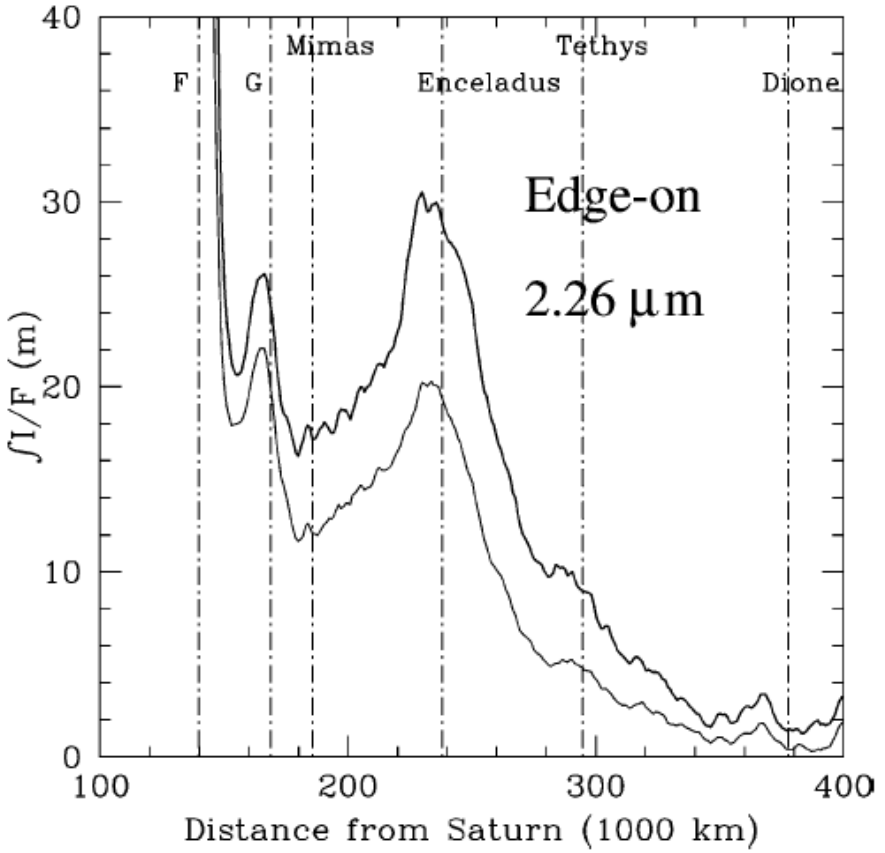

de Pater et al. (2004)

Extended OH cloud

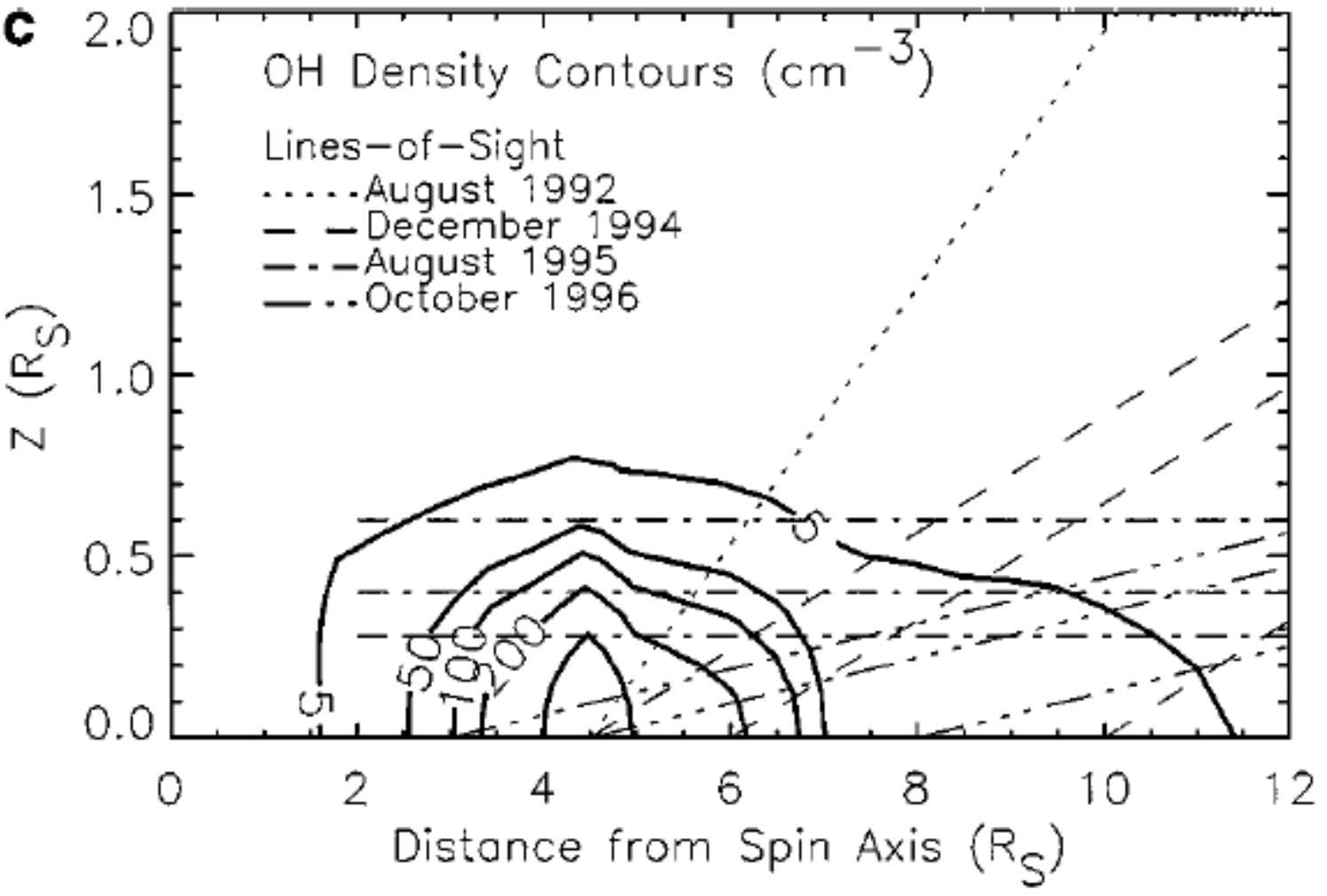

Jurac et al. (2001)

Saturnian Satellites

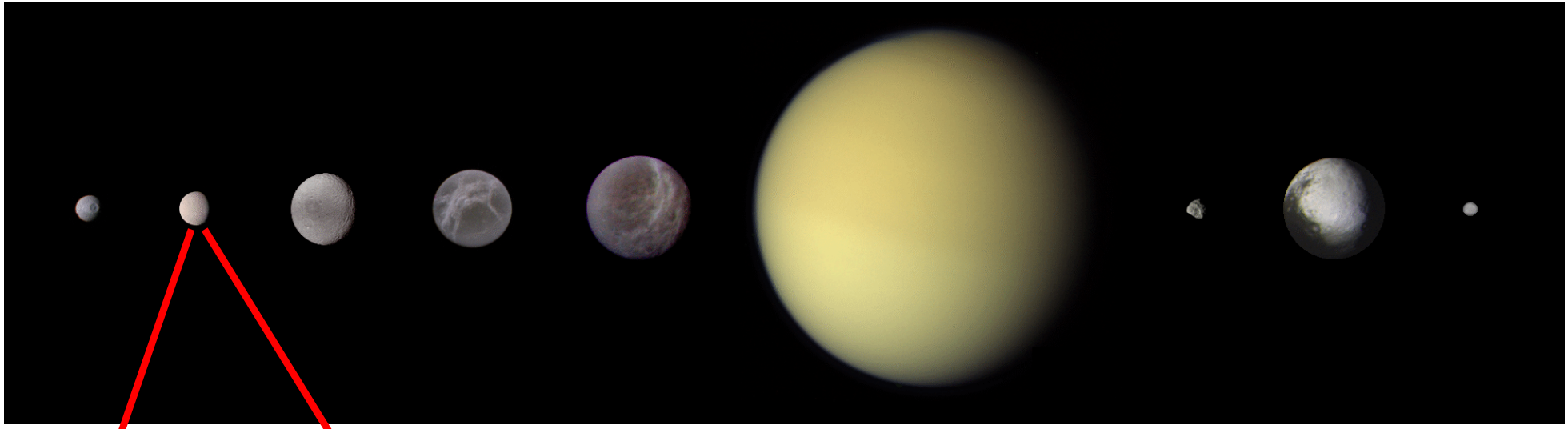

M E T D R Titan Iapetus

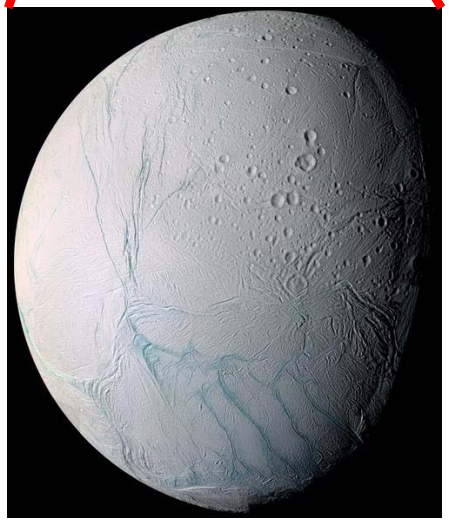

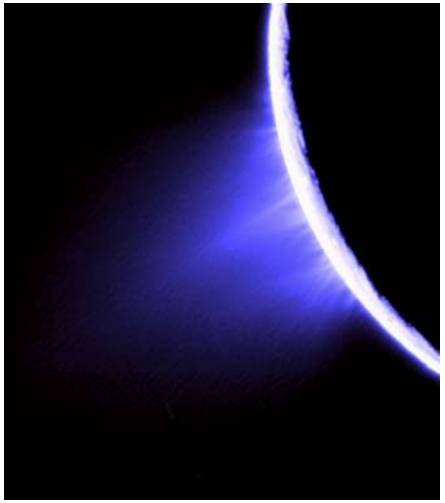

Enceladus' gas and dust plumes

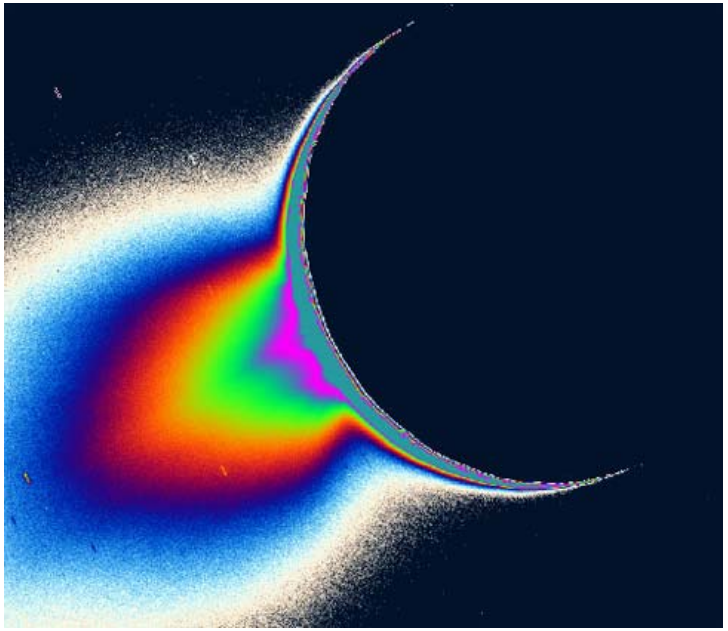

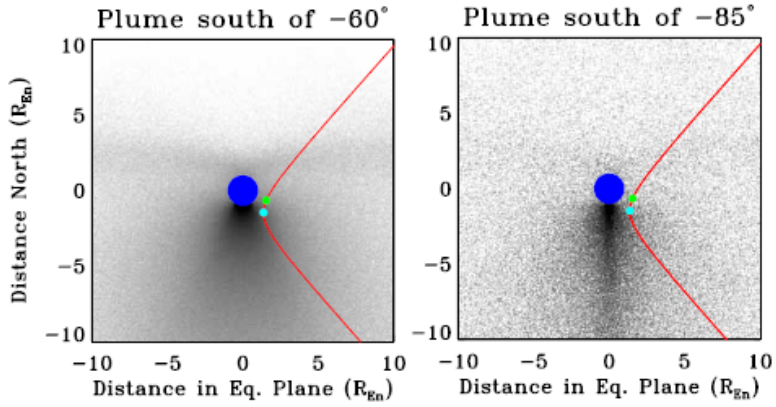

Figure 3. Comparison between plumes formed form different-sized active regions. Left, active region is south of −60° longitude. Right, active region south of −85°. The blue circle represents Enceladus' disk. The red line shows Cassini's trajectory in cylindrical coordinates (z versus $\sqrt{x^2 + y^2}$). The green dot shows the Enceladus closest approach; the light blue dot marks the point of maximum water density measured by INMS.

Burger et al. 2007

Dynamics of Saturn's E-ring dust

- $R_E = 4\ R_s$
- $N(O^+) = 100\ (R_E/a)^4$
- $T(O^+) = 100$ eV
- Perturbation effects:

  Electrostatic charging

  Planetary oblateness (J2)

  Radiation pressure force

  Plasma drag force
- Ion sputtering time ~ 50 years for 1 μm icy grains

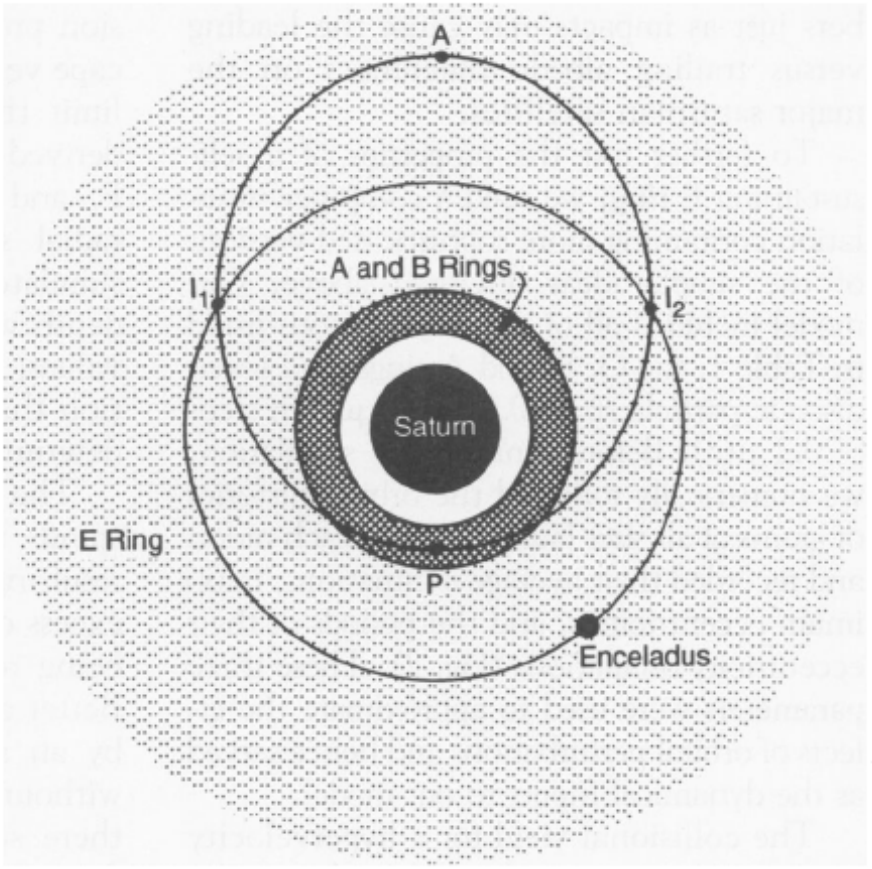

Hamilton and Burns (1994)

Grain charging by thermal plasma

- Current balance condition:

  $J_e(\Phi_d(t)) + J_i(\Phi_d(t)) + J_{sec}(\Phi_d(t)) + J_{ph}(\Phi_d(t)) = 0$

- J_{ph} is photo-electron emission currrent
- $J_{e,I}$ are electron/ion currents from the background plasma
- J_{sec} is secondary electron current

Shull (1978); Whipple (1981); Chow et al. (1993); Horanyi (1996)

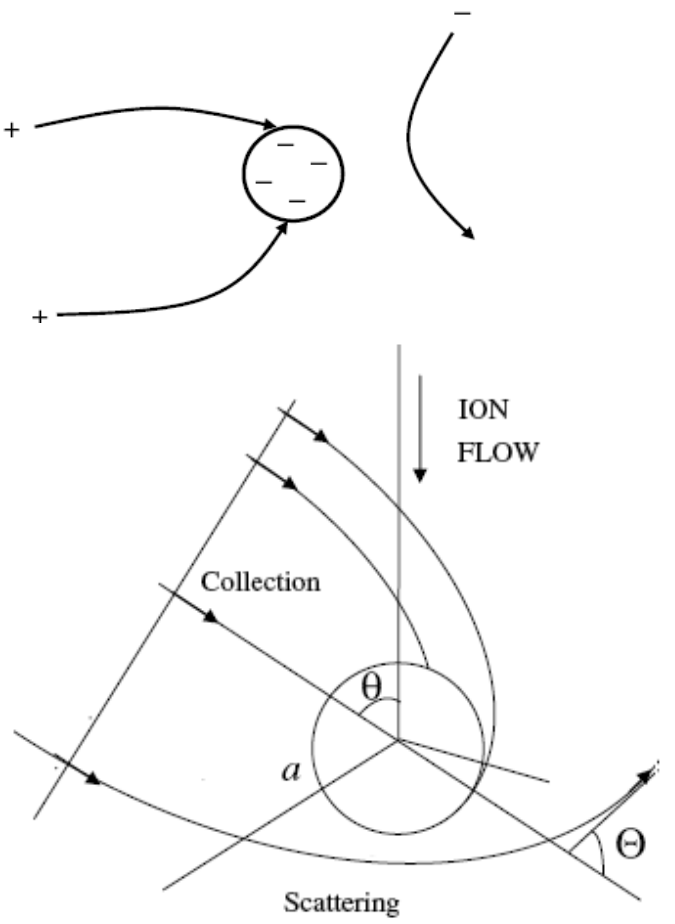

Ishihara (2007)

The charging equation

- Ion and electron currents(I_i^+ and I_e^+) for surface potential Φ_s>0(Mendis et al. ,1981):

$$I_i^+ = \tfrac{1}{2} neV\cos\theta\left[1+\mathrm{crf}\,(X_i)+\left(\pi^{1/2}U_i\right)^{-1}\exp\left(-X_i^2\right)\right]$$

$$I_e^+ = \frac{fne\alpha_e}{2\pi^{1/2}}\left\{\exp\left(-U_e^2\right)+\pi^{1/2}U_e\left[1+\mathrm{erf}\,(U_e)\right]\right\},$$

With

$$\alpha_i = \left(\frac{2kT_i}{m_i}\right)^{1/2}, \quad \alpha_e = \left(\frac{2kT_e}{m_e}\right)^{1/2},$$

$$U_i = \frac{V\cos\theta}{\alpha_i}, \qquad U_e = \frac{V\cos\theta}{\alpha_e},$$

$$X_i = U_i - \left(\frac{e\phi_s}{kT_i}\right)^{1/2}.$$

- The photoelectron current I_p^+ is

$$I_p^+ = I_0\cos\theta\exp\left(\frac{-e\phi_s}{kT_p}\right),$$

$$I_0 = \frac{2.5\times10^{10}e\chi}{d^2(\mathrm{AU})},$$

where kT_p =2 eV and X=0.1.

For Φ_s <0,

$$I_i^- = \frac{fneV\cos\theta}{2}\left[1+\mathrm{erf}\,(U_i)+\left(\pi^{1/2}U_i\right)^{-1}\exp\left(-U_i^2\right)\right]$$

$$I_e^- = \frac{ne\alpha_e}{2\pi^{1/2}}\left\{\exp\left(-X_e^2\right)+\pi^{1/2}U_e\left[1+\mathrm{erf}(X_e)\right]\right\}$$

$$I_p^- = I_0\cos\theta,$$

$$X_e = U_e - \left(\frac{-e\phi_s}{kT_e}\right)^{1/2}$$

$\mathbf{I_i - I_e + I_p = 0 \rightarrow \Phi_s = ?}$

Comparison of theoretical models with Cassini CDA observations of the electrostatic potential of the charged dust

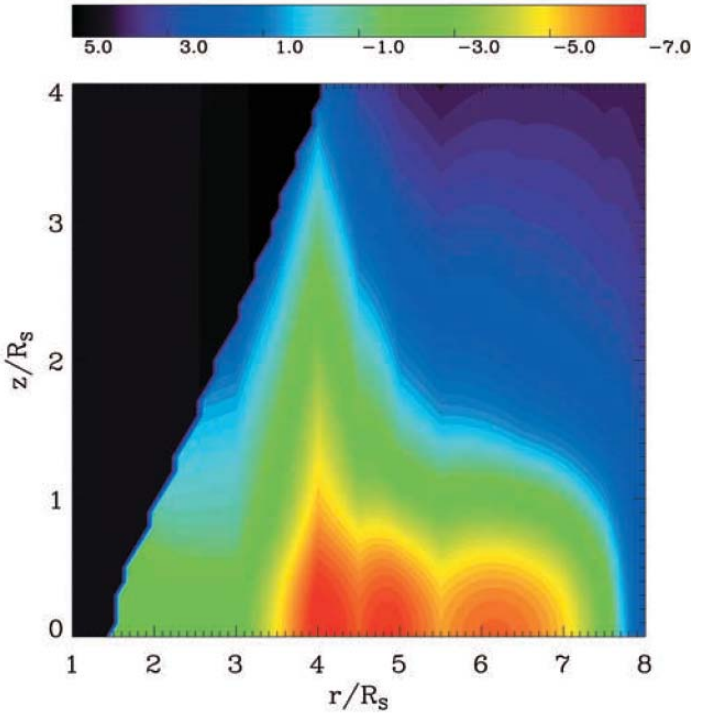

Juhasz and Horanyi (2002)

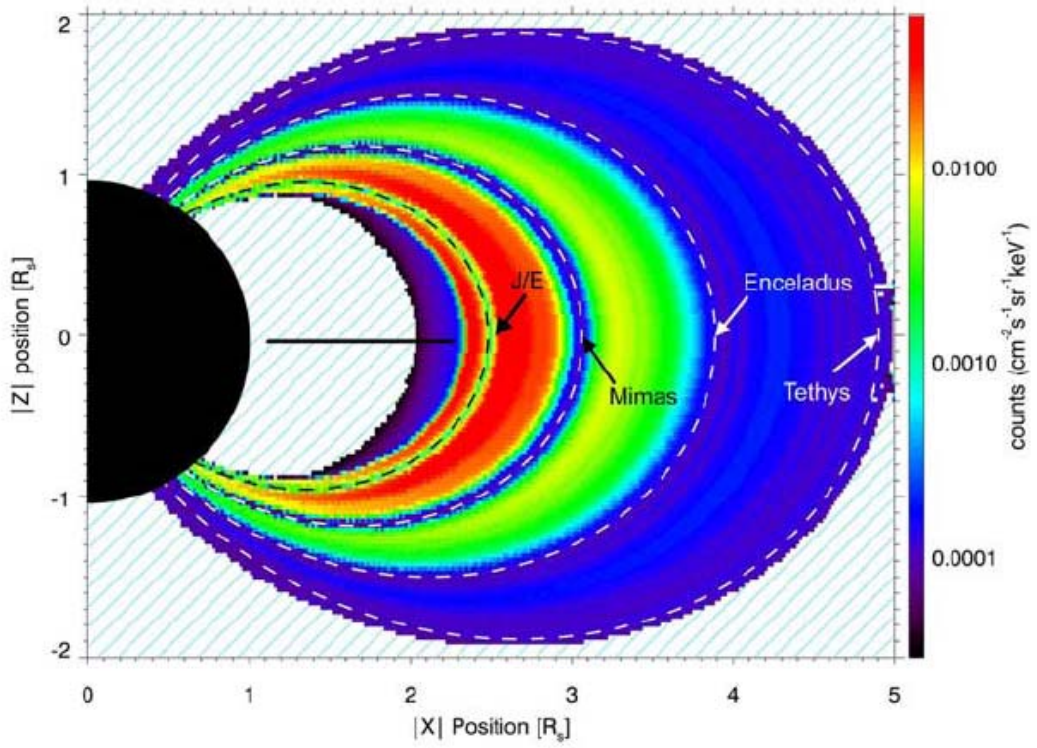

Roussos et al., (2008)

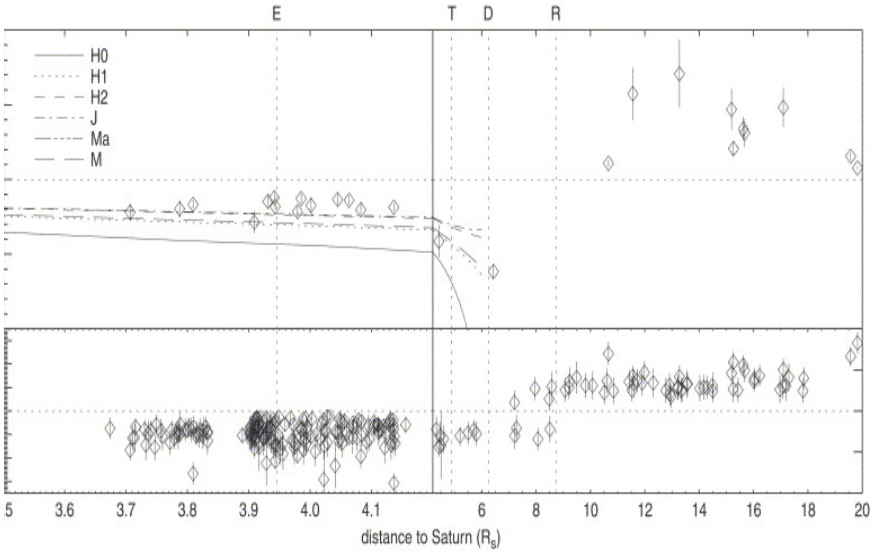

Kempf et al. (2006)

E-ring particle density distribution

- Top: r_g ~ 0.1-0.5 μm
- Middle: r_g ~ 0.5-1.0 μm
- Bottom: r_g ~ 1.0-3.0 μm

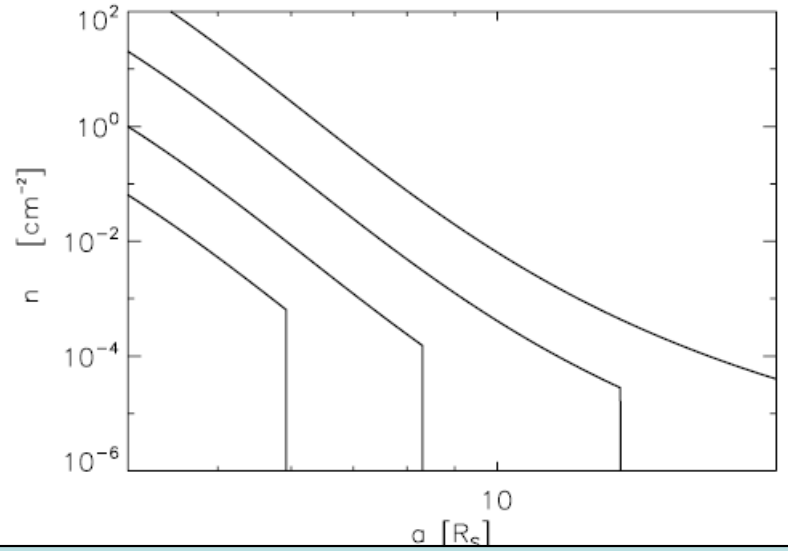

Top to Bottom: 0.1, 0.3, 1 and 3 μm

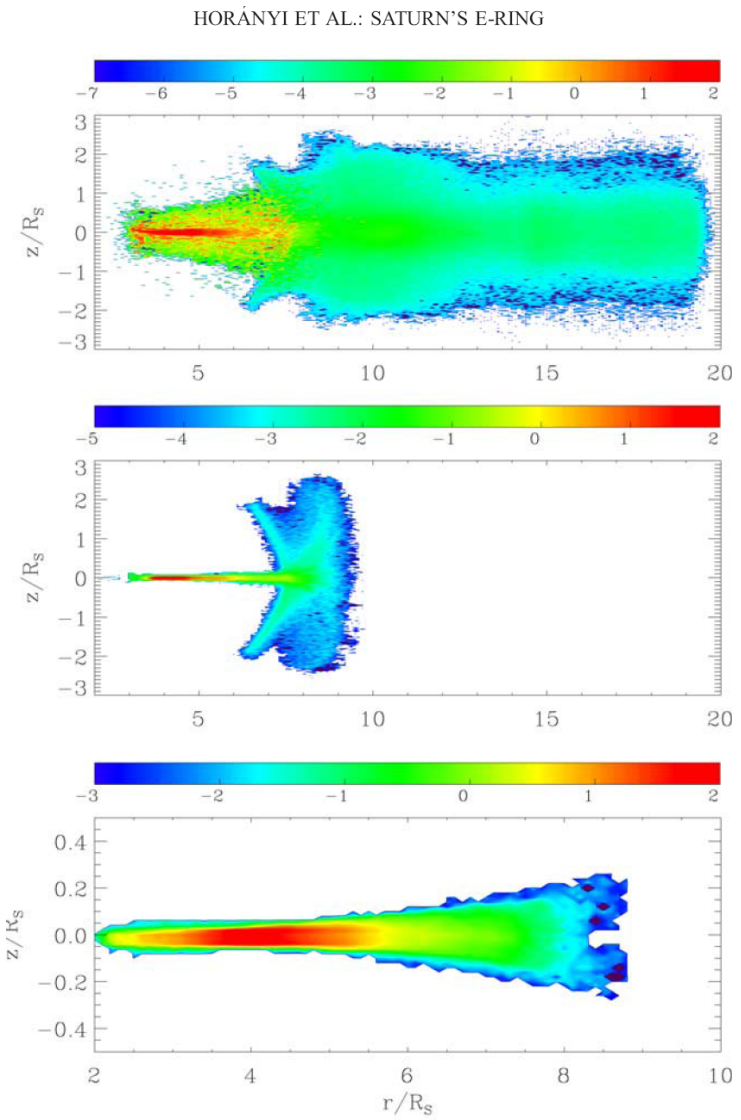

Horanyi et al., (2008)

Saturn's (B) ring spokes

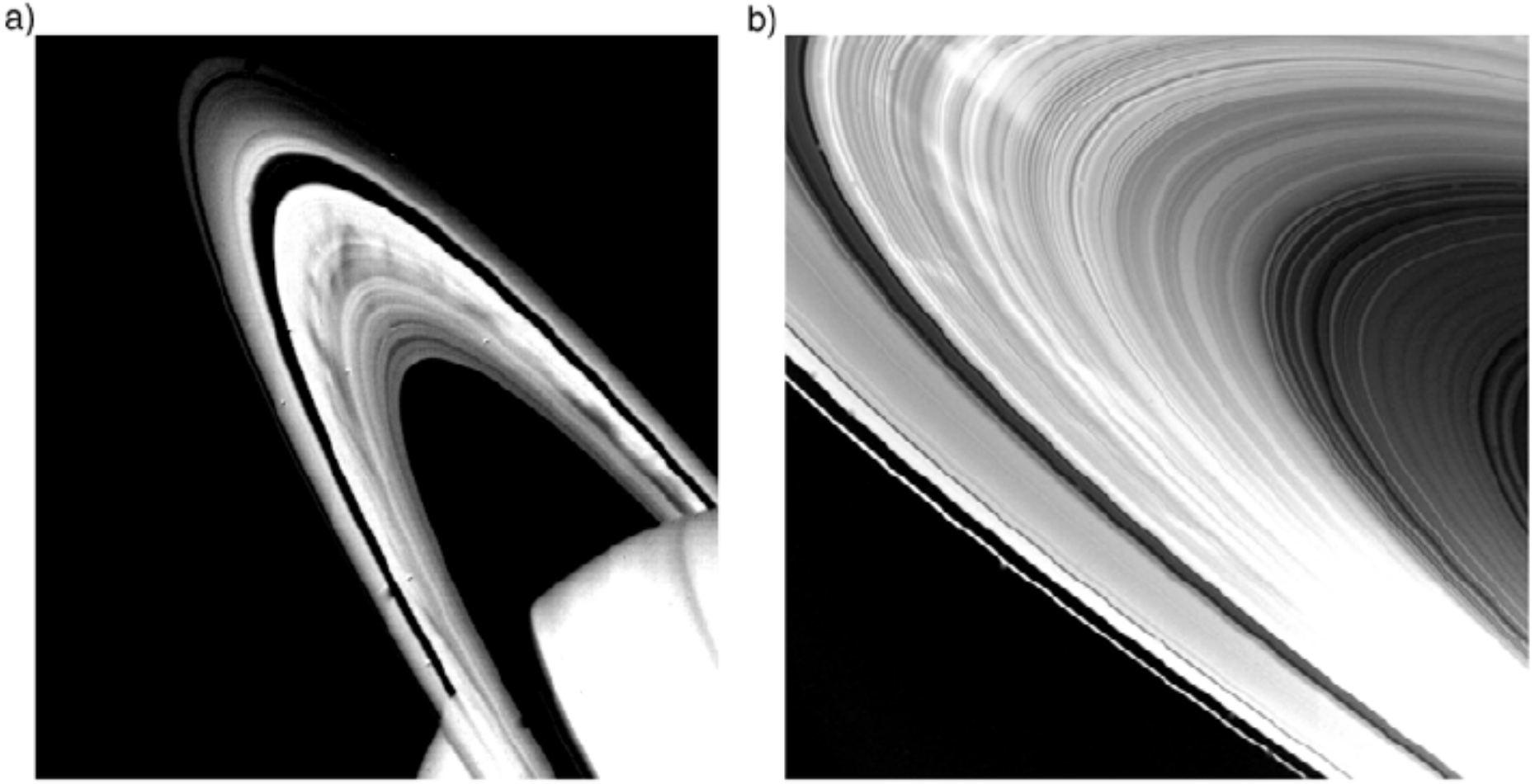

Smith et al. (1981, 1982)

Time evolution of ring spokes

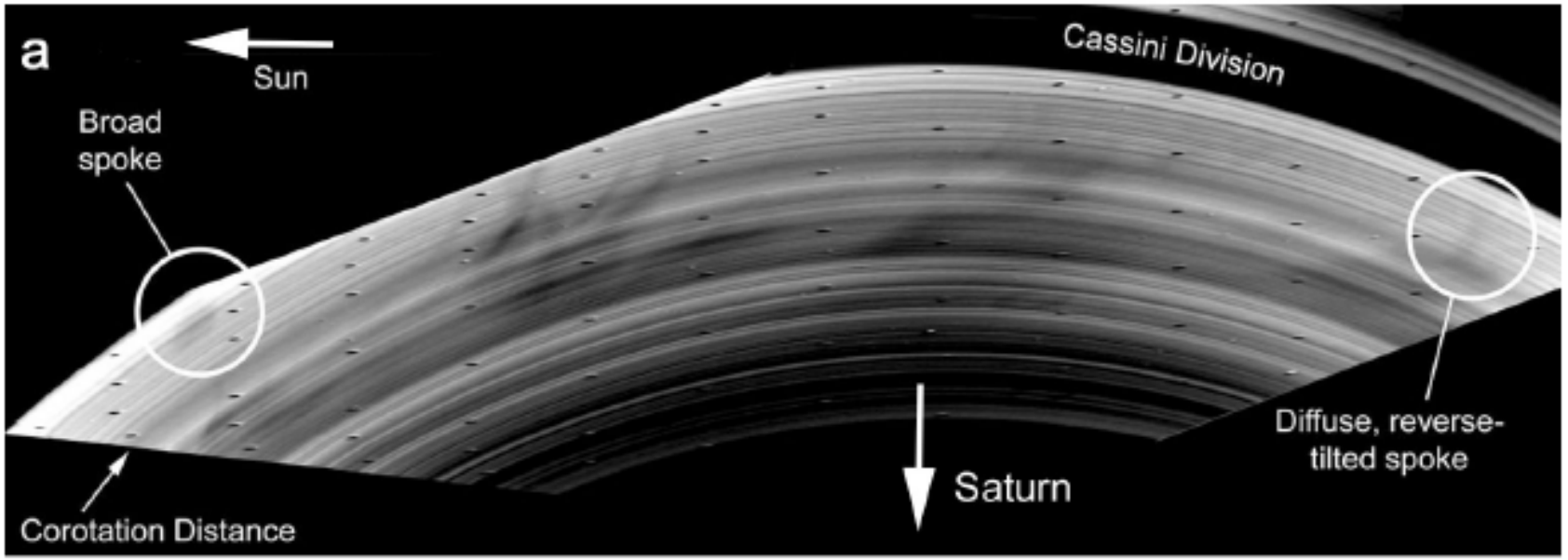

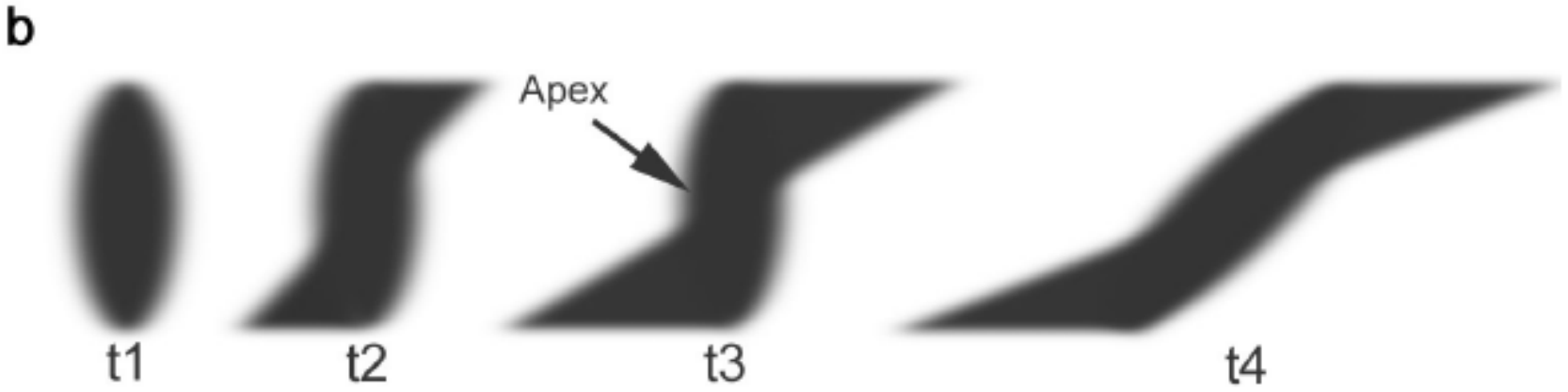

Jones et al., (2006)

Spoke statistics

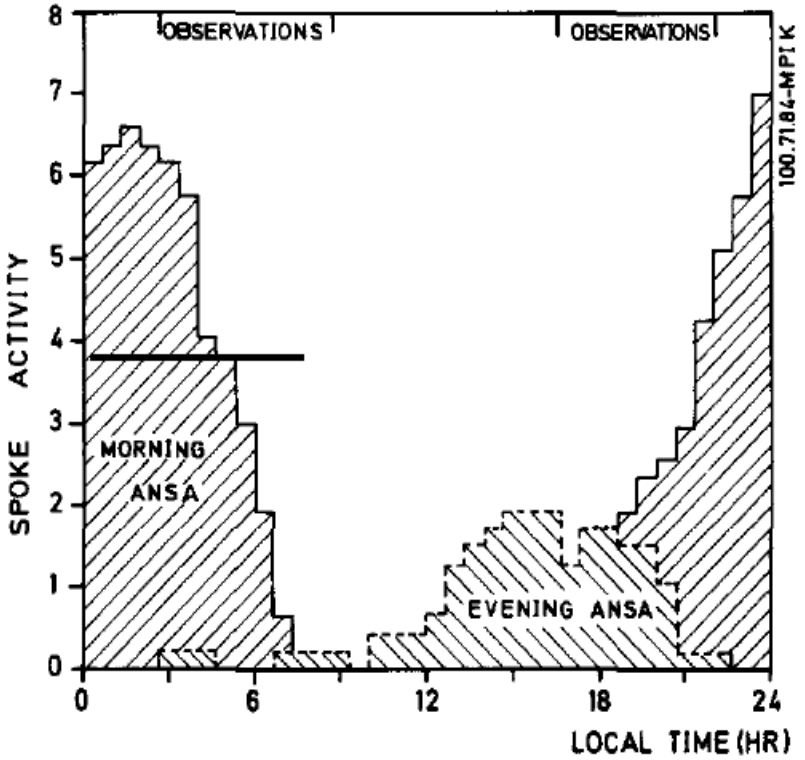

Grun et al. (1984)

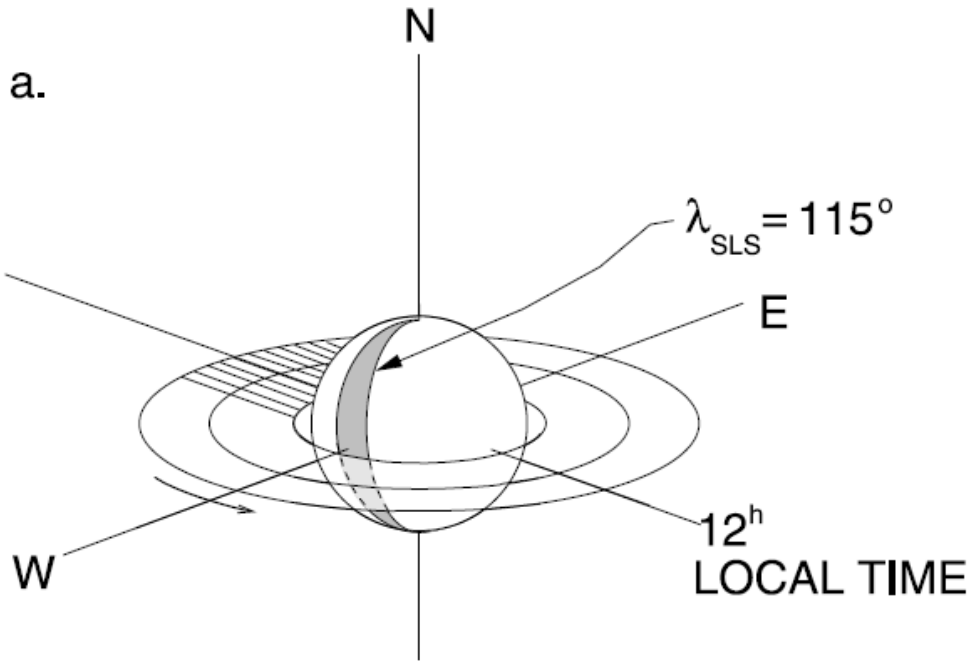

Porco and Danielson (1982)

Meteoroid-ring impact pattern

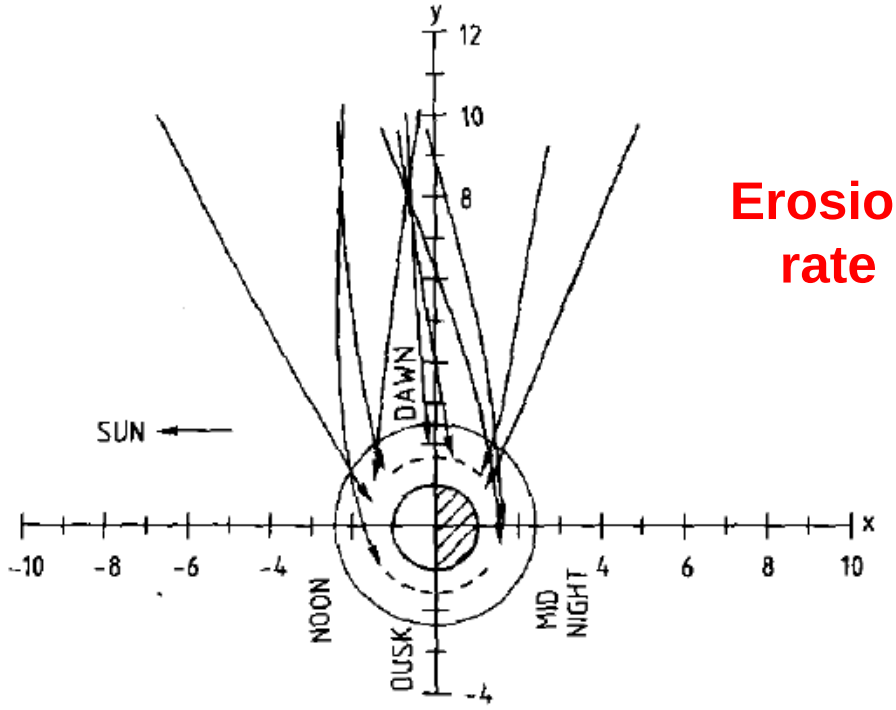

Erosion rate

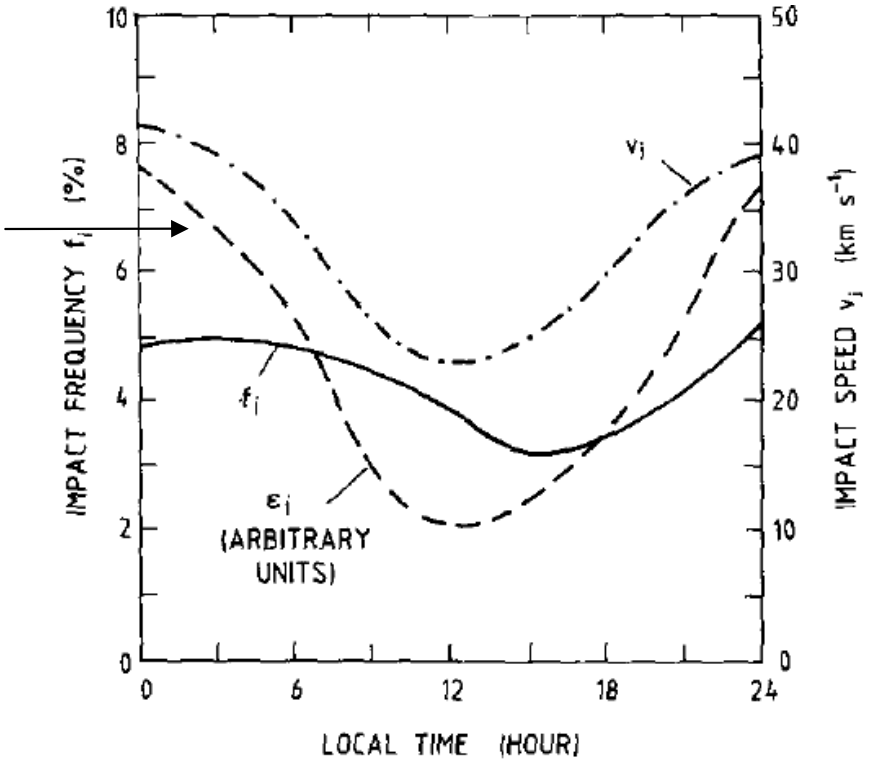

Ip (1995)

The dusty plasma cloud model of spoke generation

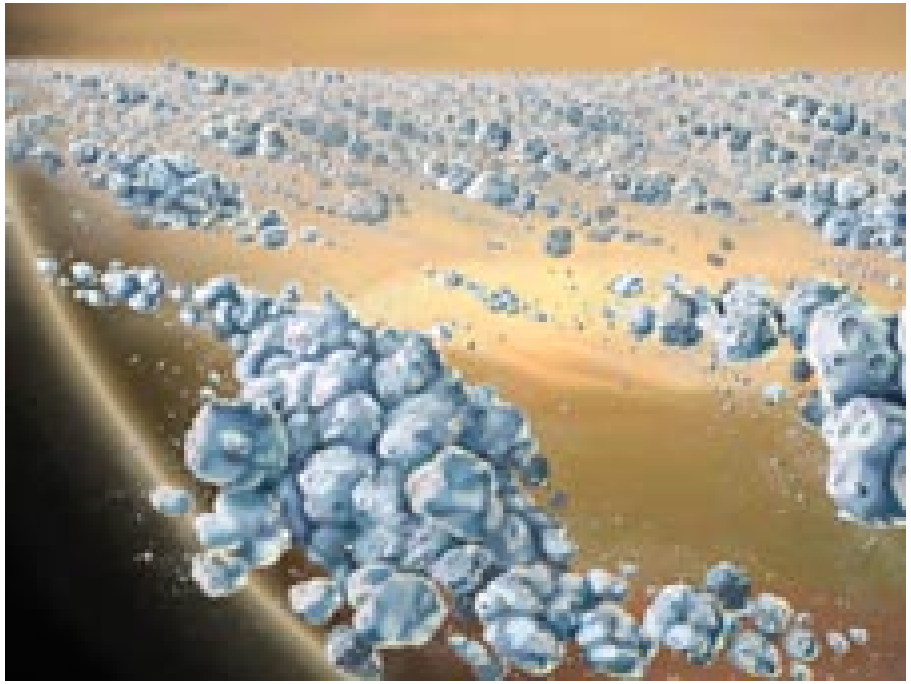

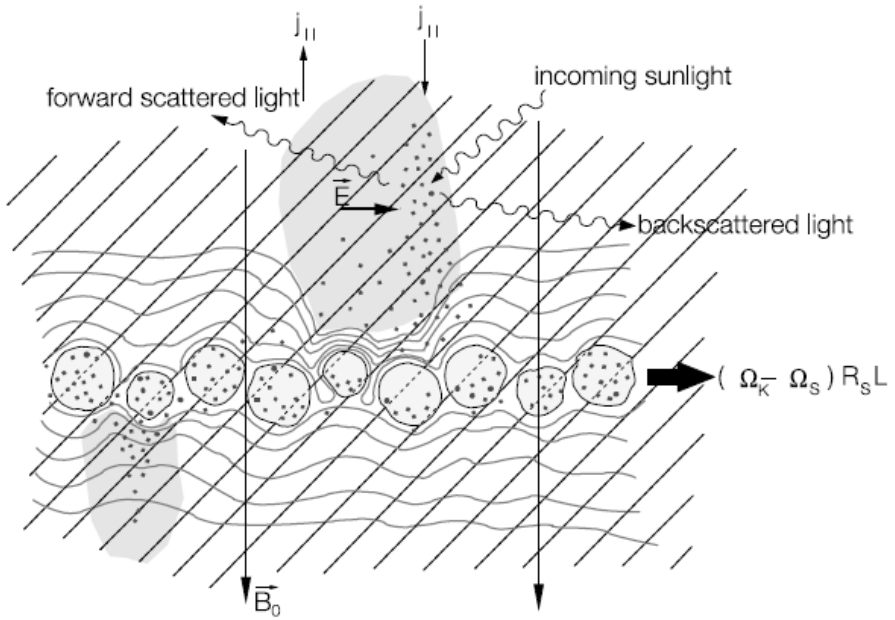

http://www.nasa.gov/images/content/
205787main_PIA10081-226.jpg

Goertz and Morfill (1983)

Spoke formation under moving plasma clouds

$$v_{px} = v\frac{\Sigma_s}{\sigma_i}b,$$

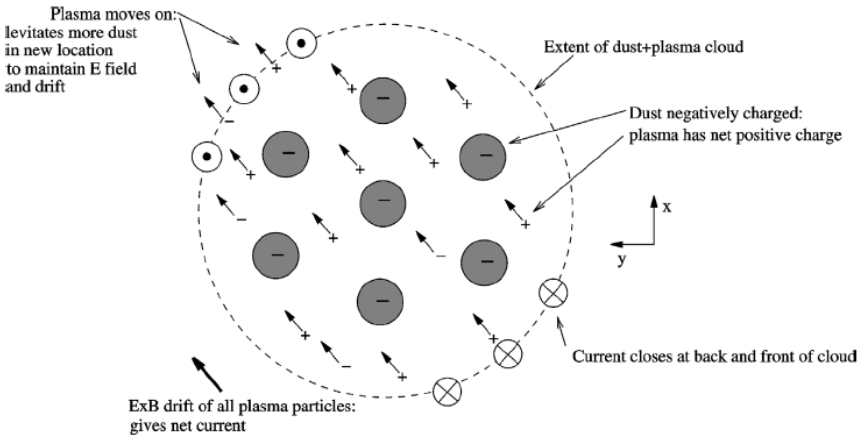

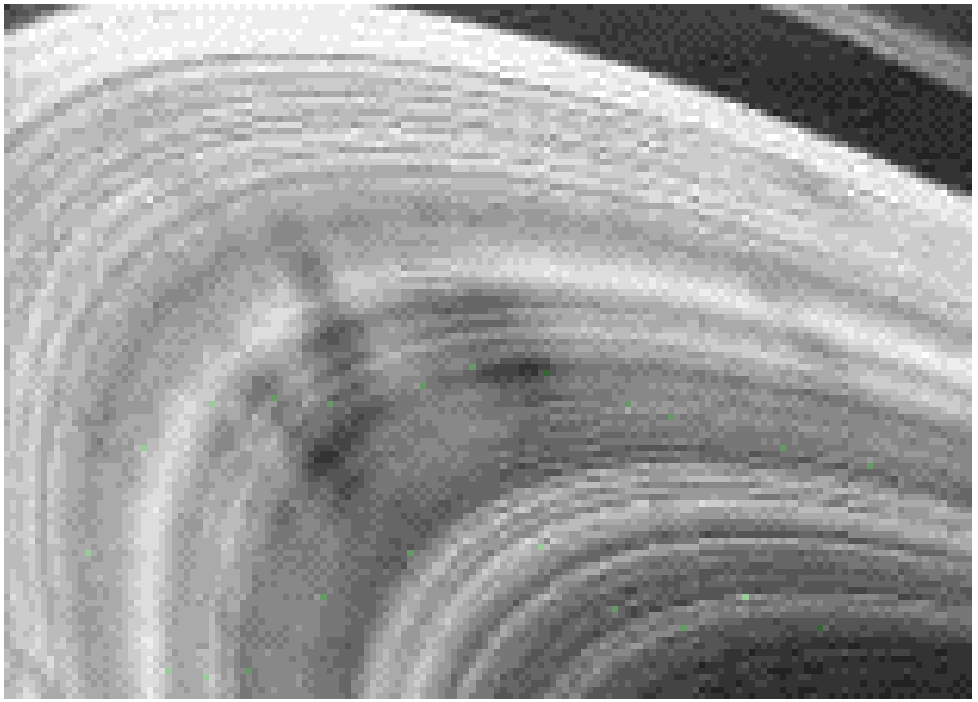

Farmer and Goldreich (2005)

Ionosphere-dust cloud coupling

$$\mathbf{v}_p = c\frac{\mathbf{E}\times\mathbf{B}}{B^2}$$

$$\mathbf{J} = \sigma\mathbf{E} + \Sigma\frac{\mathbf{B}\times\mathbf{E}}{|B|}$$

$$J_{xs} = [\sigma_s E_{xs}] - [b\Sigma_s E_{ys}],$$
$$J_{ys} = [\sigma_s E_{ys}] + b\Sigma_s E_{xs},$$
$$J_{xi} = \sigma_i E_{xi} - [b\Sigma_i E_{yi}],$$
$$J_{yi} = \sigma_i E_{yi} + [b\Sigma_i E_{xi}].$$

$$v_{px} = v\left[\frac{\Sigma_s\sigma_i - \Sigma_i\sigma_s}{\Sigma_t^2 + \sigma_t^2}\right]b,$$
$$v_{py} = v\left[\frac{\Sigma_i\Sigma_t + \sigma_i\sigma_t}{\Sigma_t^2 + \sigma_t^2}\right],$$

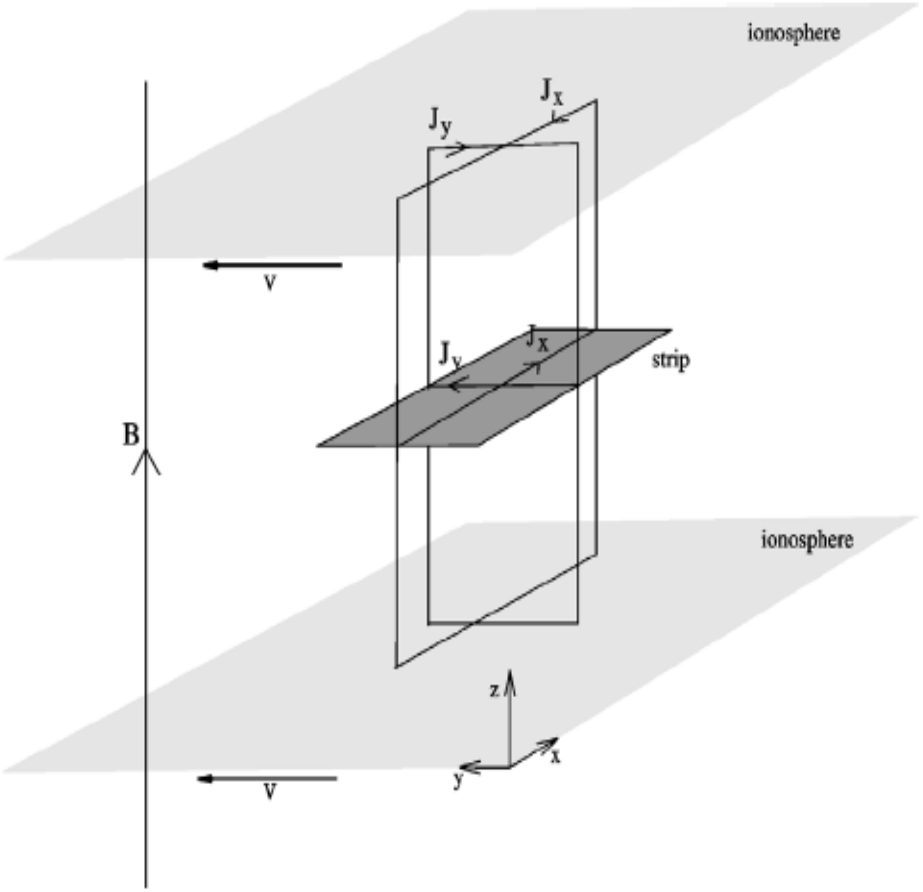

Farmer and Goldreich (2005)

Limitation to collective charging

- Surface electrostatic potential of a dust grain embedded in a dust cloud of number density (N) and Debye length (λ_D) is given by:

  $V = V_o(1+x)$ with

  $V_o = Q/a$ (a=grain radius)

  $x = 4\pi Na\lambda_D^2 e^{-R/\lambda_D} a(1+\lambda_D)$
- The corresponding charge is:

  $Q = Q_o/(1+x)$
- **The sum of many small potentials gives rise to an average plasma potential which is significantly different from zero.**

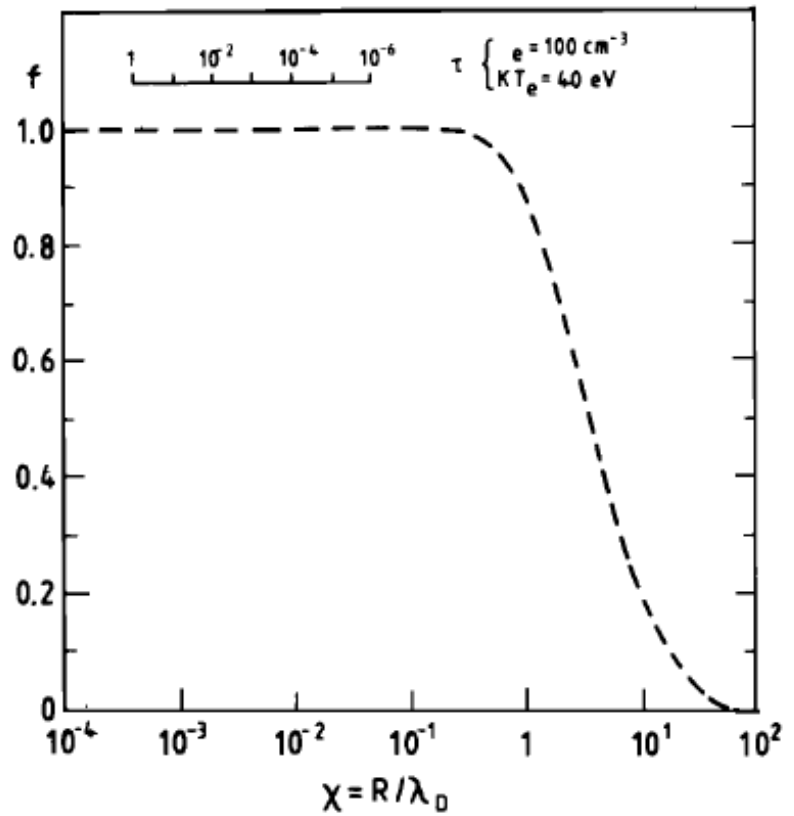

Fig. 2. The function f(z) described in the text. The insert indicates an equivalent optical depth scale corresponding to z for a plasma with n = 10^2 cm^{-3} and kT_e = 40 eV, assuming a height of 10 km.

Goertz and Ip (1984)

Ring-ionosphere coupling

- **The self-generation (i.e., floating plasma clouds) mechanism has problems.**
- **An alternative effect is to invoke external charging process, for example, by injection of energetic electron beams from the Saturnian ionosphere (Ip and Mendis, 1986).**
- **Saturn's upper ionosphere has strong diurnal variation because of precipitation of H2O and O2 molecules from the rings – as indicated by the thunderstorm-related SED (Saturn Electrostatic Discharge) emission.**

A new model is to generate Energetic electron beams by lightning.

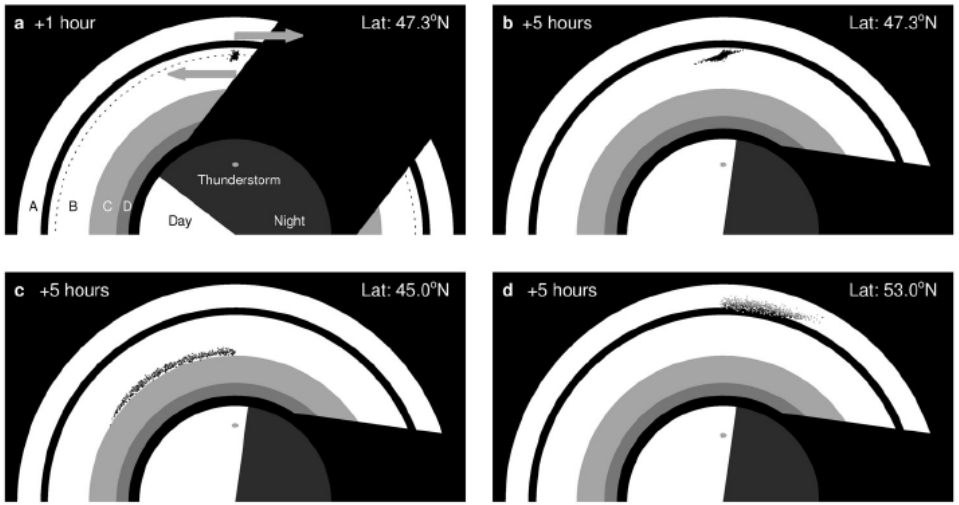

Jones et al., (2006)

Red sprites produced by atmospheric thunderstorms

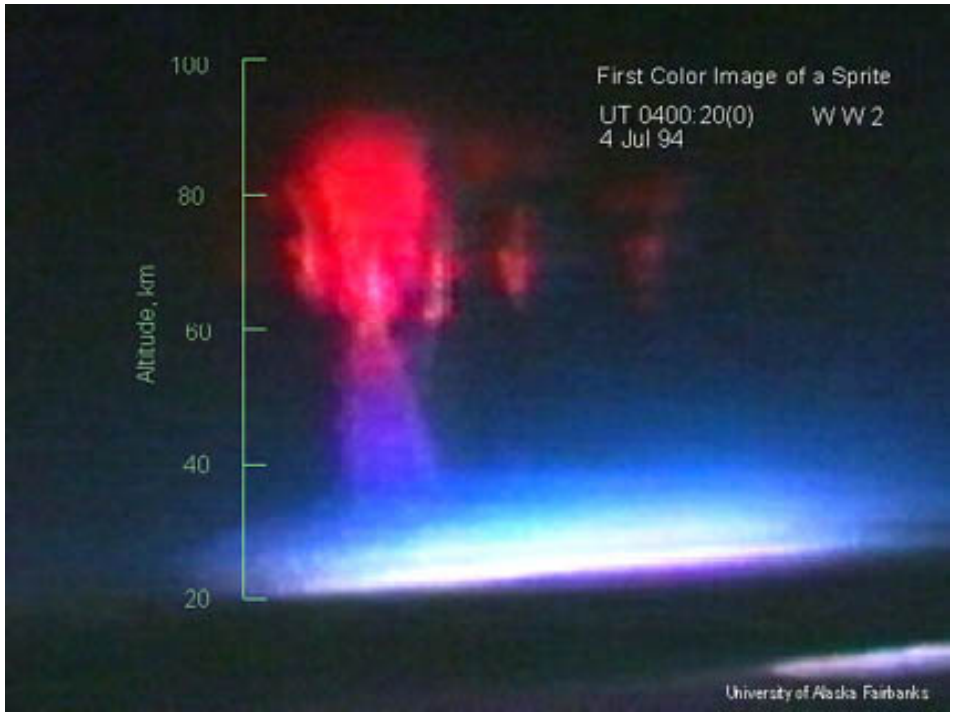

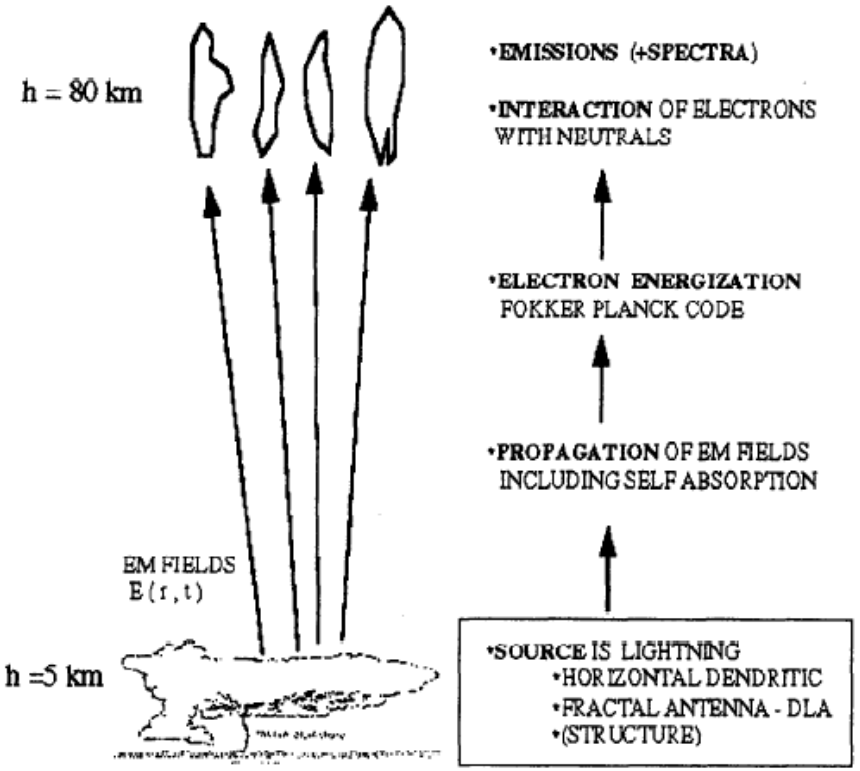

http://sprite.phys.ncku.edu.tw/new/news/0626_presss/
big_red_sprites_sentman_s.jpg

Valdivia et al. (1997)

Energetic electrons from lightning discharge

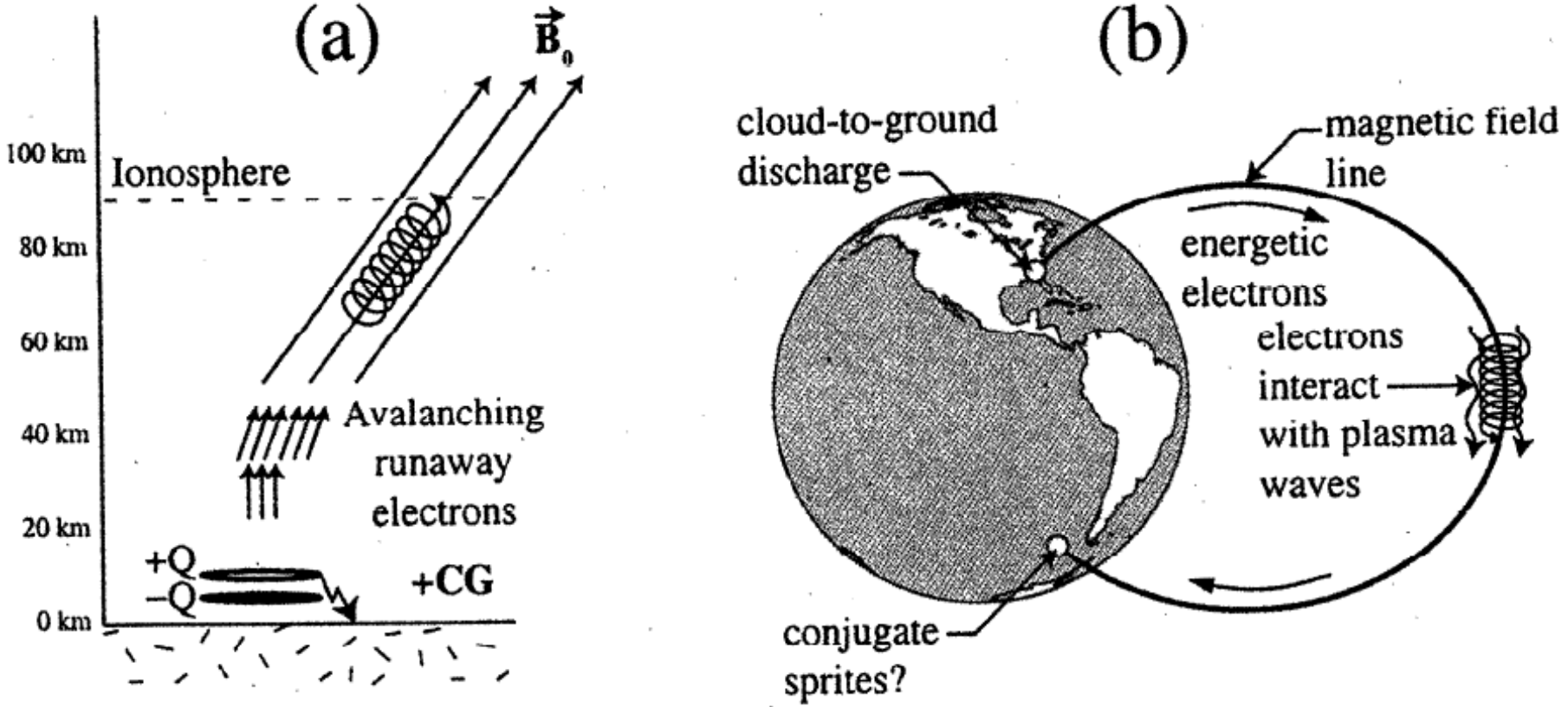

Lehtinen et al. (2001)

Lightning-induced ring spoke activity

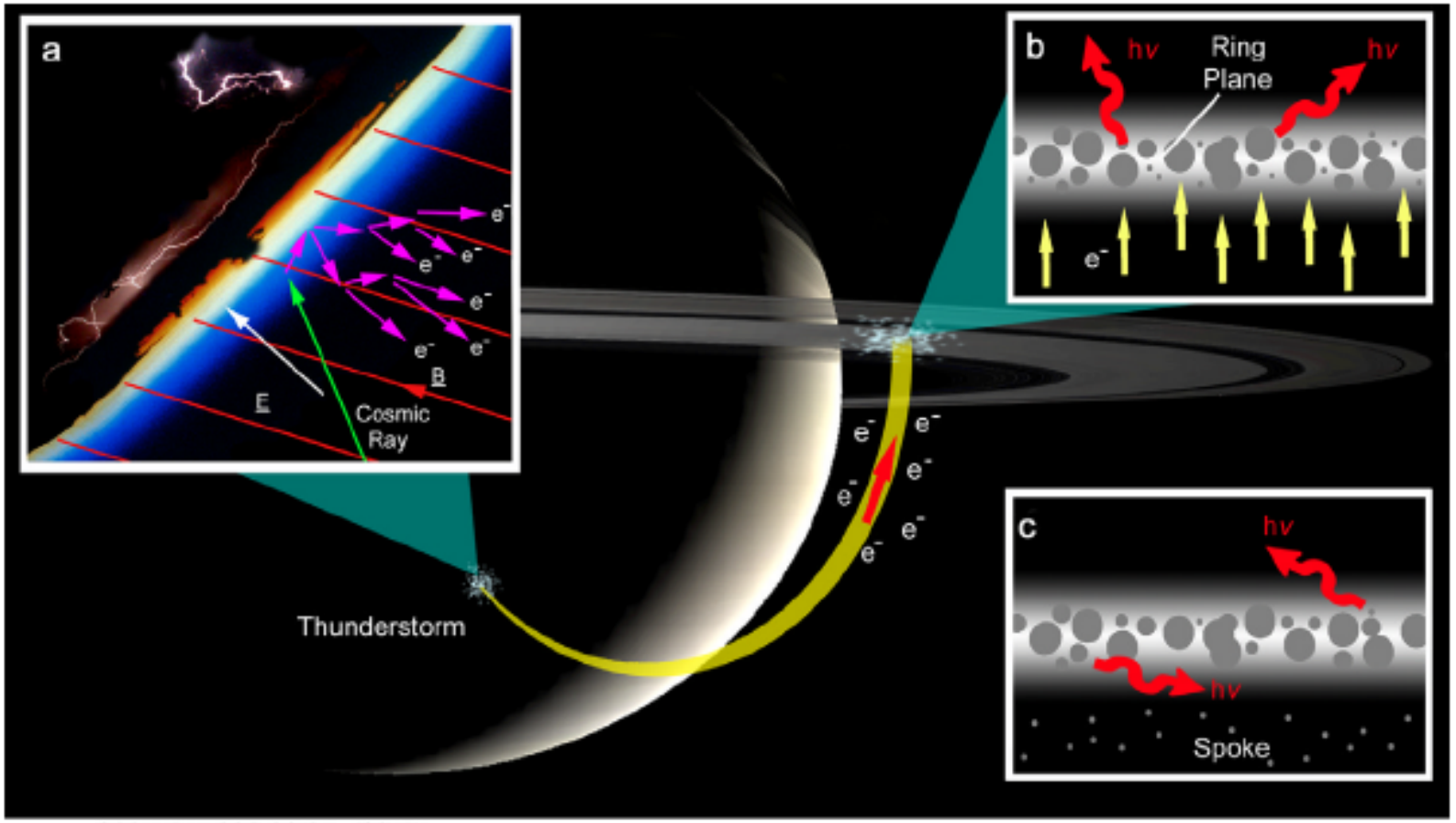

Jones et al., (2006)

Diurnal and seasonal effects of ring charging

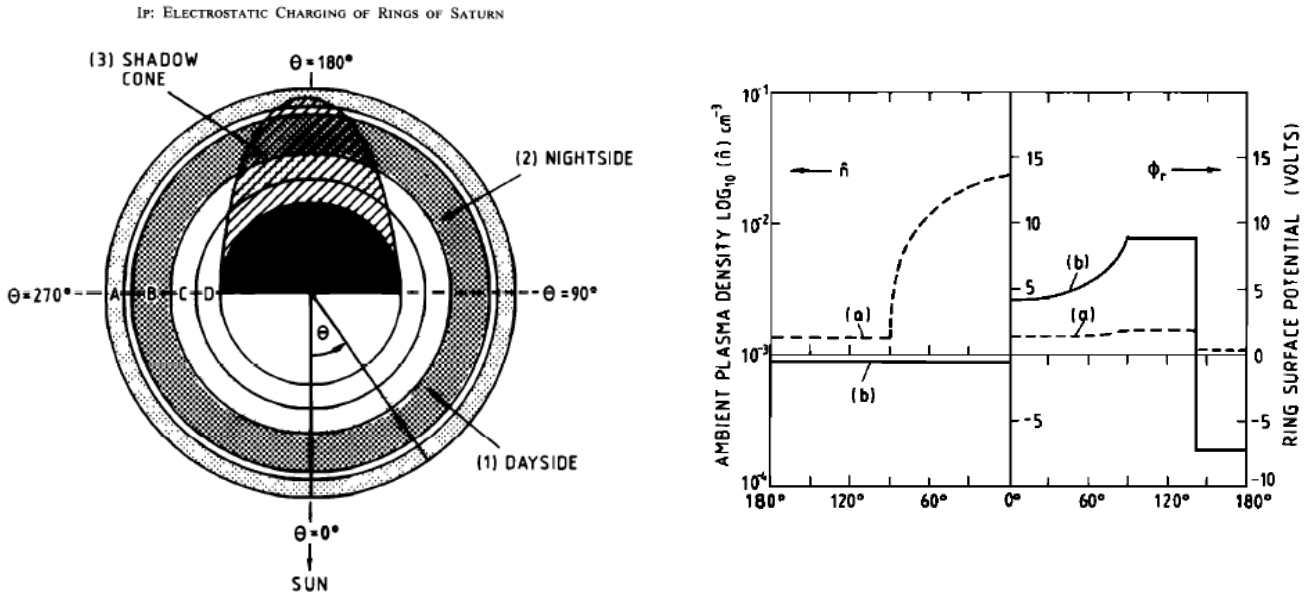

Ip (1984)

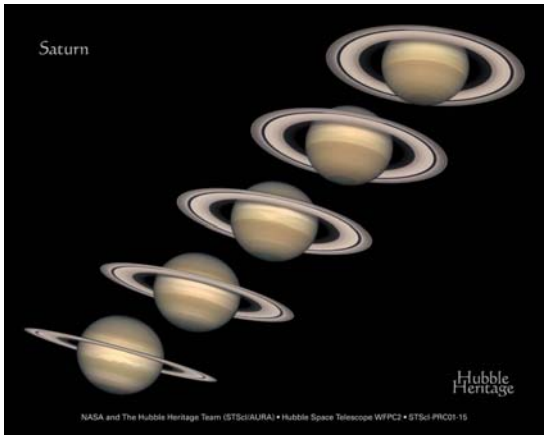

NASA

Farrell et al. (2006): Spoke formation most probable on the negatively charged side of the ring plane. This condition depends on the solar inclination angle.

Ring O_2 atmosphere and O_2^+ ionosphere

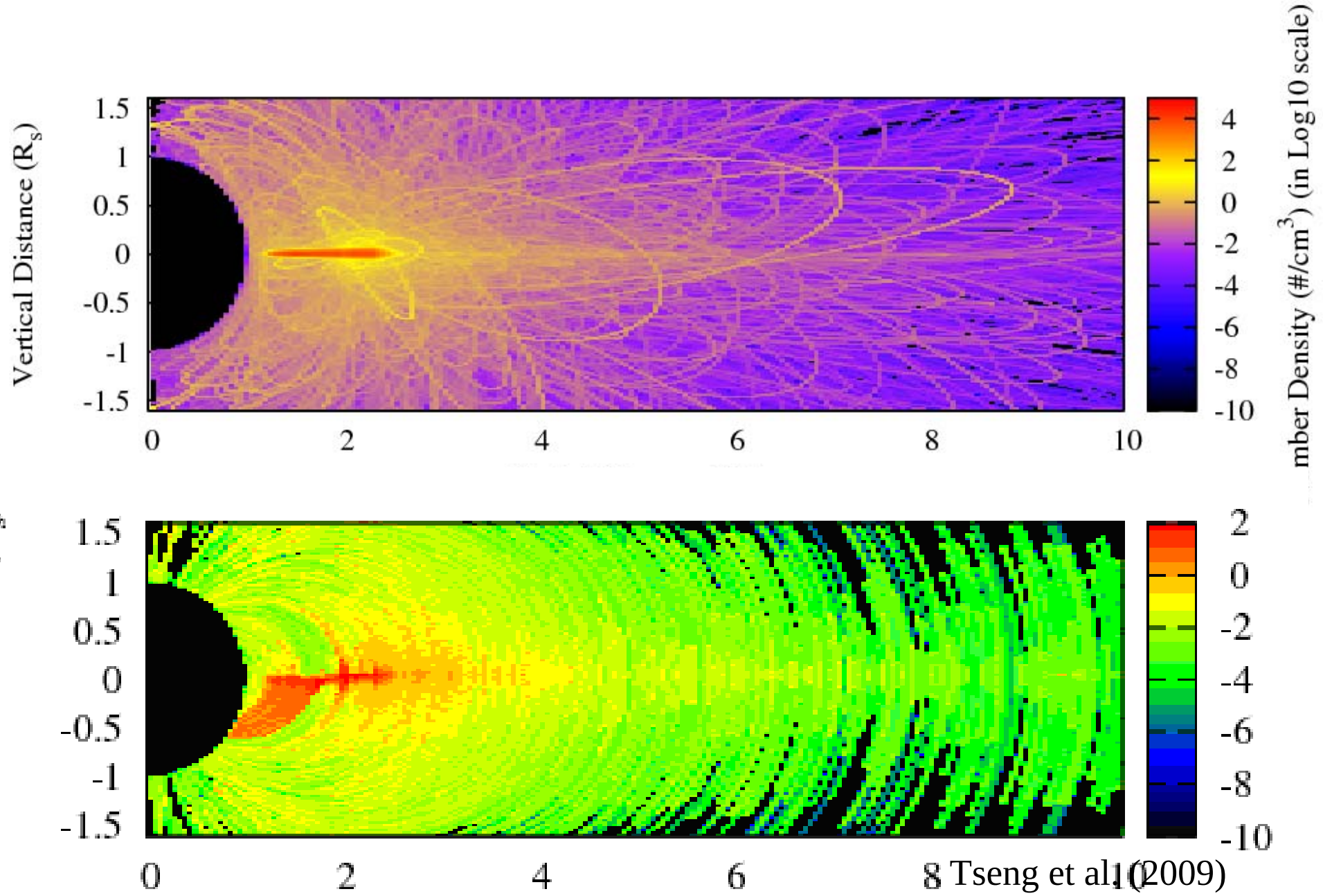

Tseng et al. (2009)

The shielding effect of an offset centered dipole field

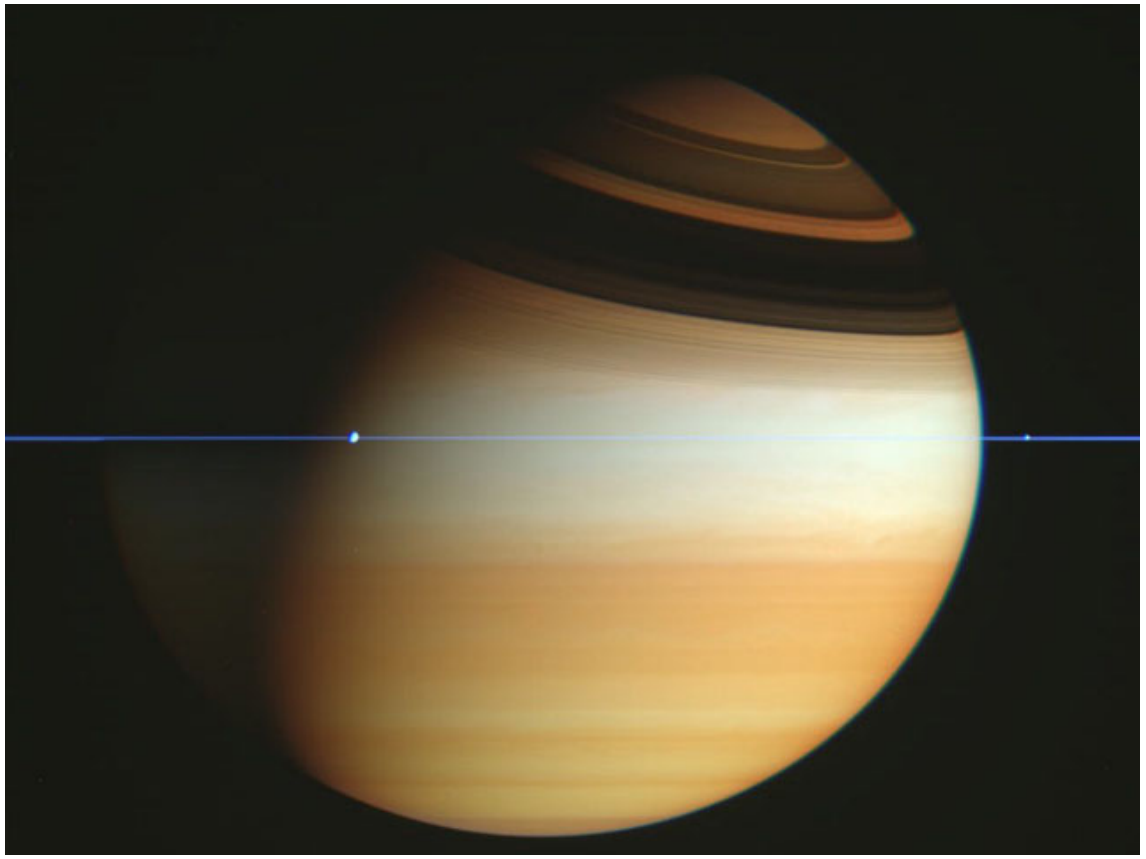

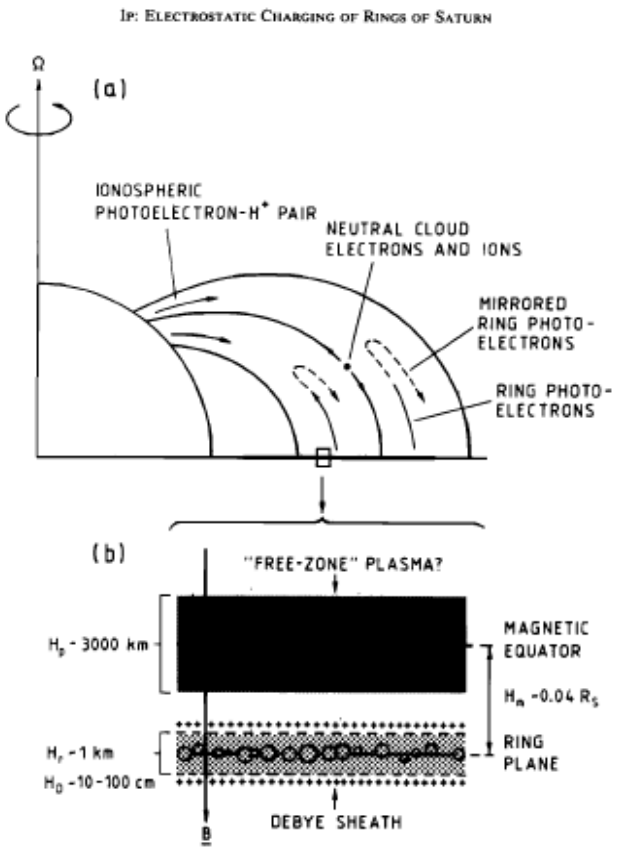

Ip (1984)

A Cassini view of the A, B and C rings

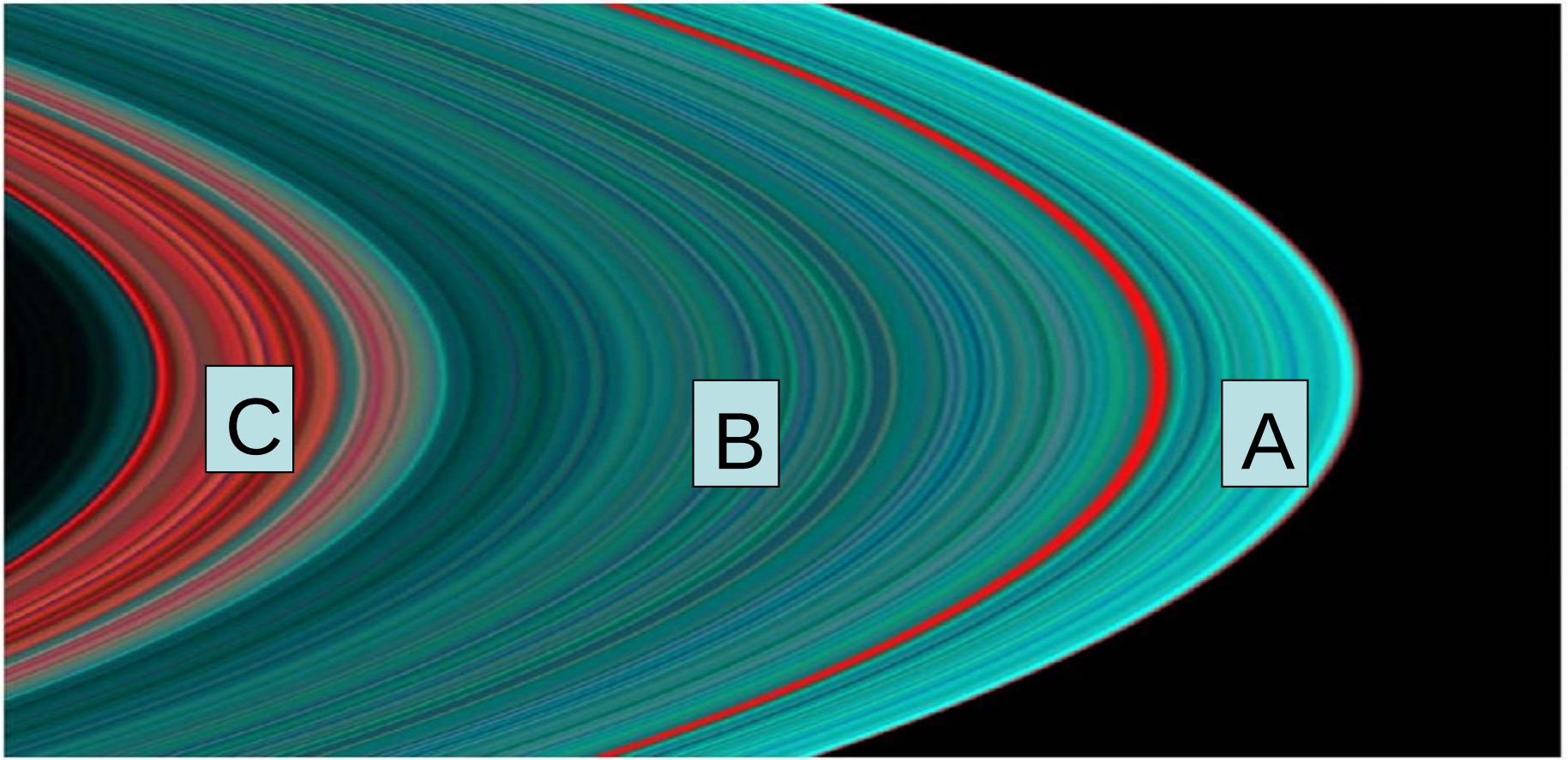

Saturnian ring opacity variation from Cassin UVSI

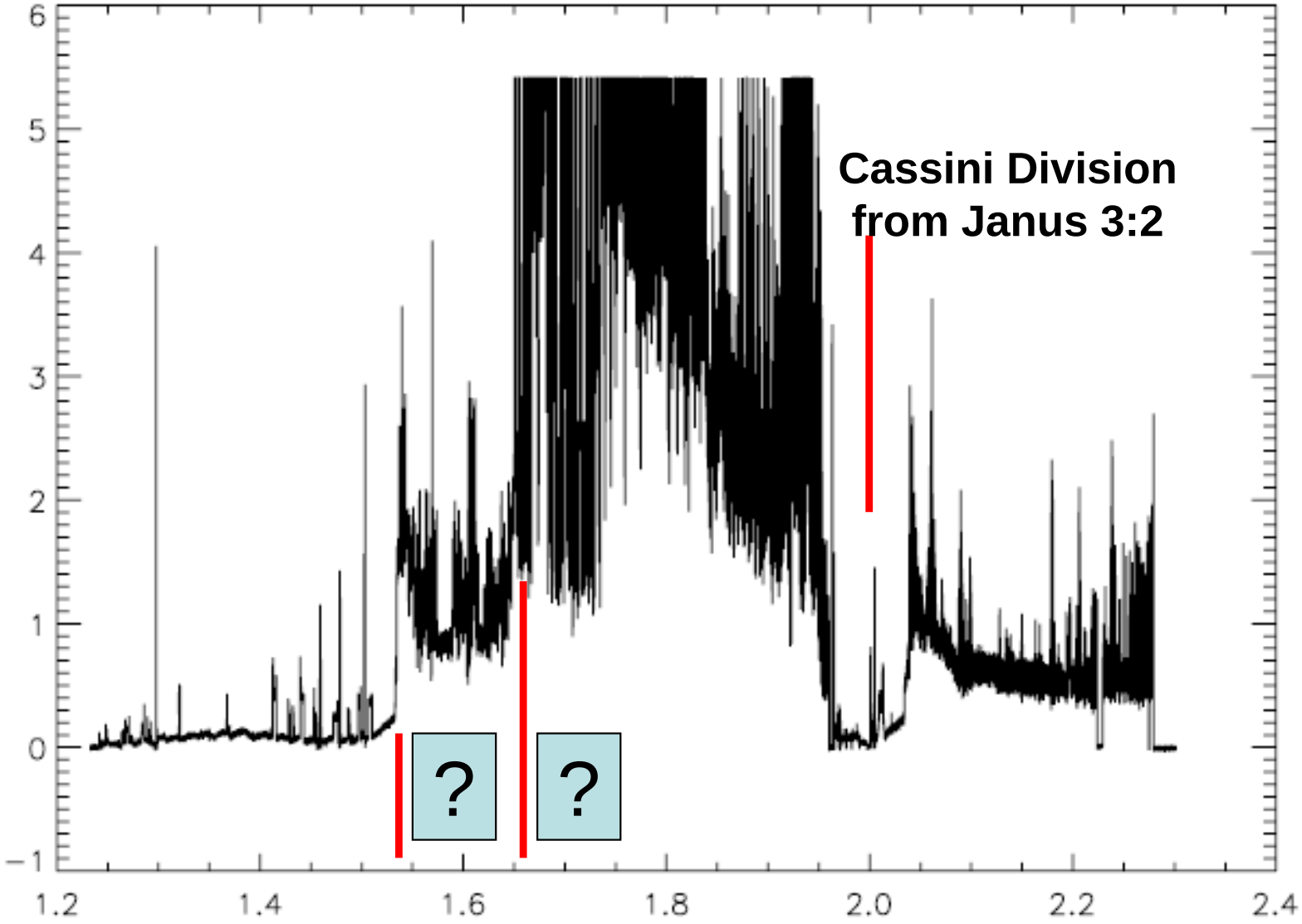

e.g., Northrop & Hill (1983)

Force equilibrium

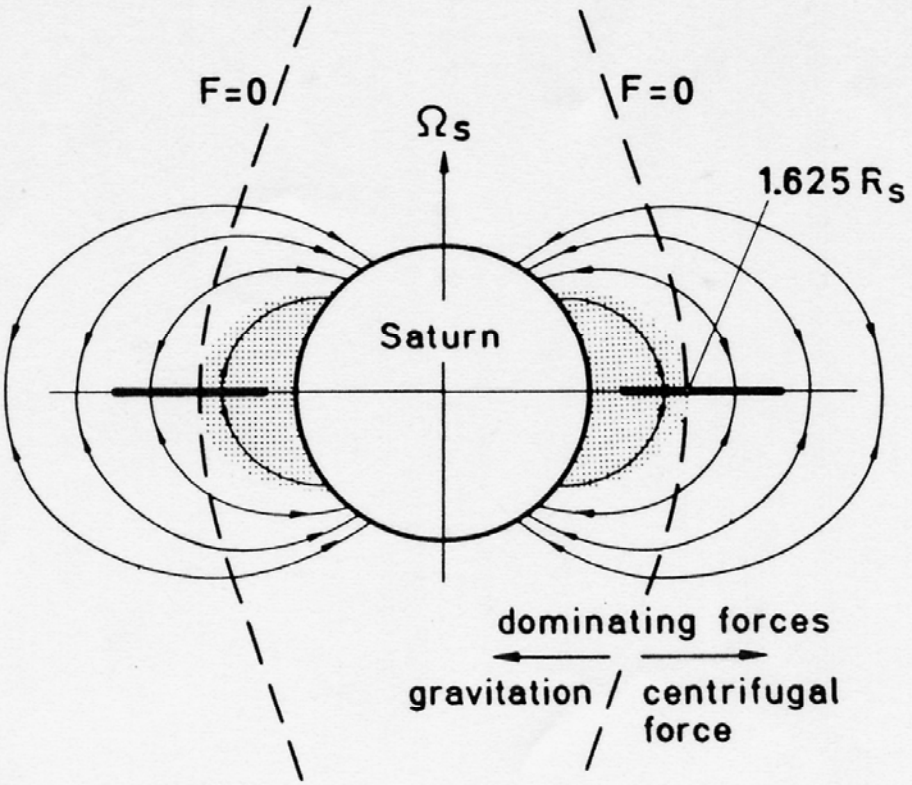

Fig. 9. Division of the rotating plasmasphere by the dashed curves $F = 0$ into two plasma regimes, according to the consideration of the balance of centrifugal and gravitational forces: (1) the upward siphon flow region denoted by the shaded area with equatorial distance $r \leqslant 1.6252\ R_S$; and (2) the equatorial confinement region with $r > 1.6252\ R_S$ (from Ip 1982).

Ip (1983)

End of Lecture 1

Lecture 2

January 7, 2009

The first generation of dusty plasma physicists

W. Ian Axford

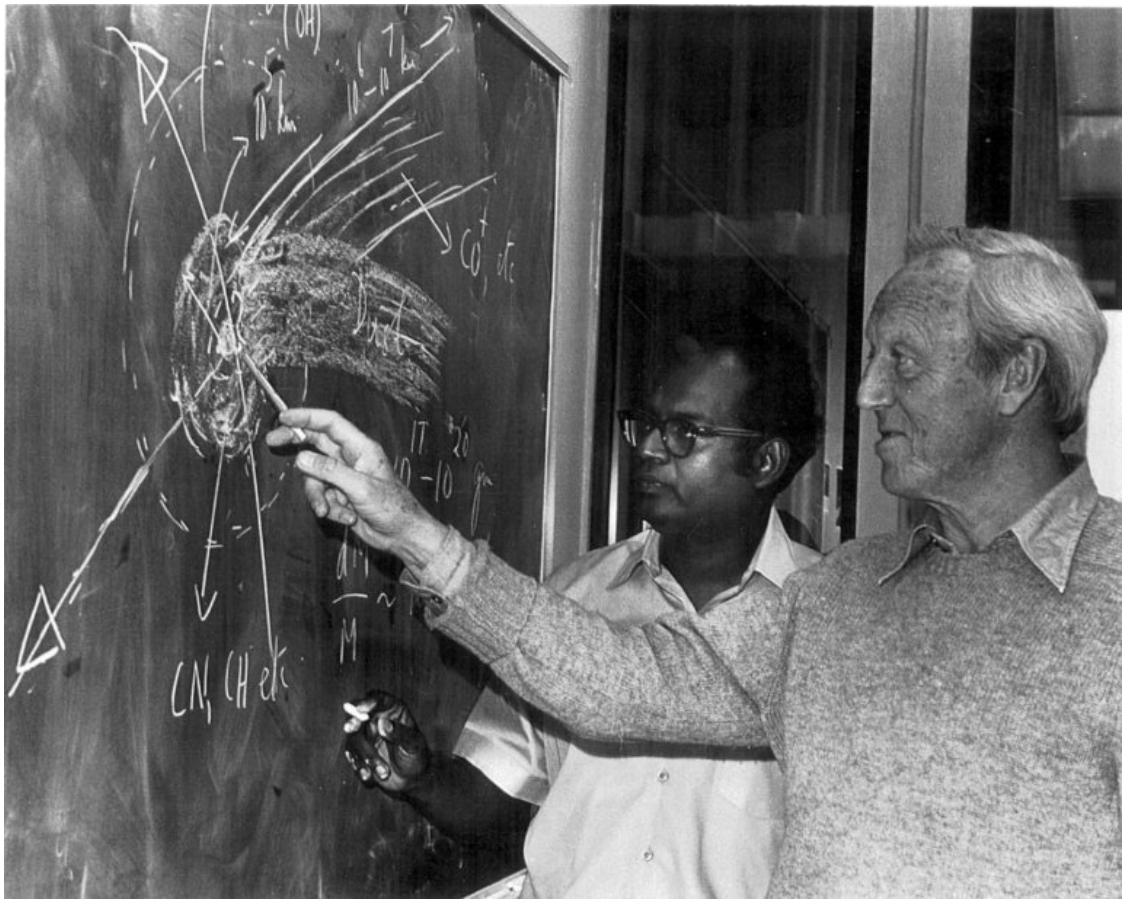

Asoka Mendis and Hannes Alfven

Annual Review of Earth and Planetary Science

SATELLITES AND MAGNETOSPHERES OF THE OUTER PLANETS

* 10029

D. A. Mendis and W. I. Axford
Department of Applied Physics and Information Science, University of California, San Diego, La Jolla, Caifornia 92037

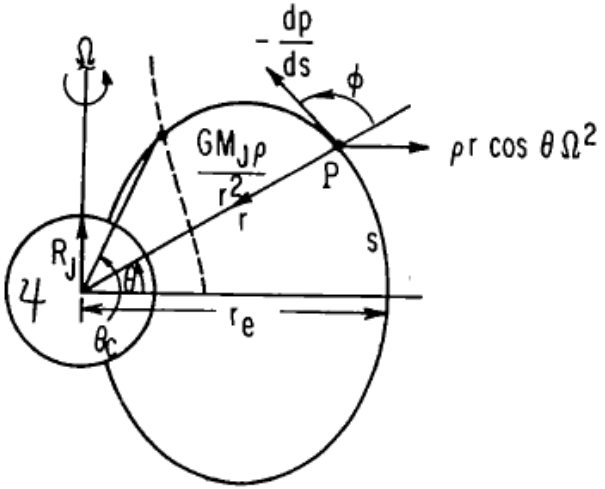

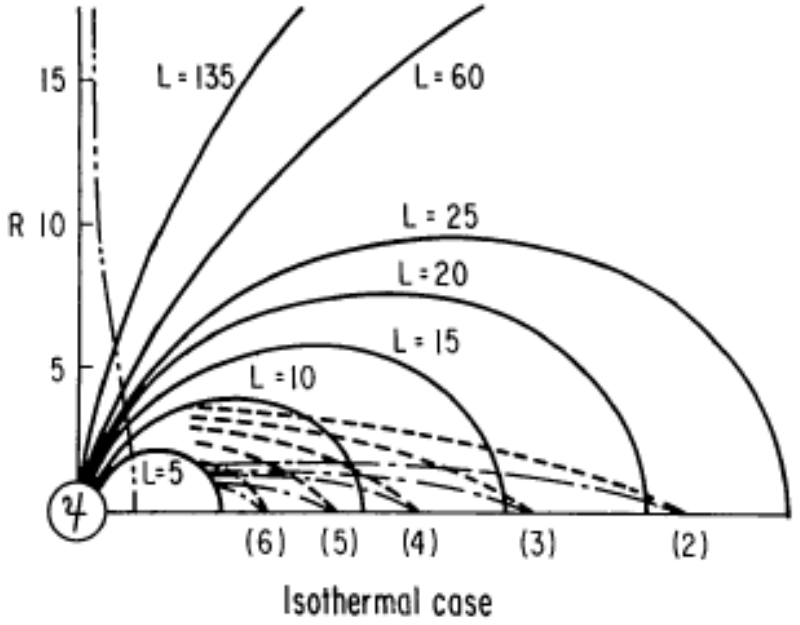

Mendis & Axford (1974)

Bottom-up model

Surface erosion mechanism of Iapetus

Meteoroids
~Ice sublimation

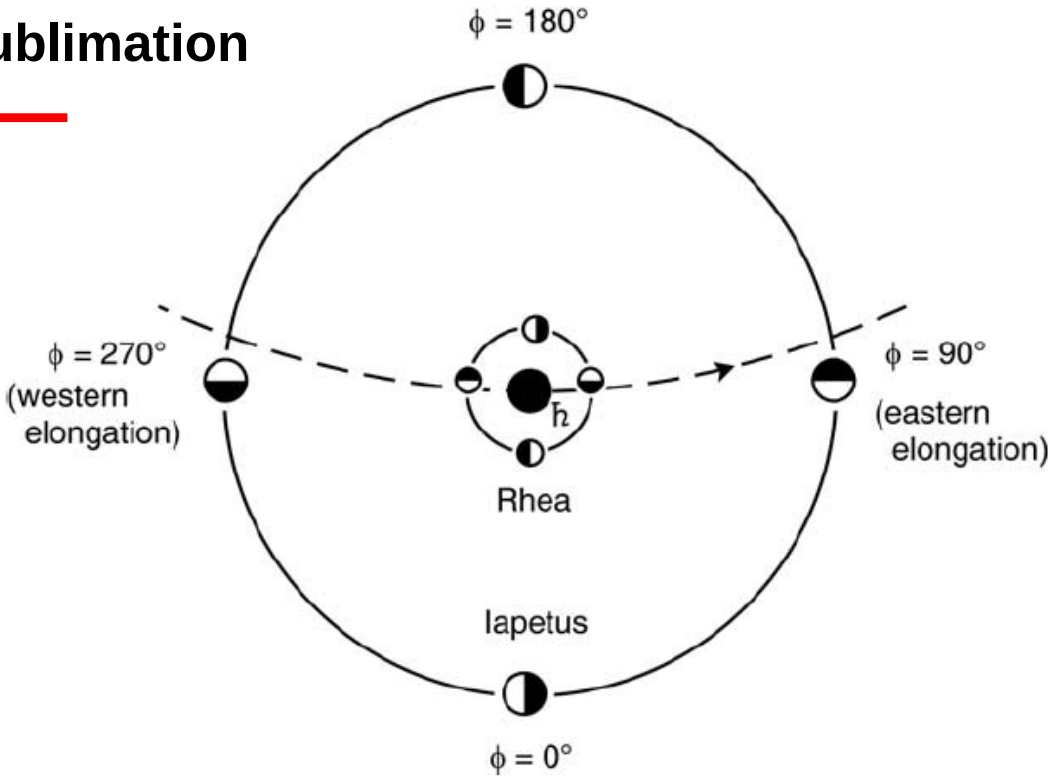

SATELLITES AND MAGNETOSPHERES OF THE OUTER PLANETS 459

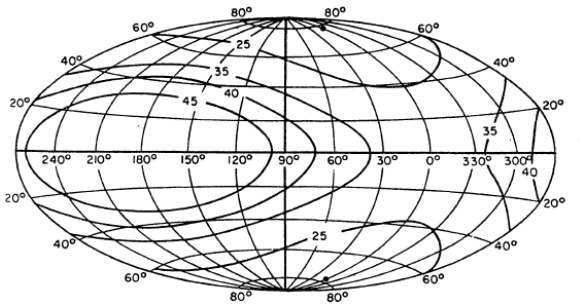

Figure 14 Lines of constant erosion rate on the complete sphere of Iapetus. Numbers are the factors by which the arrival rate of meteoroidal mass in a system at rest relative to the Sun must be multiplied to give the rate of material erosion. The center of the leading hemisphere of Iapetus in orbit about Saturn is at 180°, the trailing at 0° (Cook & Franklin, 15).

Mendis & Axford (1974)

Cassini view of the Saturnian ring system

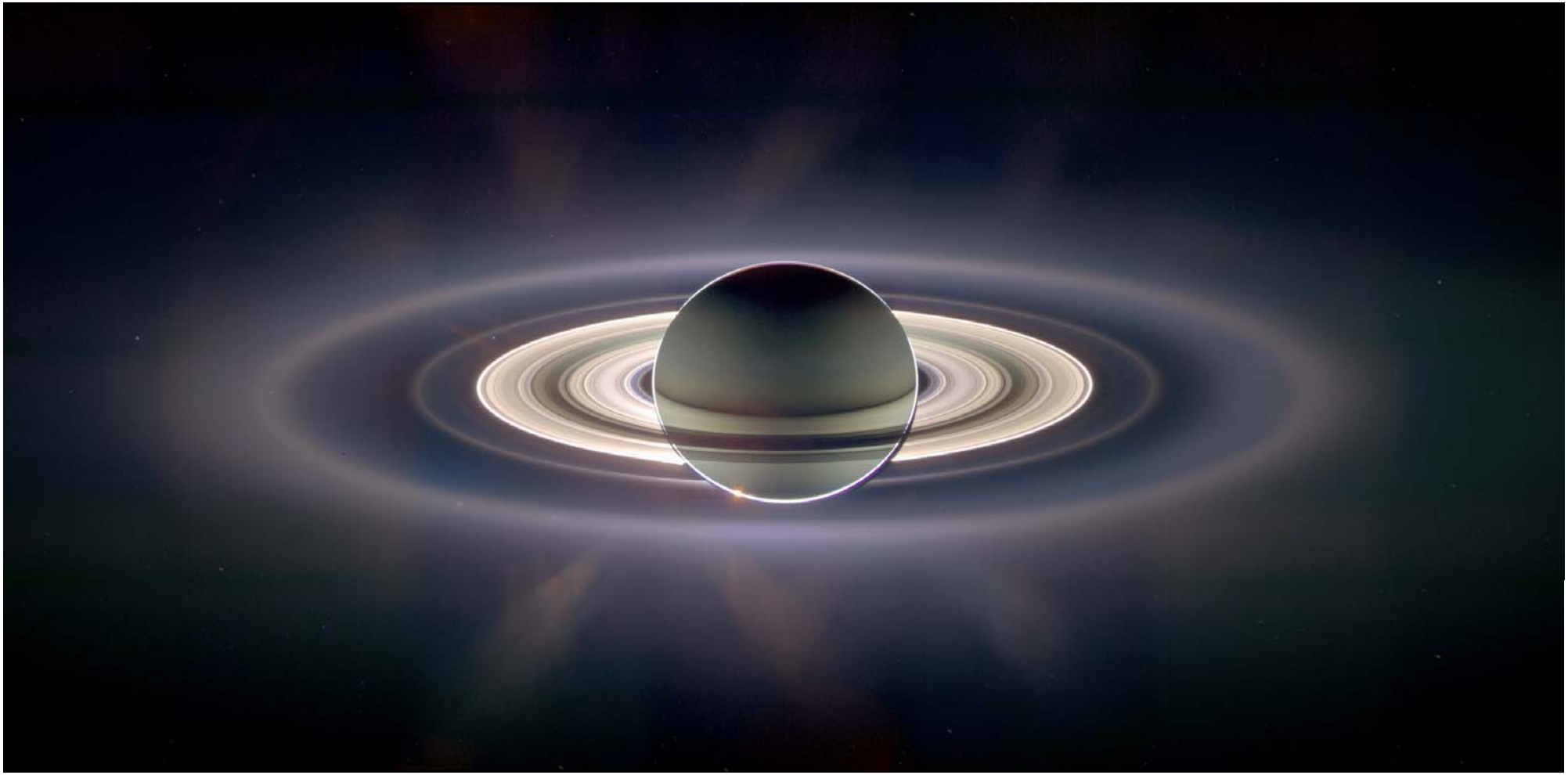

Dynamics of Saturn's E-ring dust

- $R_E = 4\ R_s$
- $N(O^+) = 100\ (R_E/a)^4$
- $T(O^+) = 100$ eV
- Perturbation effects:

  Electrostatic charging

  Planetary oblateness (J2)

  Radiation pressure force

  Plasma drag force
- Ion sputtering time ~ 50 years for 1 μm icy grains

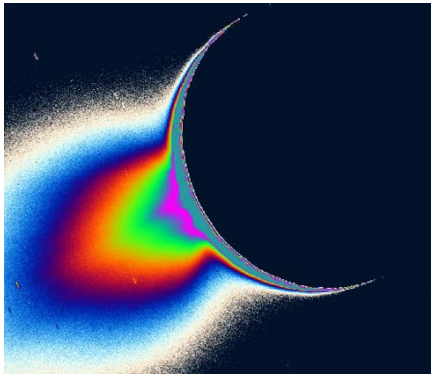

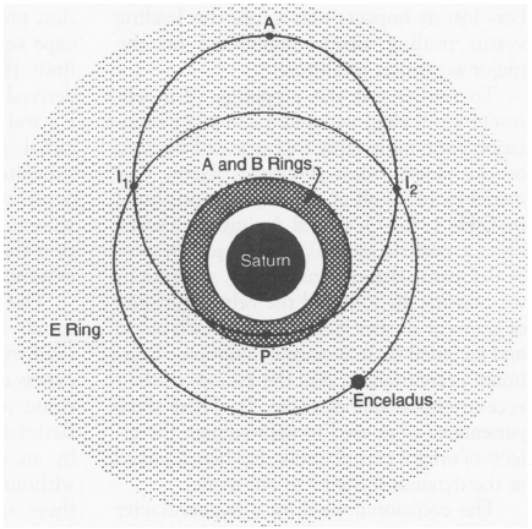

Hamilton and Burns (1994)

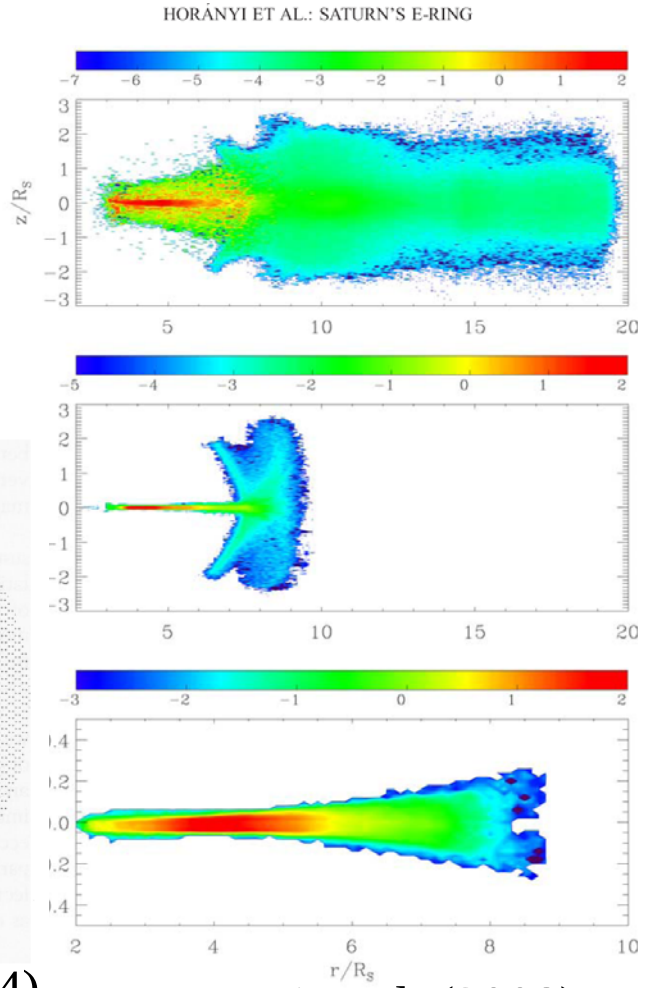

Horanyi et al. (2008)

Spoke formation on Saturn’s B ring

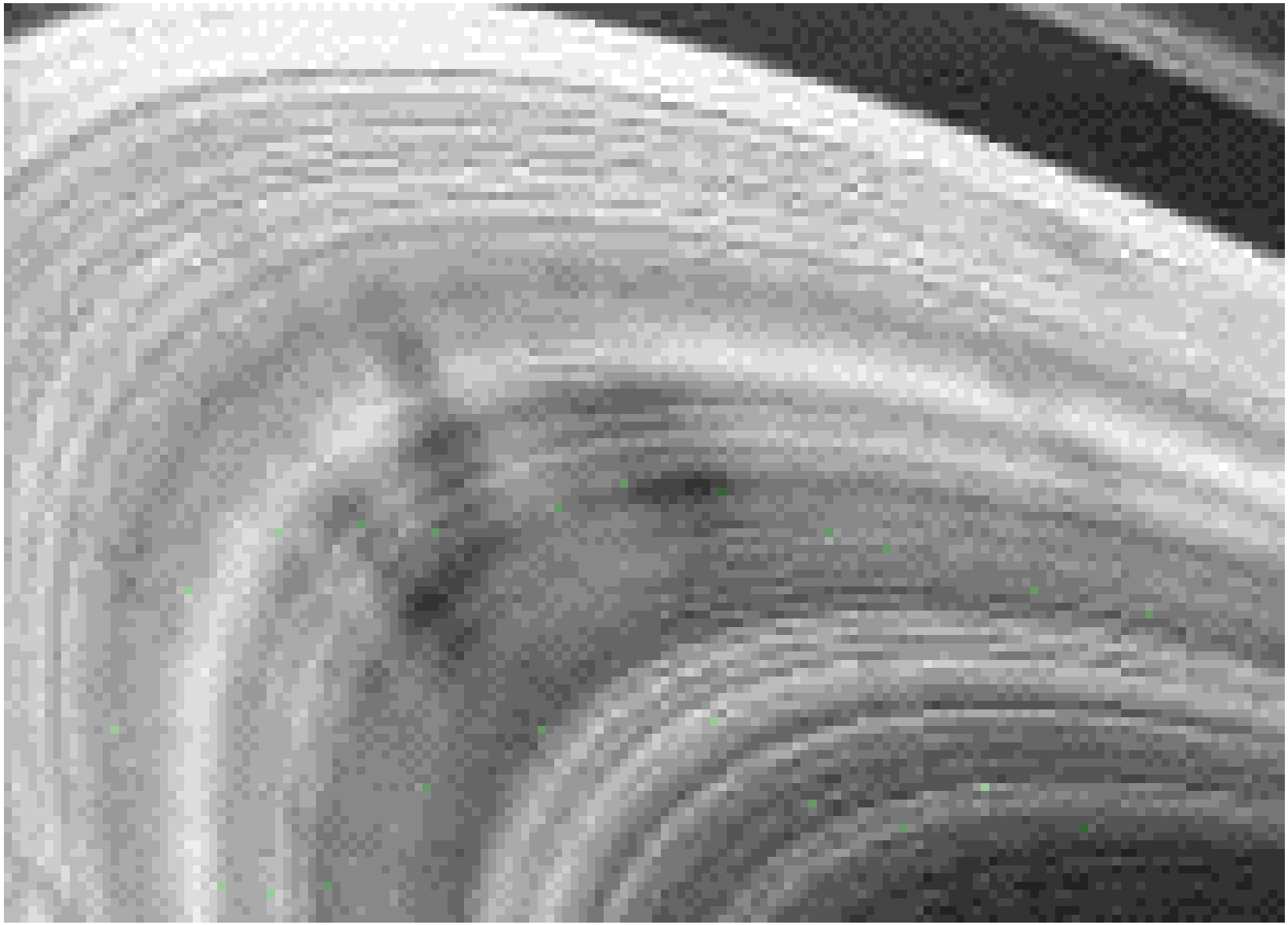

Moving plasma cloud model vs. lightning-induced electron beam model

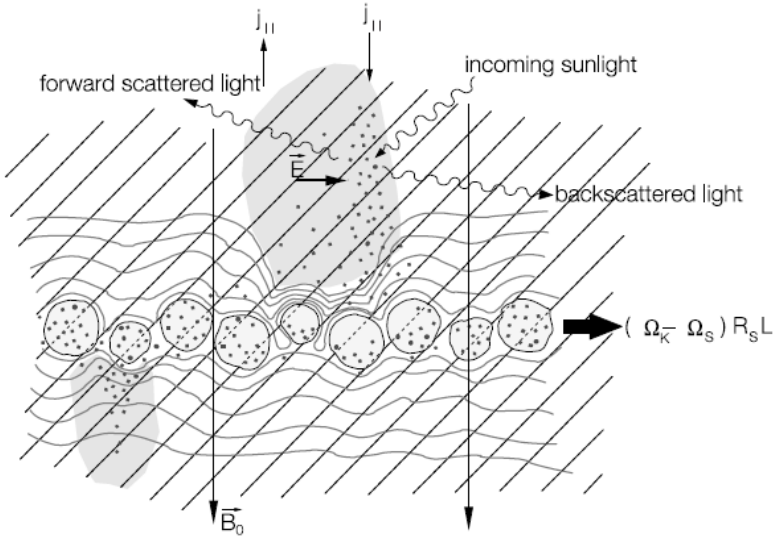

Goertz and Morfill (1983)

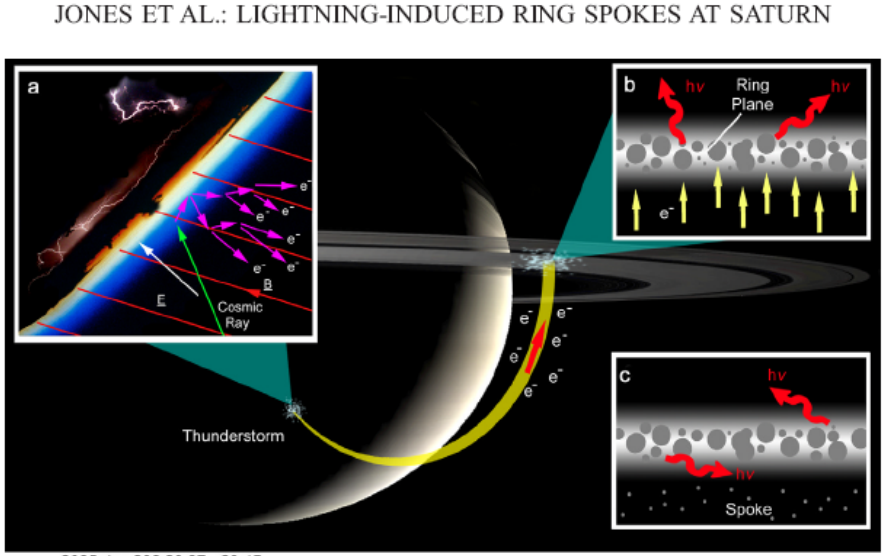

Jones et al. (2006)

Diurnal and seasonal effects of ring charging

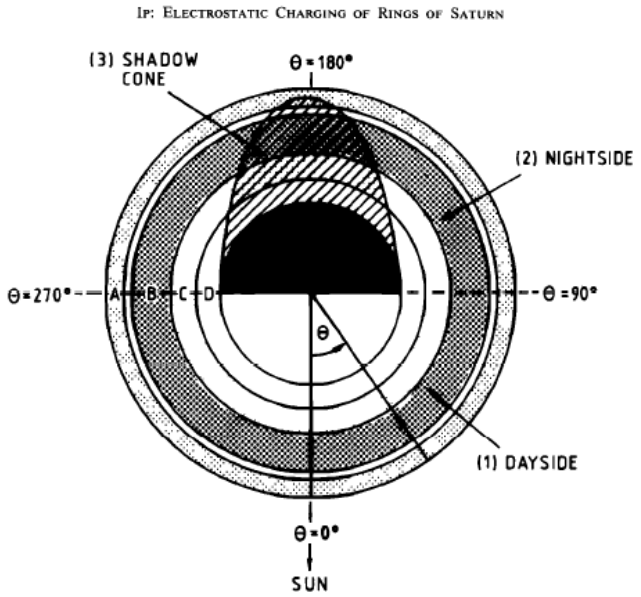

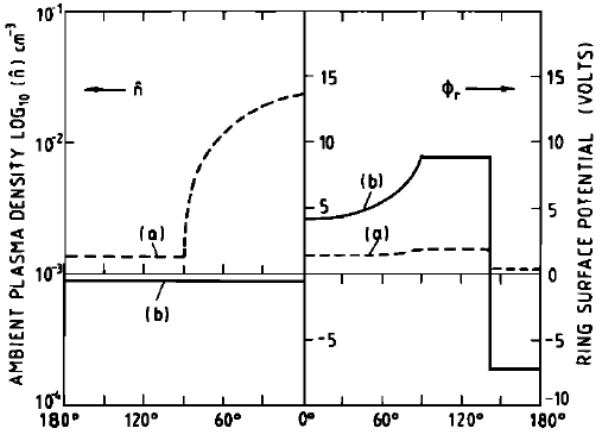

Ip (1984)

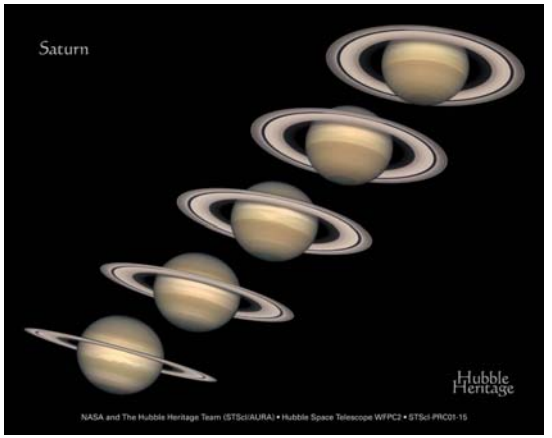

NASA

Farrell et al. (2006): Spoke formation most probable on the negatively charged side of the ring plane. This condition depends on the solar inclination angle.

Force equilibrium of charged small grains

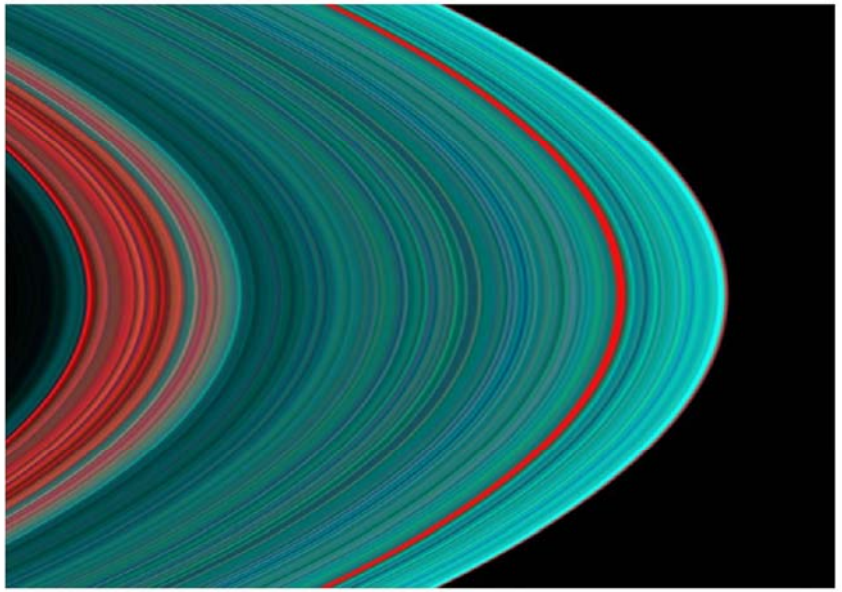

C B A

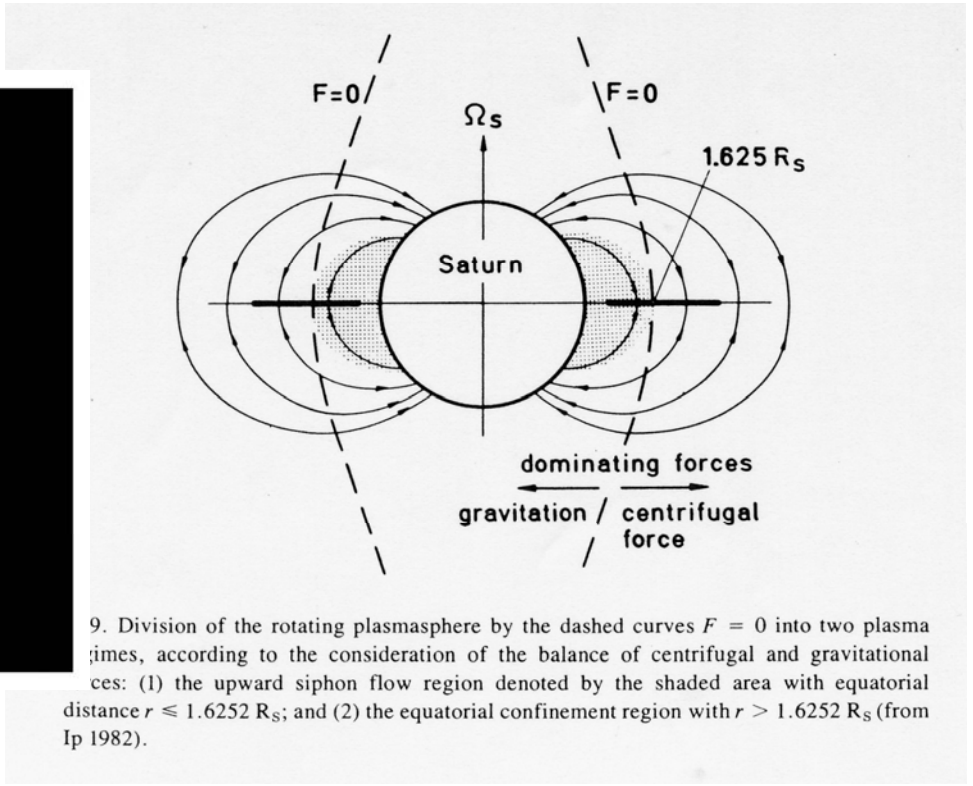

9. Division of the rotating plasmasphere by the dashed curves $F = 0$ into two plasma ;imes, according to the consideration of the balance of centrifugal and gravitational ces: (1) the upward siphon flow region denoted by the shaded area with equatorial distance $r \leq 1.6252\ R_S$; and (2) the equatorial confinement region with $r > 1.6252\ R_S$ (from Ip 1982).

Ip (1983)

3. The lunar dust

Lunar Horizontal Glow

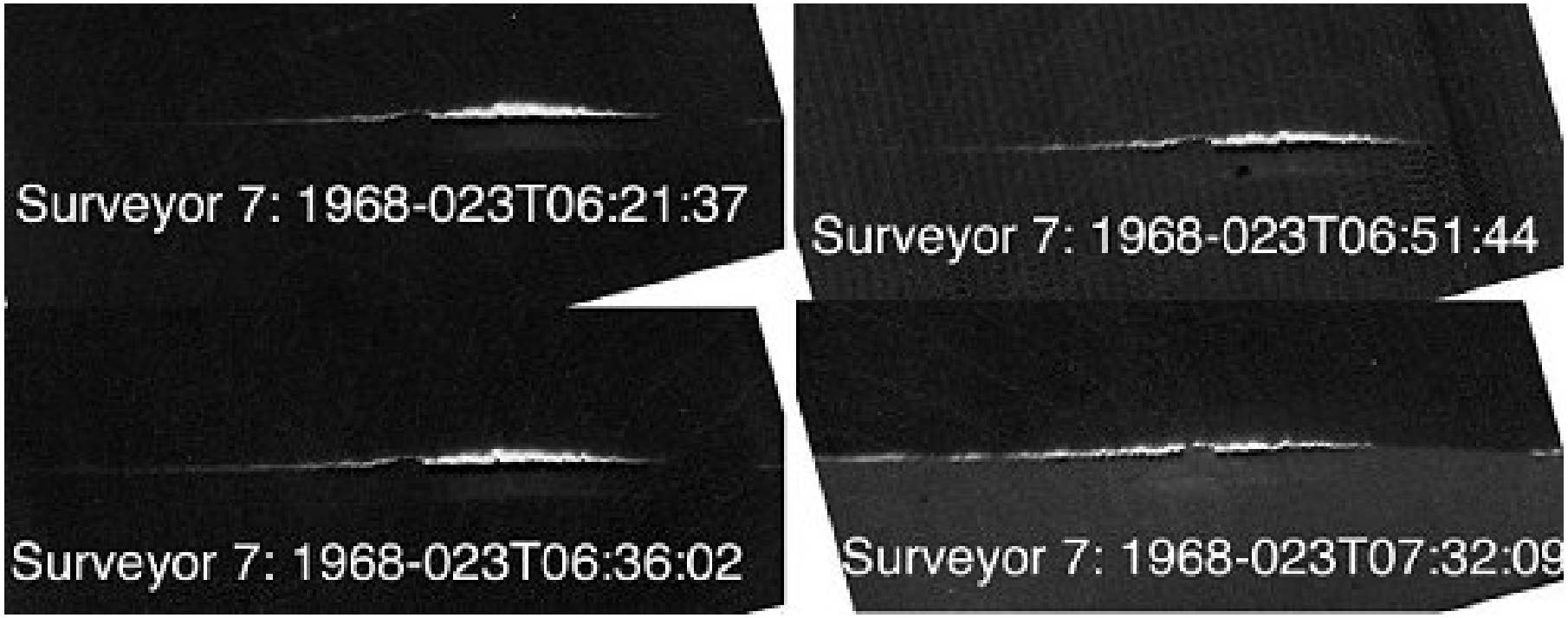

Lunar horizontal glow drawn by Apollo 17 astronauts

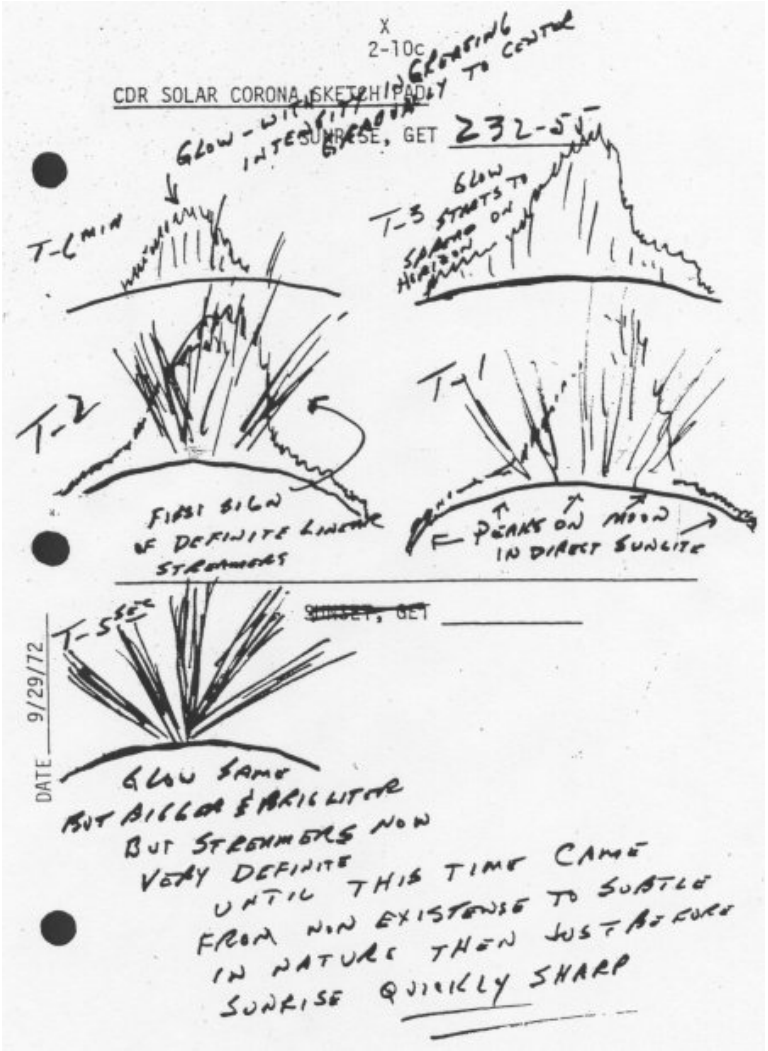

Moon-Solar Wind Interaction

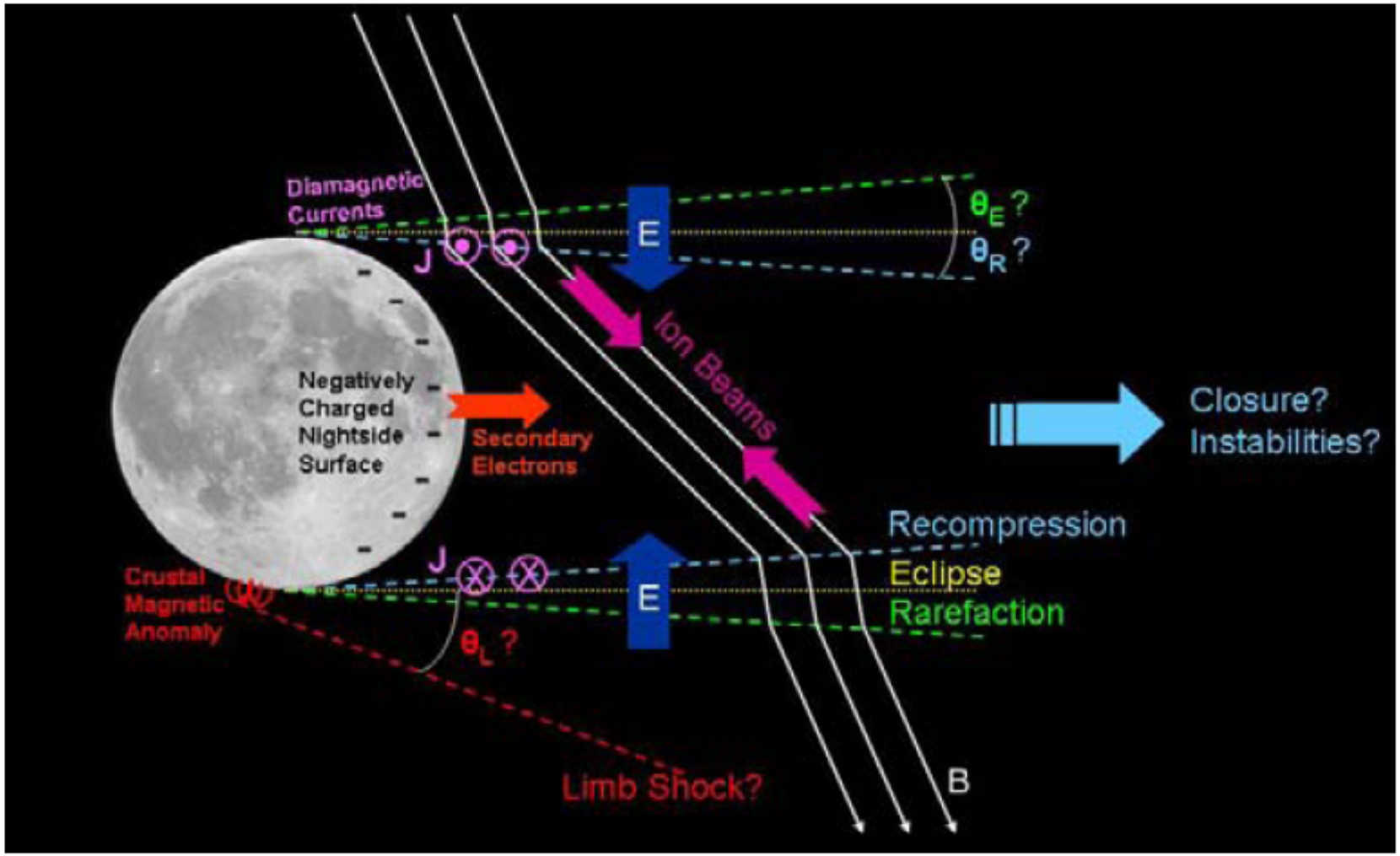

Electrostatic charging of lunar surface

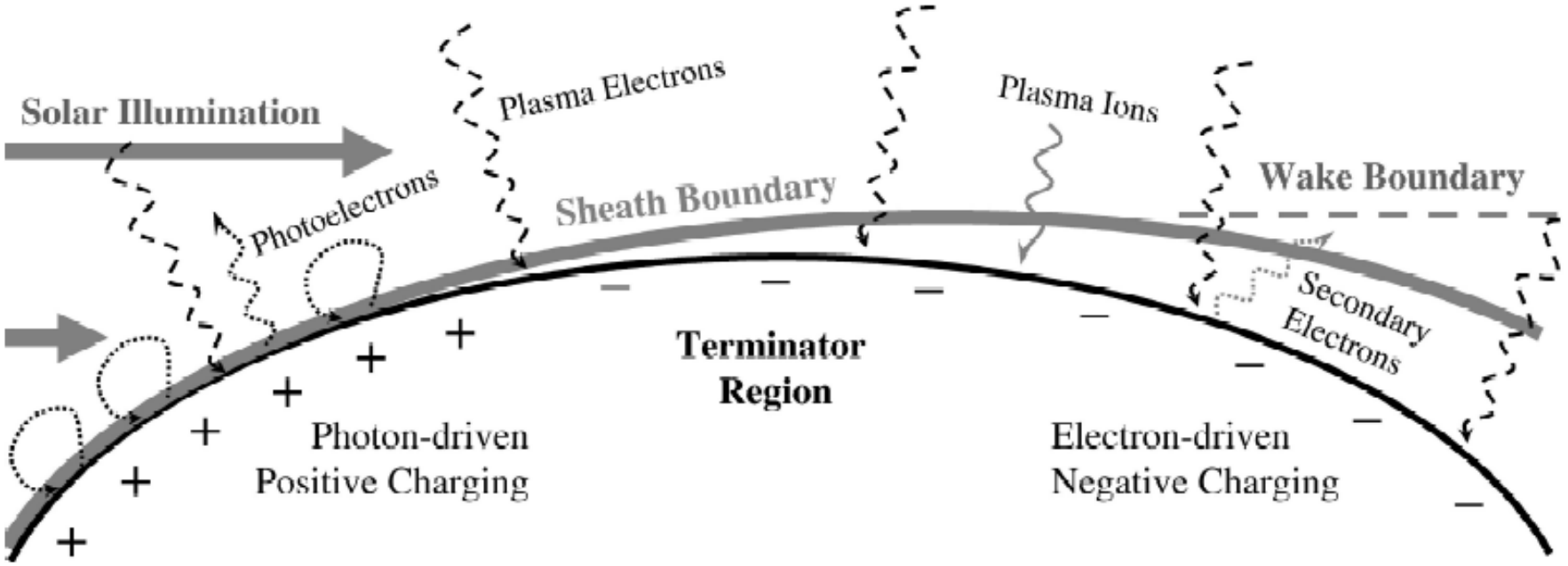

Figure 1. Schematic of the lunar electrostatic environment in the solar wind (not to scale).

roc. 'Dust in Planetary Systems', Kauai, Hawaii, USA.
6--30 September 2005 (ESA SP-643, January 2007)

Stubbs et al. 2005

Electrostatic Charging of dust grains

- Ambient plasma electron flux (I_e)
- Ambient plasma ion flux (I_i)
- Photoelectron flux (I_p)

The charging equation

- Ion and electron currents(I_i^+ and I_e^+) for surface potential Φ_s>0(Mendis et al. ,1981):

$$I_i^+ = \tfrac{1}{2} neV\cos\theta\left[1+\mathrm{crf}\,(X_i)+\left(\pi^{1/2}U_i\right)^{-1}\exp\left(-X_i^2\right)\right]$$

$$I_e^+ = \frac{fne\alpha_e}{2\pi^{1/2}}\left\{\exp\left(-U_e^2\right)+\pi^{1/2}U_e\left[1+\mathrm{erf}\,(U_e)\right]\right\},$$

With

$$\alpha_i = \left(\frac{2kT_i}{m_i}\right)^{1/2}, \quad \alpha_e = \left(\frac{2kT_e}{m_e}\right)^{1/2},$$

$$U_i = \frac{V\cos\theta}{\alpha_i}, \qquad U_e = \frac{V\cos\theta}{\alpha_e},$$

$$X_i = U_i - \left(\frac{e\phi_s}{kT_i}\right)^{1/2}.$$

- The photoelectron current I_p^+ is

$$I_p^+ = I_0\cos\theta\exp\left(\frac{-e\phi_s}{kT_p}\right),$$

$$I_0 = \frac{2.5\times10^{10}e\chi}{d^2(\mathrm{AU})},$$

where kT_p =2 eV and X=0.1.

For Φ_s <0,

$$I_i^- = \frac{fneV\cos\theta}{2}\left[1+\mathrm{erf}\,(U_i)+\left(\pi^{1/2}U_i\right)^{-1}\exp\left(-U_i^2\right)\right]$$

$$I_e^- = \frac{ne\alpha_e}{2\pi^{1/2}}\left\{\exp\left(-X_e^2\right)+\pi^{1/2}U_e\left[1+\mathrm{erf}(X_e)\right]\right\}$$

$$I_p^- = I_0\cos\theta,$$

$$X_e = U_e - \left(\frac{-e\phi_s}{kT_e}\right)^{1/2}$$

$\mathbf{I_i - I_e + I_p = 0 \rightarrow \Phi_s = ?}$

Electrostatic Fields

- Solar wind plasma

$n_{sw}(d)=5*d^{-2}\ cm^{-3}$

$T_e(d)=1.5*10^5*d^{-2/3}\ k$

$T_i(d)=10^5*d^{-2/3}\ k$

with d in AU

Debye length:

$L_{sw} = 6.9(T_e/n_{sw})^{1/2}$ cm

=38 m at d= 1 AU

- Photoelectrons

Solar photon flux($\varepsilon \geqq$ 8ev)

$F=4.5*10^{12}*d^{-2}$ photon $cm^{-2}\cdot s^{-1}$

Photoemission flux:

$I_{pe}= \int_0^{200nm} F(\lambda)X(\lambda)d\lambda$

$=2.8*10^9*d^{-2}$ electrons/cm^2/s

(Willis et al.,1973)

Photo electron energy =kT_{pe}~2 ev

Photo electron density

$n_{pe}= 2I_{pe}/V_{pe}=70\ cm^{-3}$

$L_{pe}=6.9(T_{pe}/n_{pe})^{1/2}=3.8$ m

Photoelectron density in the Debye Sheath

- $n_{pe}=n_{pe}(0)\,[1+z/\sqrt{2}\,\lambda_D]^{-2}$

with $\lambda_D = L_{pe}$

(Grard and Tunaley, 1971)

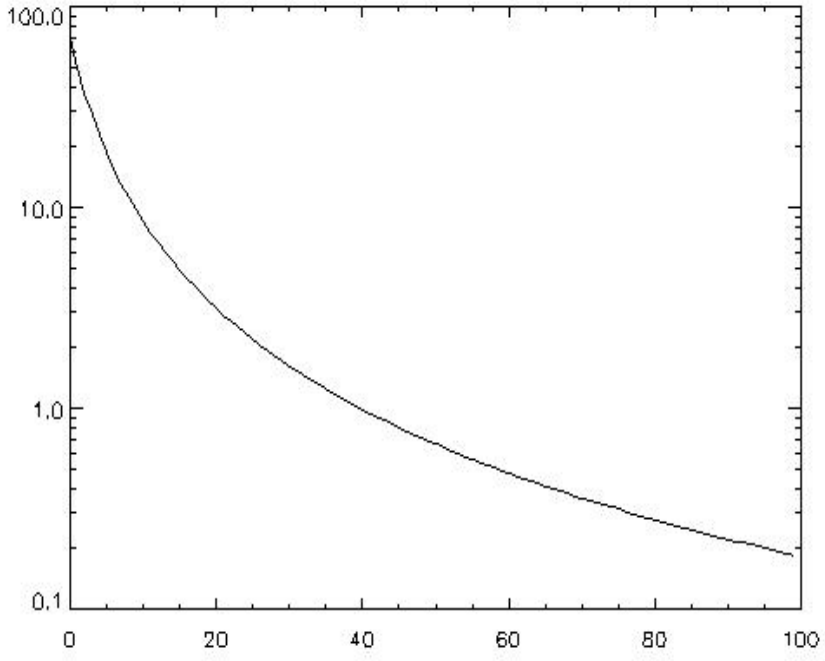

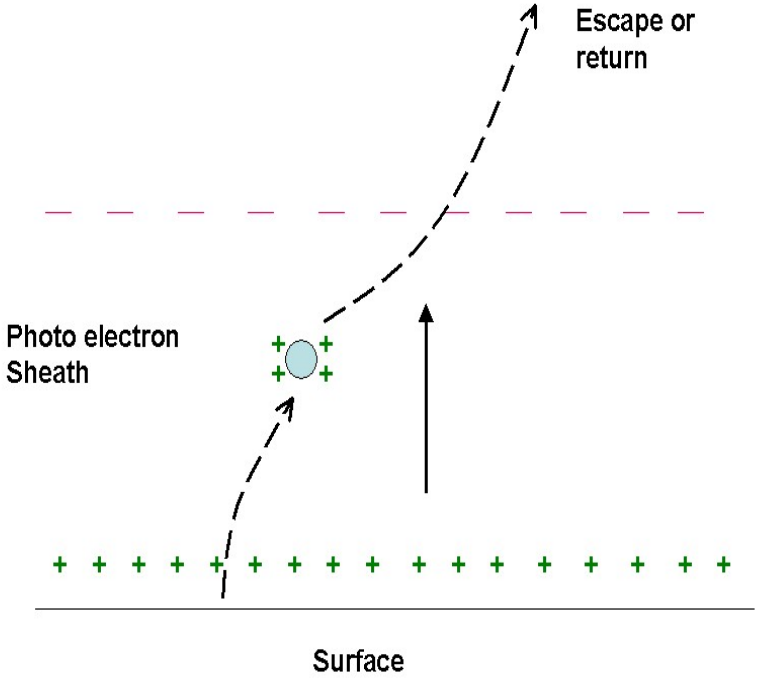

Dust levitation

Global Sunlit side charging

E ~ Φ / L_{pe} ~10-20 V/m

- Terminator Supercharging

E~1-3 KV/cm

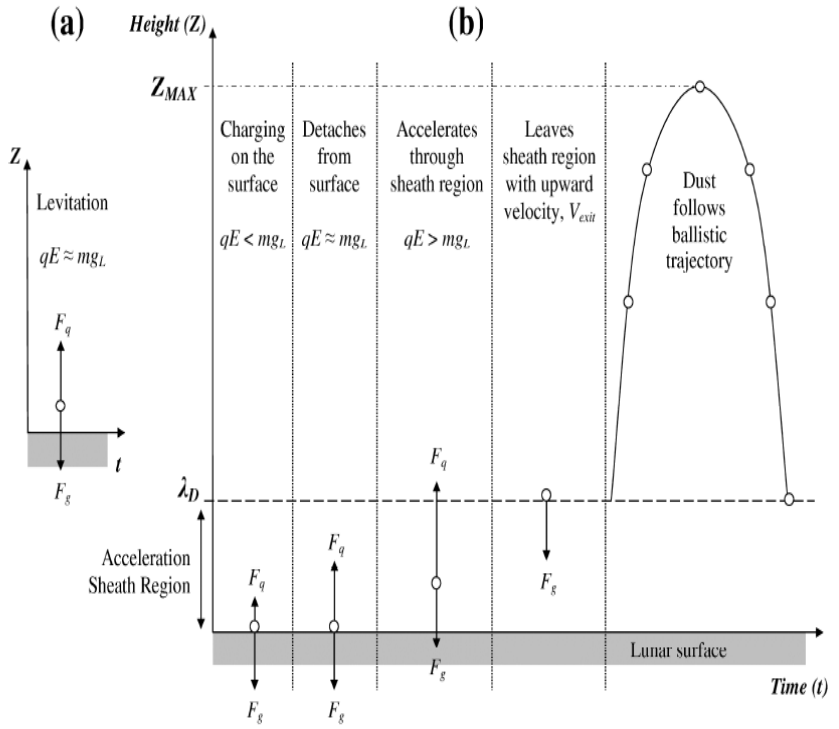

Electrostatic charging of lunar dust

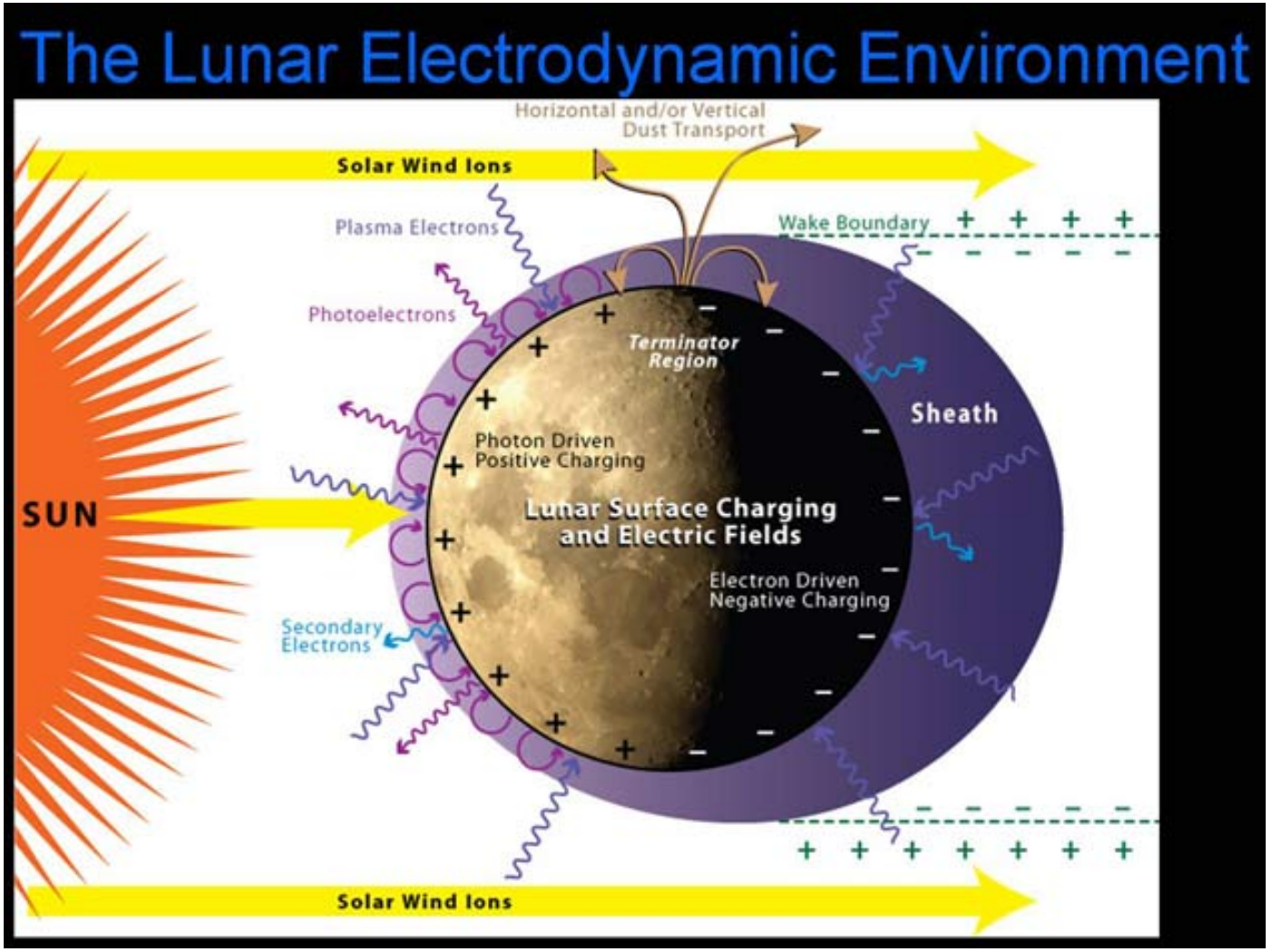

LADEE Mission of NASA (2012)

Lunar Atmosphere and Dust Environment Explorer

The objectives of the LADEE mission are:

Determine the global density, composition, and time variability of the fragile lunar atmosphere before it is perturbed by further human activity;

Determine if the Apollo astronaut sightings of diffuse emission at 10s of km above the surface were Na glow or dust and;

Document the dust impactor environment (size-frequency) to help guide design engineering for the outpost and also future robotic missions.

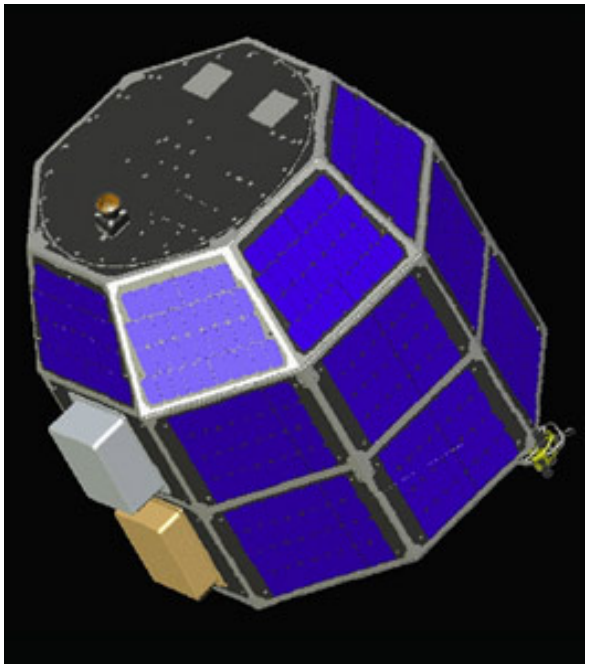

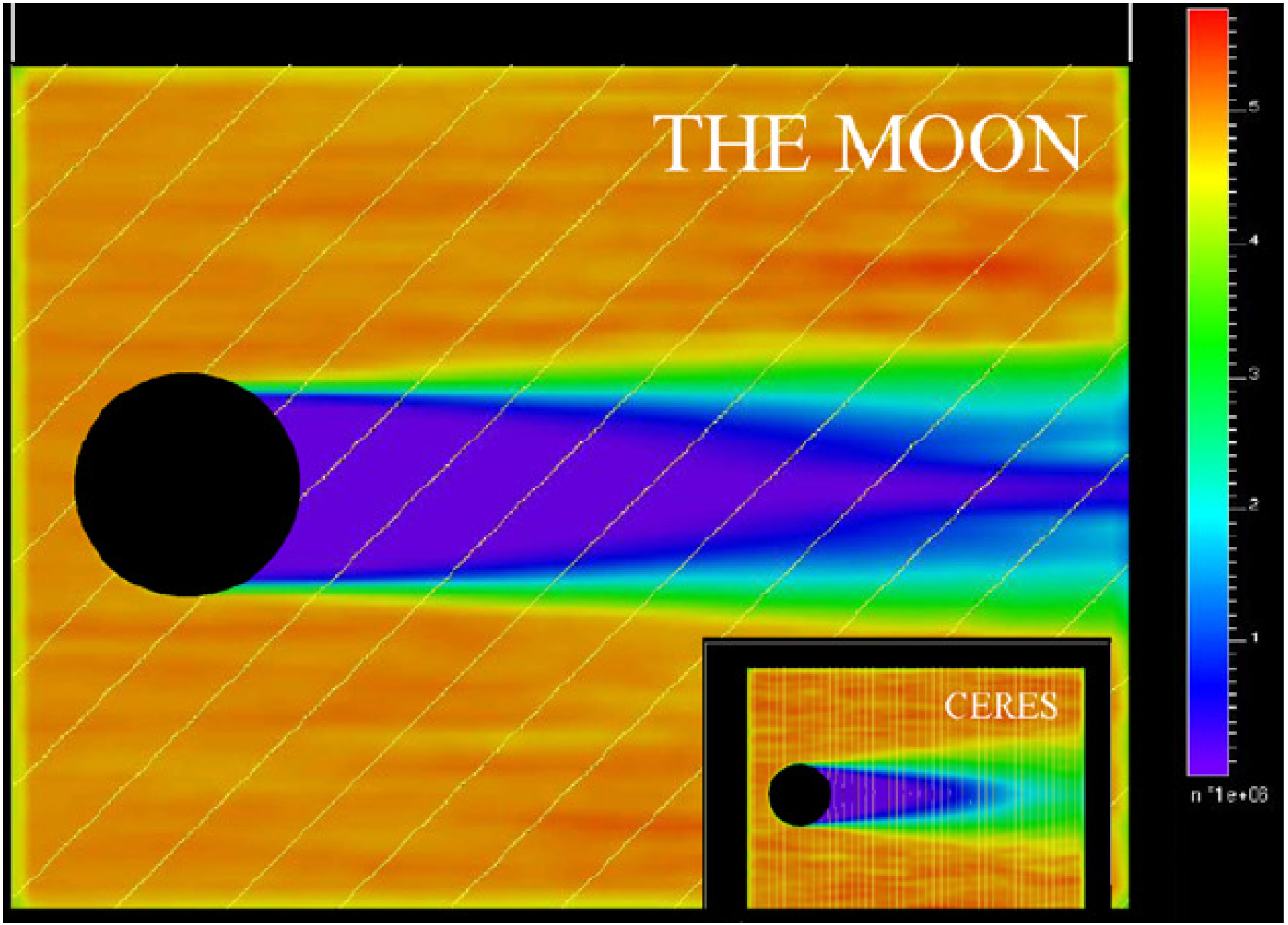
THE MOON
CERES
5
4
3
2
1
n *1e+06

The NASA Dawn Mission to Vesta and Ceres

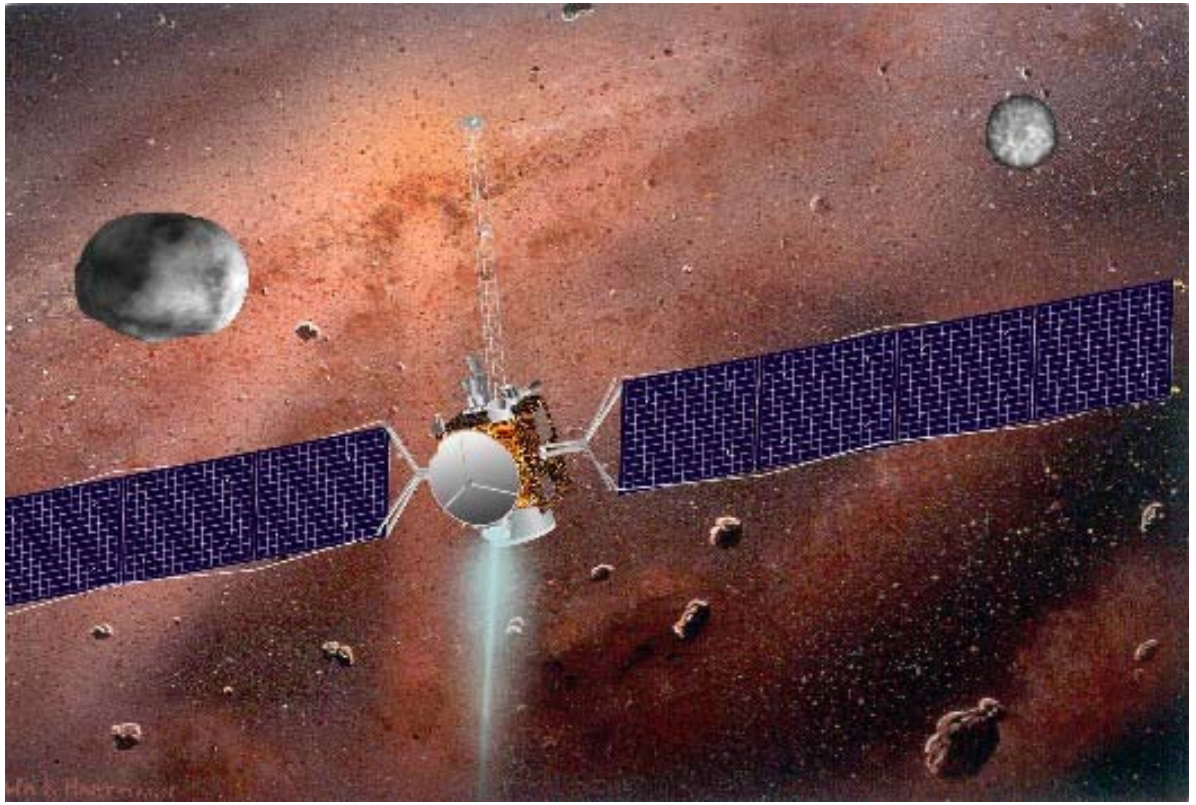

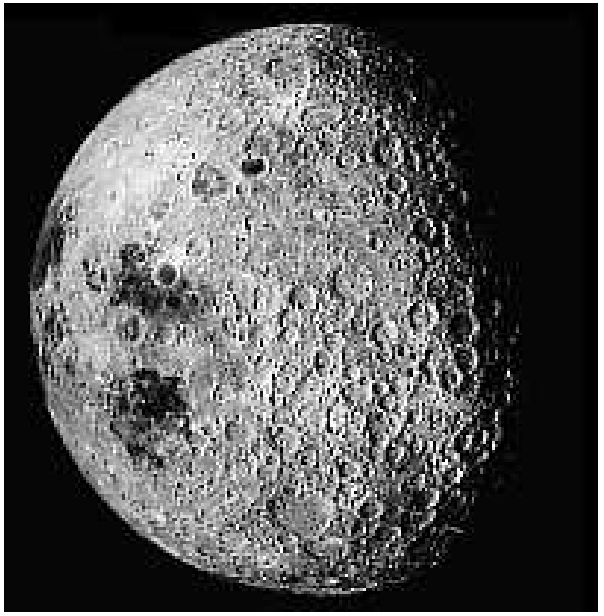

Horizontal glow at Vesta or Ceres?

Hayabusa Sample Return Mission

Rosetta Mission to 67P/Comet Churyumov-Gerasimenko (2015)

4. Laboratory dusty plasmas

Missions to Halley's Comet

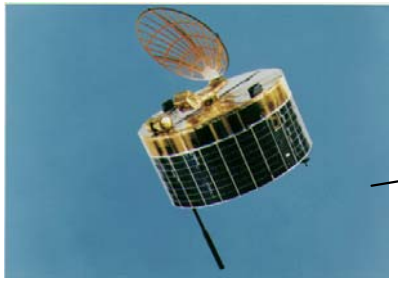

Suisei

Sakigake

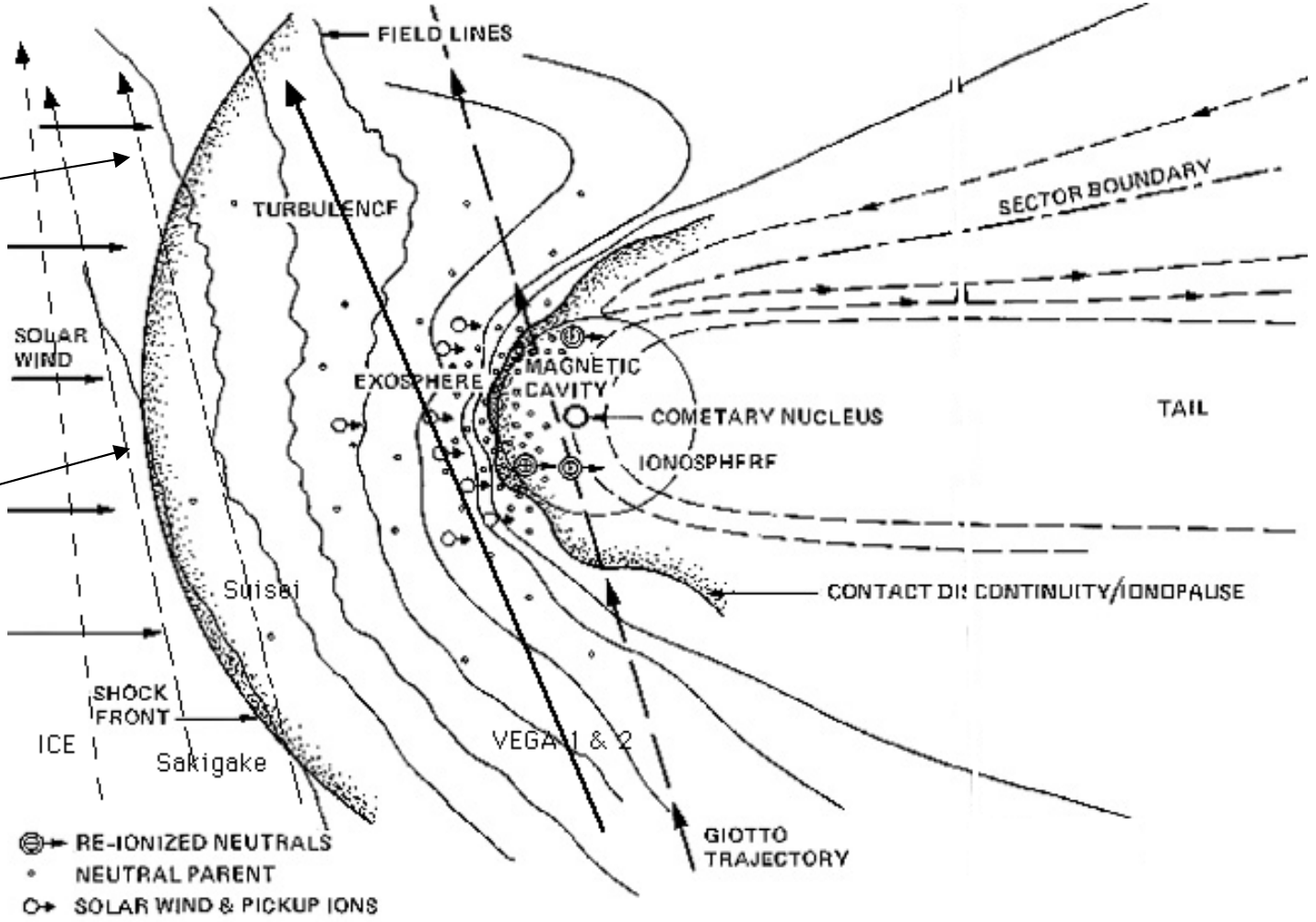

Dust acoustic waves and dust ion acoustic waves

Rao, Shukla and Yu (1990)
Shukla and Solin (1992)

$$en_e + Z|e|n + Q_g N_g = 0,$$

$$\partial_t n_j + \nabla(n_j v_j) = 0,$$

$$(\partial_t + v_j\nabla)v_j = \frac{Z_j q_j}{m_j}\left(E + \frac{1}{c} v_j \times B\right) - \frac{\gamma_j T_j \nabla n_j}{n_j m_j},$$

$$\nabla \cdot E = 4\pi \sum_j Z_j q_j n_j,$$

$$\nabla \cdot B = 0,$$

$$\nabla \times E = -\frac{1}{c}\partial_t B,$$

and

$$\nabla \times B = \frac{4\pi}{c}\sum Z_j q_j n_j v_j + \frac{1}{c^2}\partial_t E,$$

$$1 + (kr_{De})^{-2} - (\omega_{Li}/\omega)^2 - (\omega_{Lg}/\omega)^2 = 0,$$

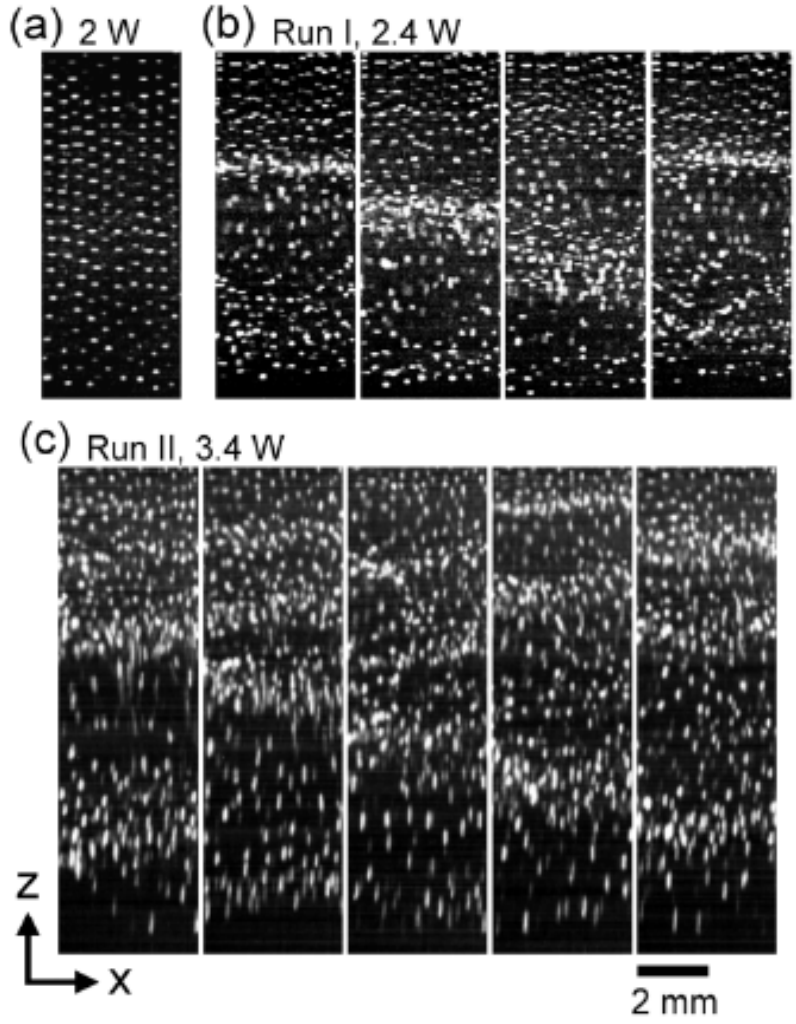

Liao et al. (2008)

The discovery of plasma crystals in 1994

Direct observation of Coulomb crystals and liquids in strongly coupled rf dusty plasmas
J.H. Chu and Lin I
Phys. Rev. Lett., 72, 4009, 1994

- The strongly coupled dusty plasmas are formed by suspending negatively charged SiO2 fine particles with 10 μm diameter in weakly ionized rf Ar discharges. The Coulomb crystals and liquids are directly observed for the first time using an optical microscope. By properly controlling the system parameters, hexagonal, fcc and bcc crystal structures and solids with coexisting different crystal structures can be formed. Increasing the rf power causes the transition to the more disordered liquid state.

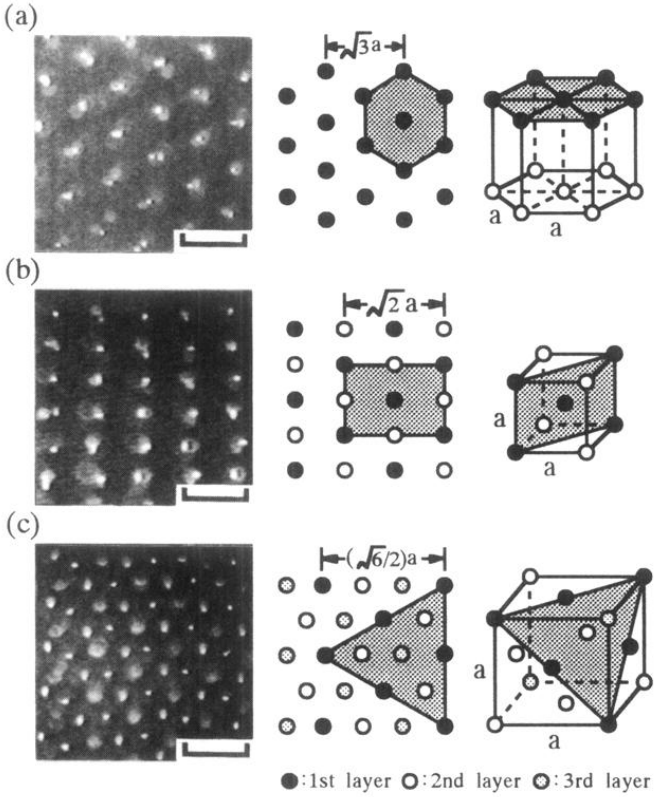

FIG. 3. Micrographs and sketches of the different crystal structures. (a) Hexagonal; (b) bcc; (c) fcc. The center column corresponds to the structures in the micrographs. The graded areas in the sketches are normal to the optical axis. The bars correspond to 200 μm.

The discovery of plasma crystals in 1994

Plasma crystal: Coulomb crystallization in a dusty plasma
H. Thomas, G.E. Morfill, V. Demmel, J. Goree, B. Feuerbacher and D. Moehlmann
Phys. Rev. Lett., 73, 652, 1994

- A macroscopic Coulomb crystal of solid particles in a plasma has been observed. Images of a cloud of 7- μm "dust" particles, which are charged and levitated in a weakly ionized argon plasma, reveal a hexagonal crystal structure. The crystal is visible to the unaided eye. The particles are cooled by neutral gas to 310 K, and their charge is >9800e, corresponding to a Coulomb coupling parameter Γ >20 700. For such a large Γ value, strongly coupled plasma theory predicts that the particles should organize in a Coulomb solid, in agreement with our observations.

FIG. 2. Image of the particle cloud in a plane above the lower electrode. The area shown is 7.7 × 7.7 mm^2 and contains 724 particles of 7-μm diameter.

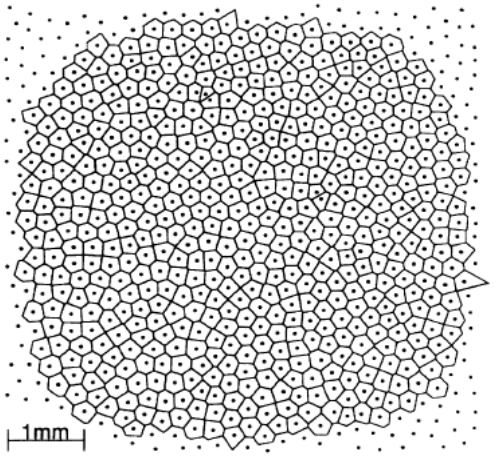

3D dust clusters (Yukawa balls)

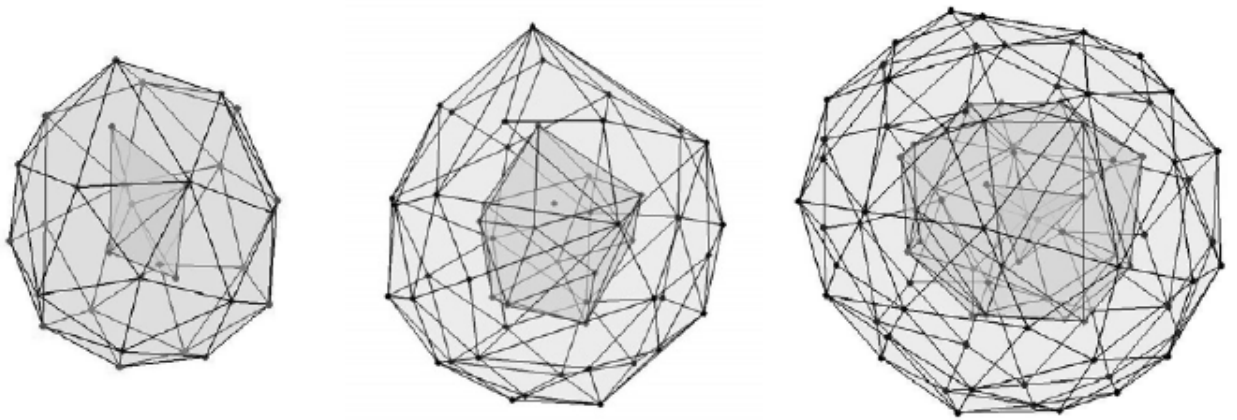

N=31 N=52 N=91

Melzer, Kading, Block and Piel (2008)

Laser heating of 2D Yukawa monolayer of dusty plasmas: Transition from solid to liquid

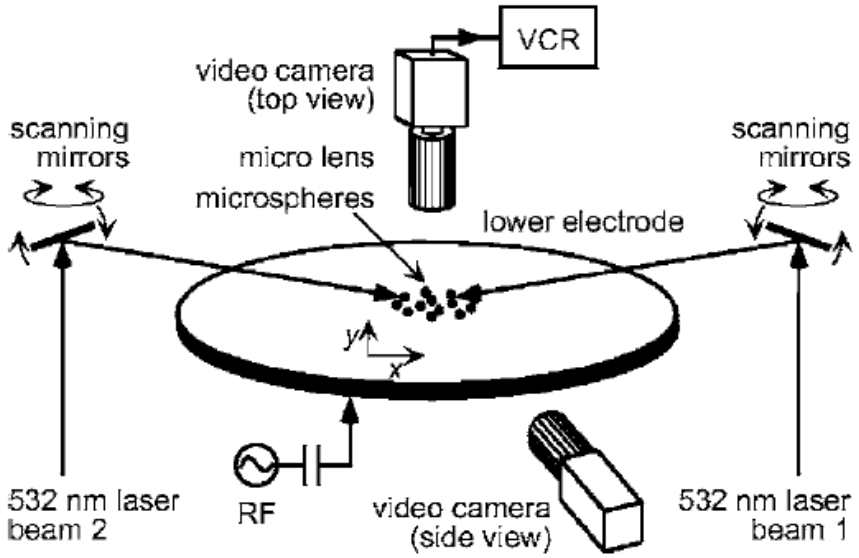

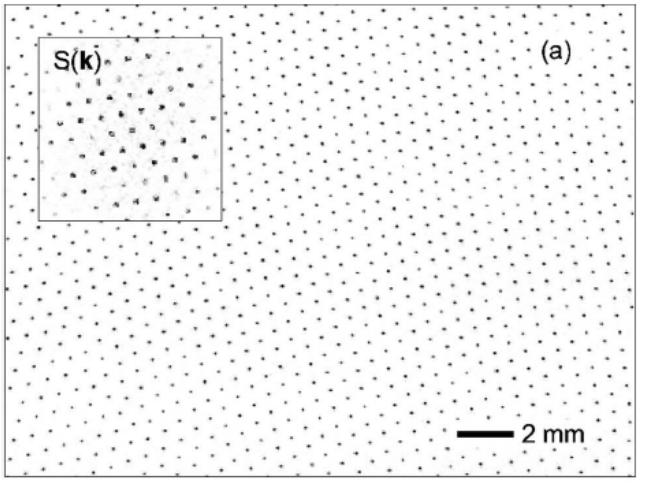

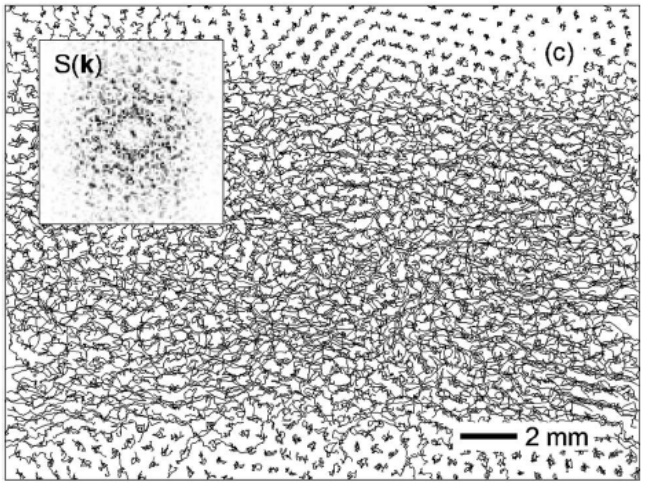

Nosenko and Goree (2006)

Plasma condensation in laboratory experiments and Tokamaks

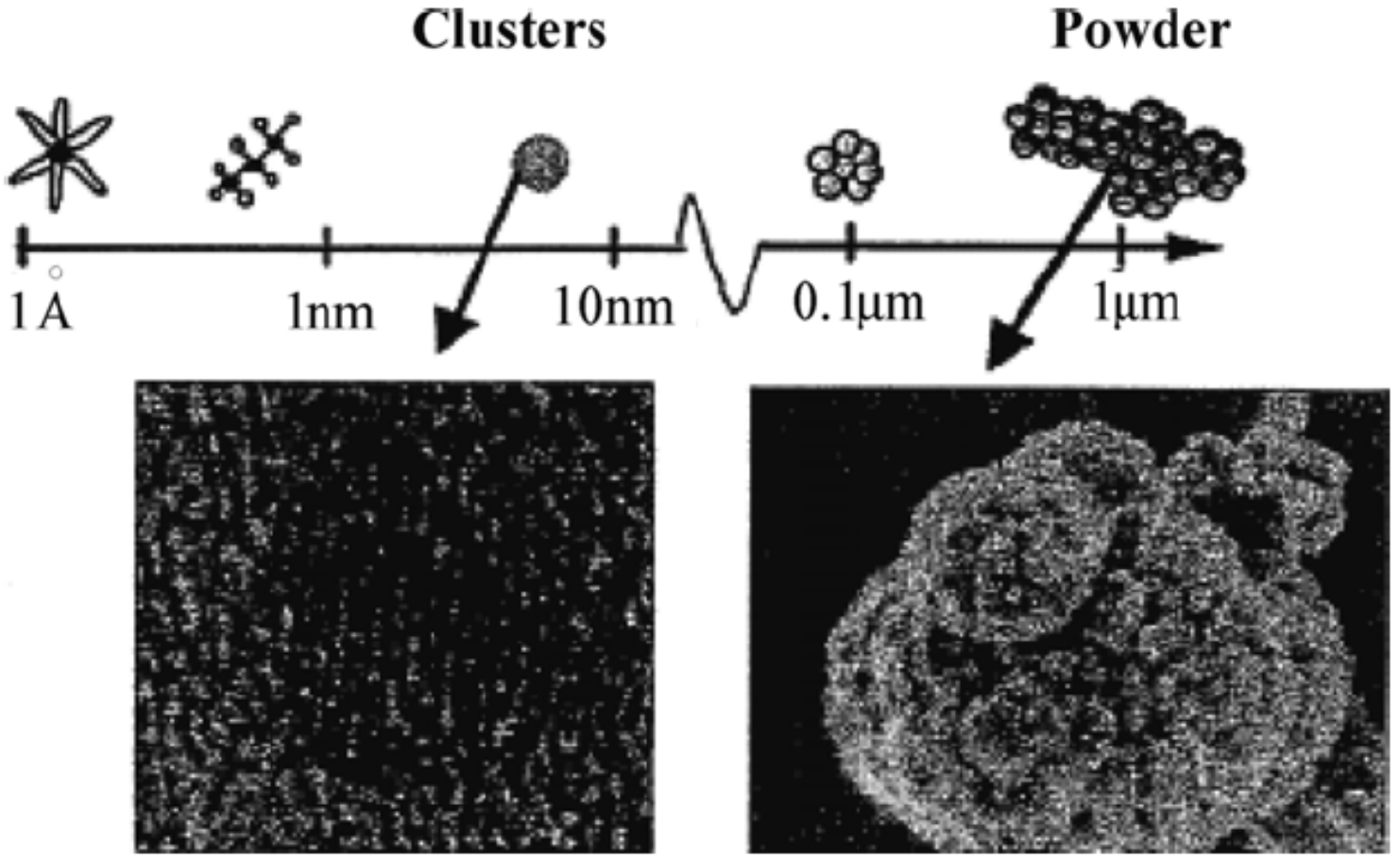

Ishihara (2007)

Plasma condensates and interplanetary dust

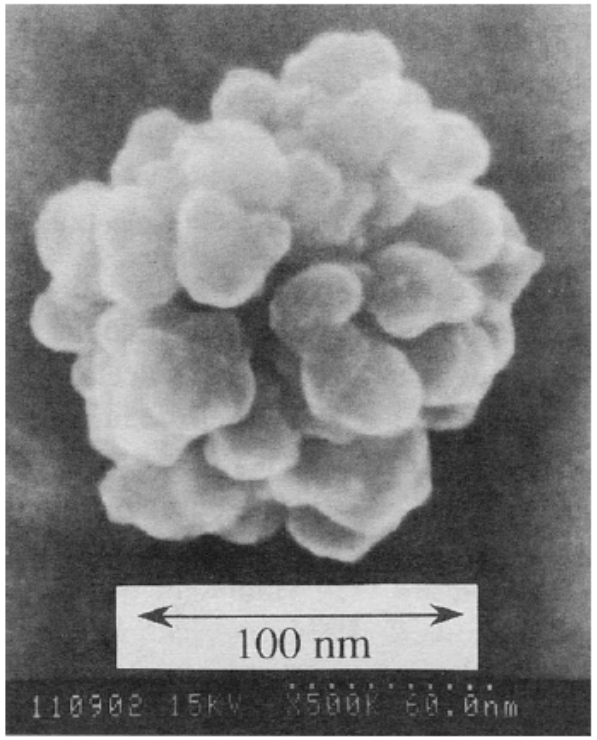

Figure 16. SEM photograph of a particle collected in the GS phase [2]. Experimental conditions: 5% SiH_4 + He, 30 sccm, 80 Pa, 40 W and $T_{on} = 4$ s.

Watanabe (2006)

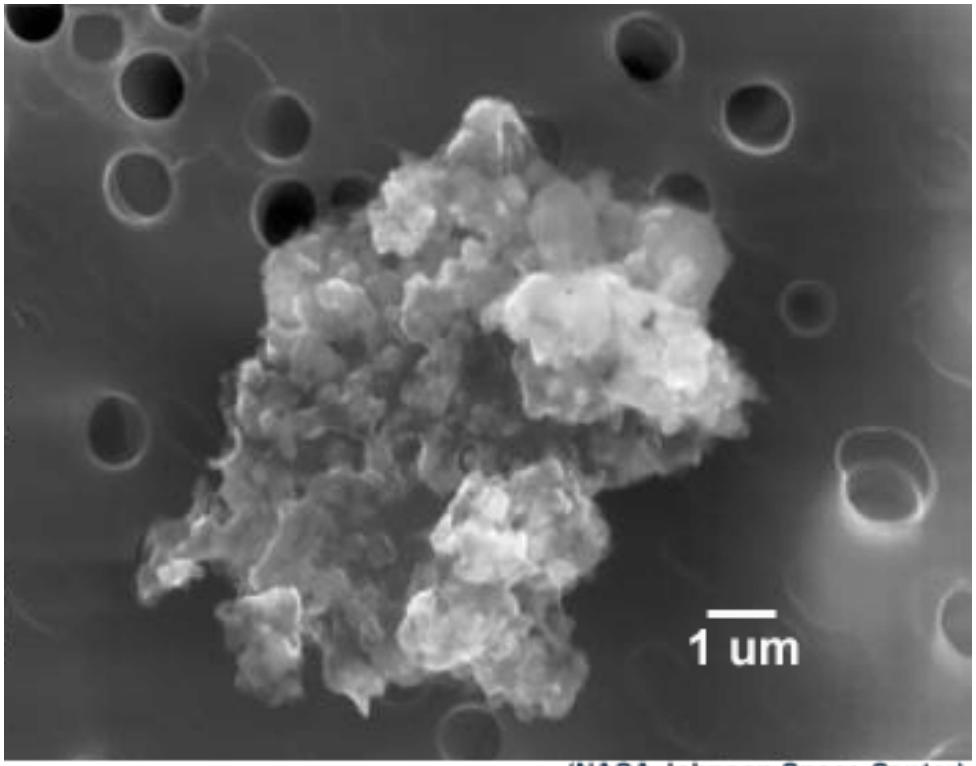

(NASA Johnson Space Center)

Dust formation and sedimentation

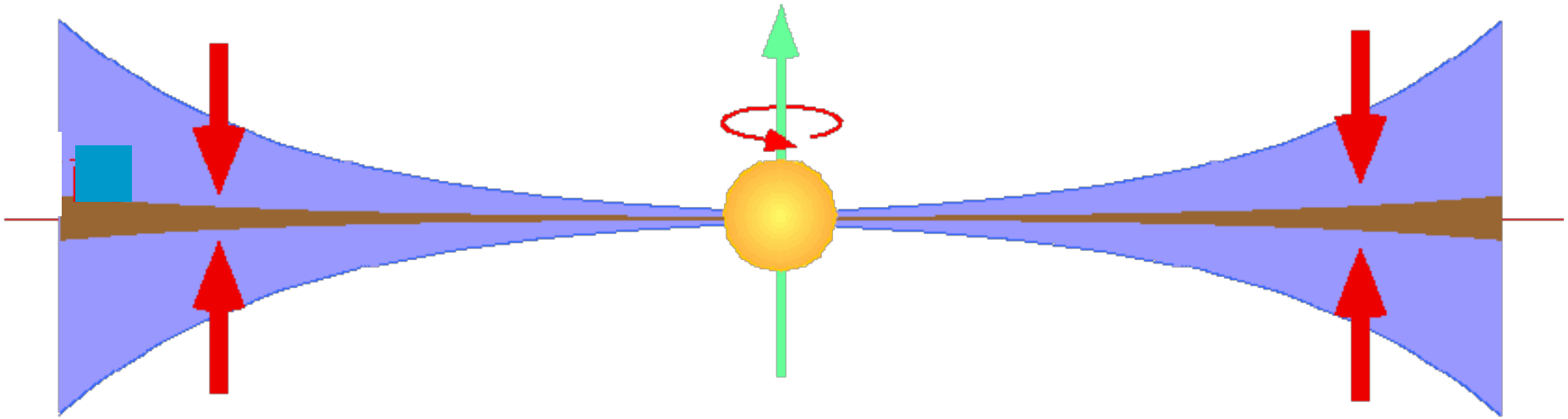

From Sho Sasaki

The upper layer of the solar nebula is subject to the Balbus-Hawley instability in driving the turbulence/viscosity while the mid-plane is a dead zone.
The first generation of dust condensation must be influenced by charging effect.

Cometary ice & interstellar grains

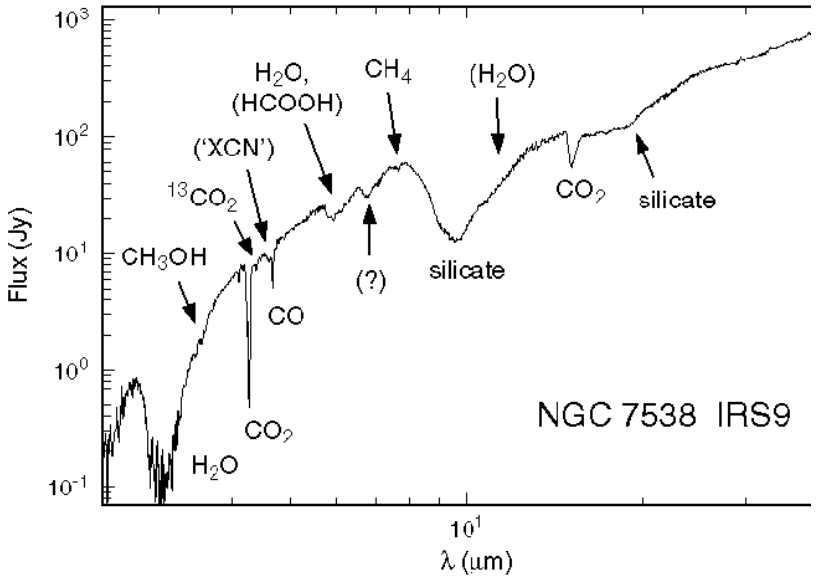

TABLE 1. *Abundances of interstellar ices toward proto-stars and cometary volatiles.*

Species	Proto-stars	Comets
H_2O	100	100
CO	1-50	5-7
CO_2	15	2-10
CH_4	0.9-1.9	0.2-1.2
H_2CO	3-7	1
OCS	0.1	0.1
CH_3OH	2-5	0.3-5
NH_3	3	1-2
C_2H_6	<0.4	0.4-1.2

FIR Spectroscopy of icy grains analogs

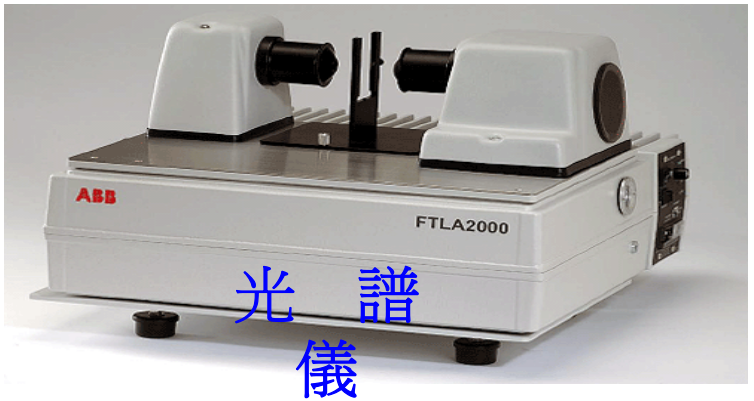

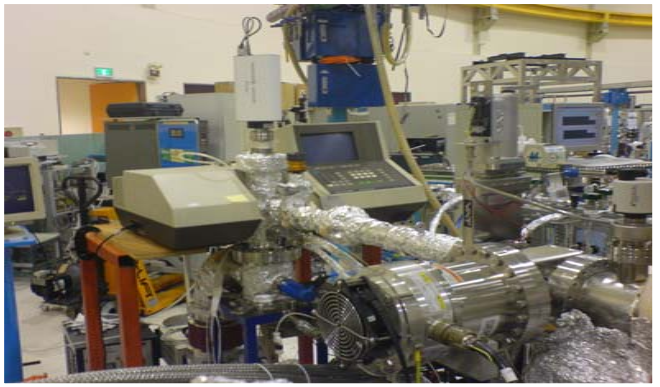

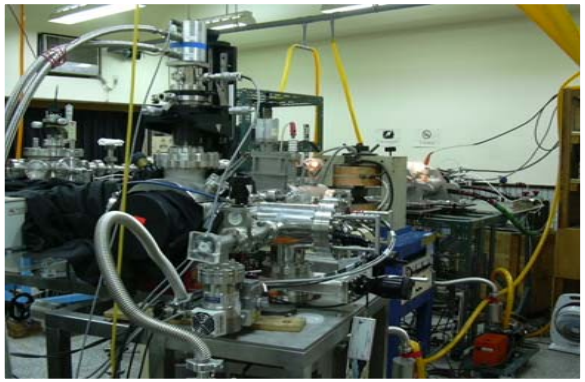

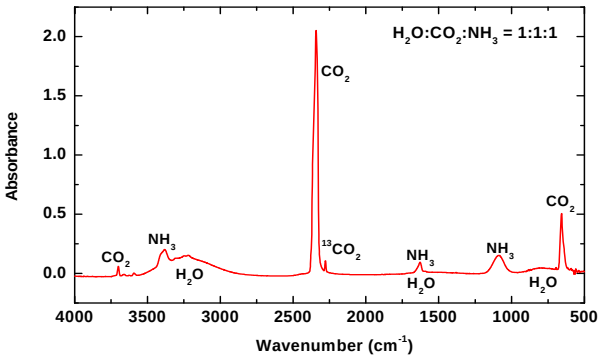

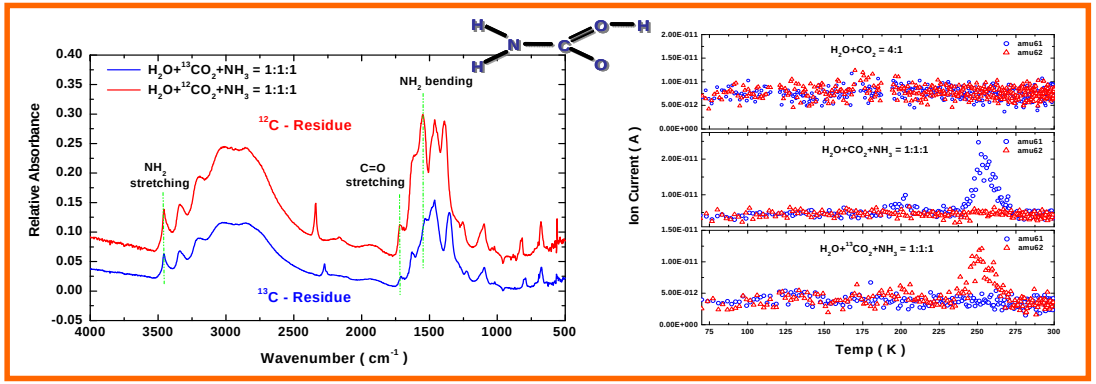

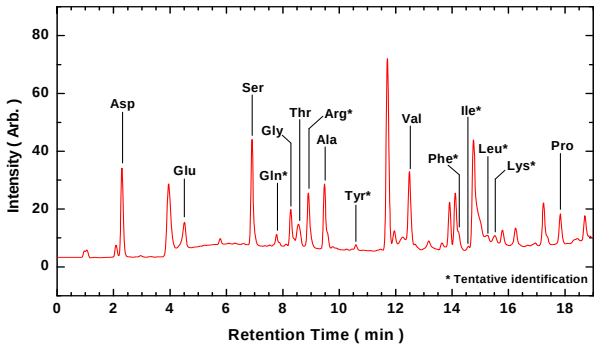

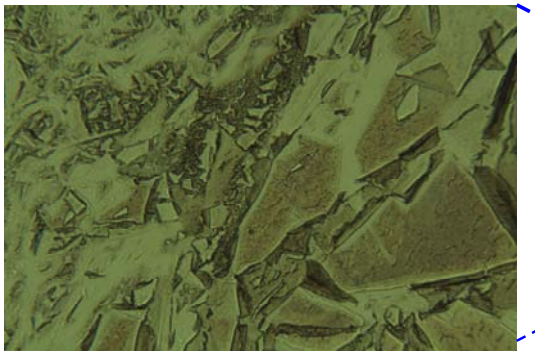

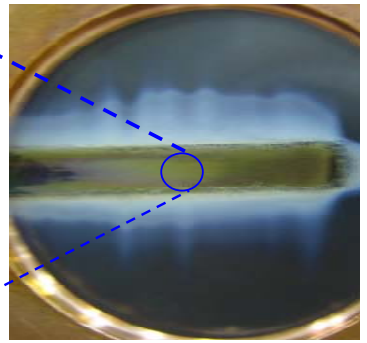

Amino acids!

Dusty plasmas are life-giving!

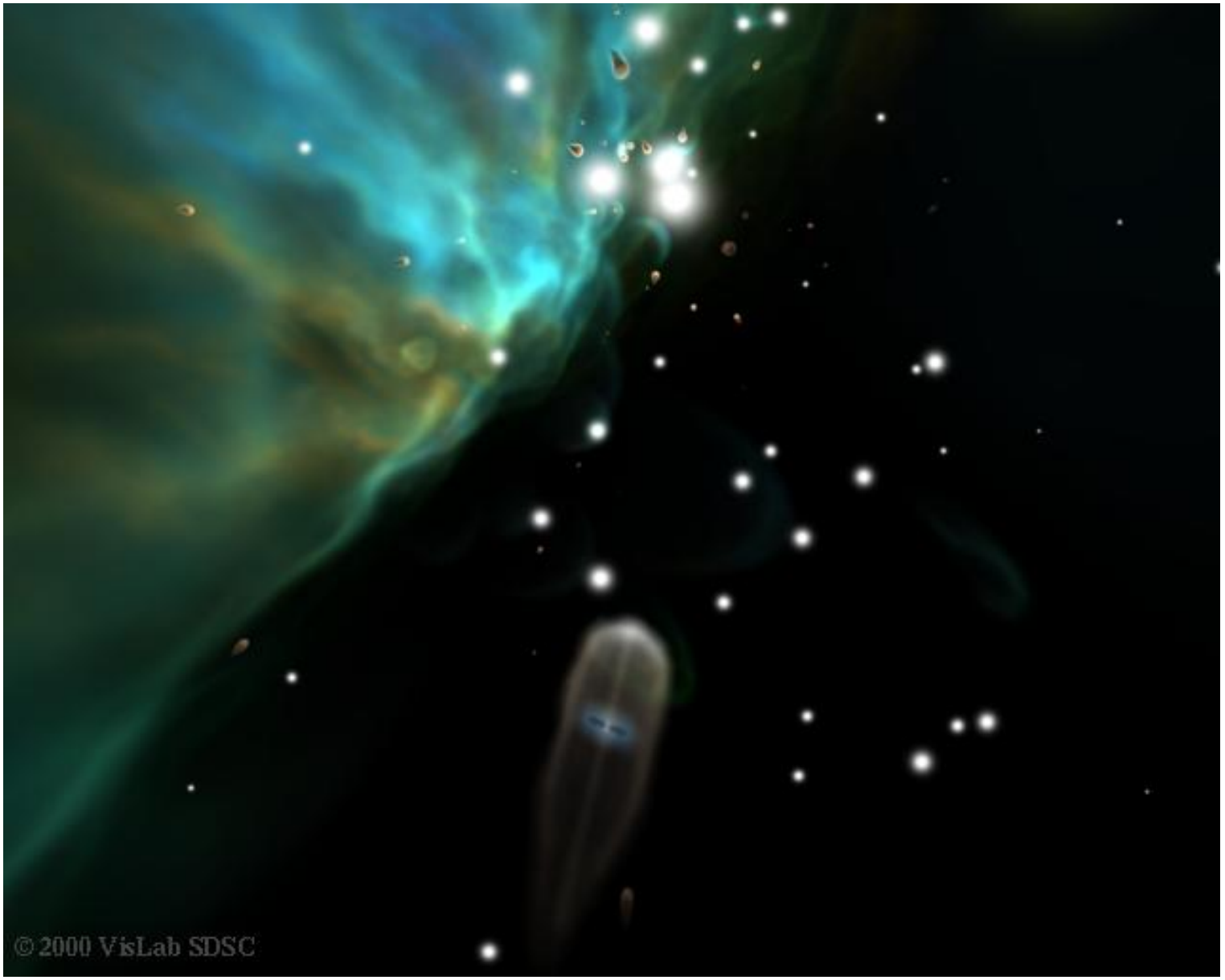

Summary

- Dusty plasma effects play an important role in small-scale (spokes) and large-scale structures (mass distribution) of the Saturnian main rings and the E ring.
- Many small solar system bodies including the Moon and Ceres could be covered by a sheath of dusty plasmas.
- Laboratory experiments led to discovery of plasma crystals which have wide applications (including solid state physics, Tokamaks and quark-gluon plasma after Big Bang).
- Plasma condensation and ion- or photon-interaction with dust grains could be important in astrophysical and planetary environments.

We are working on all four topics of dusty plasmas at National Central University.
Scientific collaborations are very welcome.

Epilogue

Iapetus from Cassini

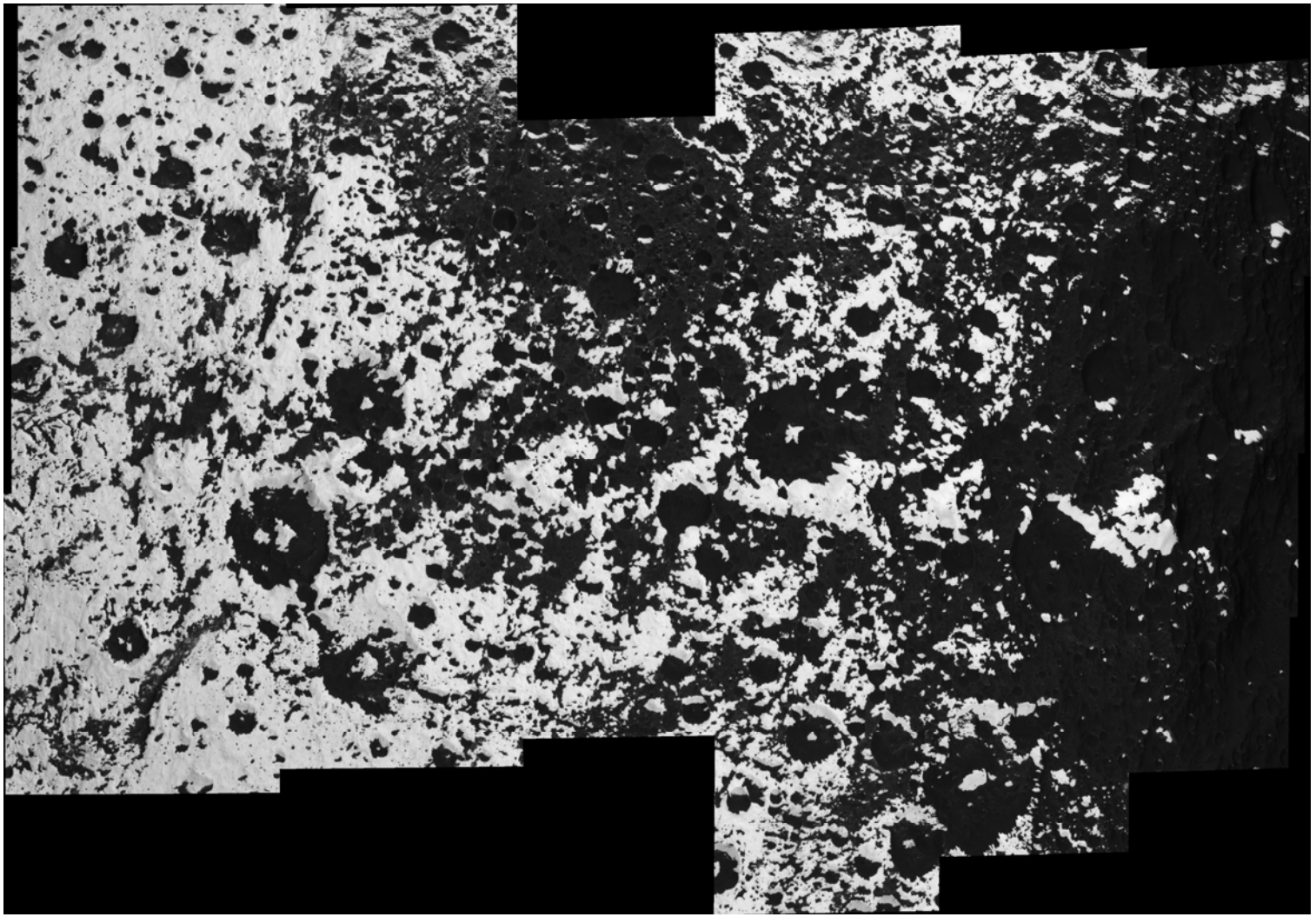

Revisiting Iapetus after Cassini

JOURNAL OF GEOPHYSICAL RESEARCH, VOL. 113, A11217, doi:10.1029/2008JA013532

Revisiting Iapetus following recent Cassini observations

D. A. Mendis[1] and W. I. Axford[2]

Received 23 June 2008; revised 4 September 2008; accepted 11 September 2008; published 22 November 2008.

[1] The recent observations of the Saturnian satellite Iapetus by the Cassini spacecraft support the theory proposed by us, over three decades ago, explaining the large brightness asymmetry between the leading and trailing faces of this synchronous satellite. Here we will revisit the question of the observed brightness variations, with orbital phase, not only of the outermost large Saturnian satellite Iapetus but also of the large inner ones (Tethys, Dione, Rhea, and Titan). While Titan (which has a significant atmosphere) shows no brightness variation with orbital phase, the remaining inner satellites show small but definite brightness variations with orbital phase, which, curiously, are in the sense opposite to that of Iapetus. In other words, while the leading face of Iapetus is much darker than its trailing face, the leading faces of the large inner satellites (with the exception of Titan) are slightly brighter. Here we provide an explanation of the latter effect too by invoking the impact on the trailing faces of these inner satellites by a class of negatively charged dust grains in the E-ring, moving in near-circular orbits, with super Kepler speeds.

Citation: Mendis, D. A., and W. I. Axford (2008), Revisiting Iapetus following recent Cassini observations, , A11217, doi:10.1029/2008JA013532.

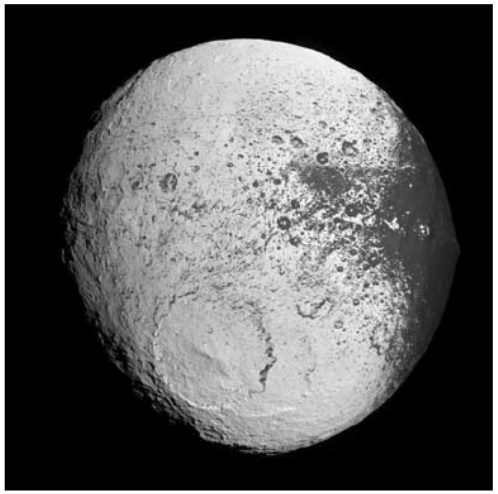

Mendis and Axford (2008)

End of Lecture 2

References

- Burger, M. H., Sittler, E. C., Johnson, R. E., et al. 2007, JGR, 112, A06219
- Burns, J. A., Hamilton, D. P., Mignard, F., et al. 1996, ASPC, 104, 179
- Chow, V. W., Mendis, D. A., & Rosenberg, M. 1993, JGR, 98, 19065
- Chu, J. H., & I, Lin. 1994, PhRvL, 72, 4009
- de Pater, I., Martin, S. C., & Showalter, M. R. 2004, Icarus, 172, 446
- Farmer, A. J., & Goldreich, P. 2005, Icarus, 179, 535
- Farrell, W. M., Desch, M. D., Kaiser, M. L., et al. 2006, GeoRL, 33, L07203
- Goertz, C. K., & Ip, W.-H. 1984, GeoRL, 11, 349
- Goertz, C. K., & Morfill, G. 1983, Icarus, 53, 219
- Grard, R. J. L., & J. K. E. Tunaley 1971, JGR, 76, 2498
- Grun, E., Garneau, G. W., Terrile, R. J., et al. 1984, AdSpR, 4, 143
- Hamilton, D. P., & Burns, J. A. 1994, Science, 264, 550
- Horanyi, M. 1996, ARA&A, 34, 383
- Horanyi, M., Juhasz, A., & Morfill, G. E. 2008, GeoRL, 35, L04203
- Ip, W.-H. 1983, JGR, 88, 819
- Ip, W.-H. 1984, JGR, 89, 3829

References

- Ip, W.-H. 1995, Icarus, 115, 295
- Ip, W.-H., & Mendis, D. A. 1983, GeoRL, 10, 207
- Ishihara, O. 2007, JPhD., 40, R121
- Jones, G. H., Krupp, N., Kruger, H., et al. 2006, GeoRL, 33, L21202
- Juhasz, A., & Horanyi, M. 2002, JGRA, 107, 1066
- Jurac, S., Johnson, R. E., & Richardson, J. D., 2001, Icarus, 149, 384
- Kempf, S., Beckmann, U., Srama, R., et al. 2006, P&SS, 54, 999
- Krivov, A. V., & Banaszkiewicz, M. 2001, P&SS, 49, 1265
- Lehtinen, N. G., Inan, U. S., & Bell, T. F., 2001, JGR, 106, 28841
- Liao, C.-T., Teng, L.-W., Tsai, C.-Y., Io, C.-W., & I, L. 2008, PhRvL, 100, 185004
- Melzer, A., Kaeding, S., Block, D., & Piel, A. 2008, JPCM, 20, 4204
- Mendis, D. A., & Axford, W. I. 1974, AREPS, 2, 419
- Mendis, D. A., Hill, J. R., Houpis, H. L. F., et al. 1981, ApJ, 249, 787
- Northrop, T. G., & Hill, J. R. 1983, JGR, 88, 6102
- Nosenko, V., Avinash, K., Goree, J., & Liu, B. 2004, PhRvL, 92, 085001

References

- Nosenko, V., & Goree, J. 2004, PhRvL, 93, 155004
- Porco, C. A., & Danielson, G. E. 1982, AJ, 87, 826
- Rao, N. N., Shukla, P. K., & Yu, M. Y. 1990, P&SS, 38, 543
- Roussos, E. et al. 2008, GeoRL, 35, L22106
- Shukla, P. K. 1992, PhyS, 45, 504
- Shull, J. M. 1978, ApJ, 226, 858
- Smith, B. A., Soderblom, L., Beebe, R. F., et al. 1981, Science, 212, 163
- Smith, B. A., Soderblom, L., Baston, R., et al. 1982, Science, 215, 504
- Soter, S., 1974, IAU Colloq. 28
- Stubbs, T. J., Halekas, J. S., Farrell, W. M., et al. 2005, LPICo, 1280, 139
- Thomas, H., Morfill, G. E., Demmel, V., et al. 1994, PhRvL, 73, 652
- Valdivia, J. A., Milikh, G., & Papadopoulos, K. 1997, GeoRL, 24, 3169
- Watanabe Y. 2006, JPhD, 39, R329
- Whipple, E. C. 1981, RPPh, 44, 1197